Investigation of the effect of hydroxycitric acid on urinary calcium oxalate risk factors for kidney stone formation in artificial urine: theoretical modelling and in vitro crystallisation experiments

A dissertation submitted to

University of Cape Town

In fulfilment of the requests for the degree

Master's thesis 2020

By

Amouna Ahmed

Supervisor

Prof. Neil Ravenscroft

Co-supervisors

Prof. Graham Jackson and Prof. Allen Rodgers

Department of Chemistry

University of Cape Town

Rondebosch

7701

March 2020

DEDICATION

I dedicate this entire thesis to my husband (Mohammed Makki), my family and my children (Ahmed, Eyadd, Omer and Alla) they supported me with their love.

Acknowledgements

First and foremost, praises and thanks to my gratitude to Allah for giving me the strength and ability to complete this Master's work. I ask his almighty that this work would be another tool to help in the treatment of kidney stones. I would like to precise my deep and sincere gratitude to my research Co-supervisor, Prof. Graham Jackson, for allowing me to do research and providing me invaluable guidance throughout the path doing this research. He educates me the methodology to carry out the study. It was a great privilege to work and study under his guidance. I am incredibly grateful for what he has offered me. I would like to sincerely thank Prof. Allen Rodgers for too, for his excellent Co-supervision and tremendous contribution towards shaping this thesis.I would like to thank for Fatin Elmagbari and Ahmed Hammouda for constant guidance.Last but notleast, I would like to thank my family for starting with my husband, Dr Mohammed for his support and great patience at all times, and to my parents who have given me their unbelievable comfort throughout the way.

Abstract

Nephrolithiasis, or urolithiasis, commonly known as kidney stones, is a common medical problem. Kidney stones are composed of different mineral types. Calcium Oxalate is the most common kind of stone.

The principal aim of this research was to establish whether hydroxycitrate (HCA) affects and/or inhibits calcium oxalate crystallisation. A three-pronged approach was adopted, involving the determination of thermodynamic binding constants for Ca, Mg and Zn-HCA complexes, theoretical modelling of HCA-complex formation in artificial urine and *in vitro* crystallisation experiments. A potentiometric analysis was conducted to determine thermodynamic binding constants. These were included in the database of the JESS computer program to model the effect of HCA on the urinary supersaturation of calcium salts. A 1 mM HCA concentrations successfully decreased the concentration of ionised calcium and hence the urinary supersaturation of calcium salts. The solution structures of H^{+}, Ca^{2+}, Mg^{2+}, and Zn^{2+}-HCA complexes were investigated using ^{1}H-NMR. For protonation, the results showed that the *pK*a values were too close to resolve and that several microstates were in rapid exchange. Similarly, for the metal complexes, several species were found to be in rapid exchange. Crystallisation experiments were conducted in artificial urine, to determine the effect of HCA on the thermodynamics and kinetics of crystallisation of calcium oxalate, which is the most common component of kidney stones. The effect of HCA on calcium oxalate metastable limit (MSL) and crystallisation kinetics were measured. The results confirmed those predicted by theoretical

modelling. The MSL was significantly affected by 1 mM HCA. Also, 1 mM HCA increased the rate of CaOx crystallisation. Both these effects are favourable and decrease the risk of *in vivo* crystal and stone formation. This augurs well for the potential application of HCA as a therapeutic agent in the management of kidney stone disease. Such an outcome needs to be tested in human trials.

LIST OF ABBREVIATIONS AND SYMBOLS

AUA	Anhydrous uric acid
AU	Artificial urine
Cit	Citrate
COM	Calcium oxalate monohydrate
COD	Calcium oxalate dihydrate
CaOx	Calcium oxalate
CaP	Calcium phosphate
CT	Computed tomography
ESRD	- end –stage renal disease
ESTA	Equilibrium simulation for titration Analysis
HCA	Hydroxycitric acid
IUPAC	International union of pure and applied
JESS	Joint expert speciation system
K	Equilibrium constant
K_W	Dissociation constant of water

log β	Logarithm (to base10) of the cumulative equilibrium Constants
Iog *K*	Logarithm (to base10) of the cumulative equilibrium Constants
MSL	Metasable limit
NMR	Nuclear magnetic resonance
n_P	Number of titration points
n_t	Number of titrations
pH	(- Iog H^+)- A measure of acidity or alkalinity
JESS	Joint Expert Speciation System
Q_M-bar	The deprotonation function

R_f^H	The Hamiltonian R-factor
R^H_{Lim}	R_{Lim} is the hamiltonian R-Limit
SI	Saturation index
SS	Supersaturation
T_H	Total proton concentration (mol dm^{-3})
T_L	Total ligand concentration (mol dm^{-3})
UAA	Anhydrous uric acid
UA	Uric acid renal calculi
U_{obj}	Objective function
Z_i	The charge of the ion
Z_{H-bar}	The protonation function
Z_{M-bar}	The metal formation function

LIST OF FIGURES

LIST OF TABLES

TABLE OF CONTENTS

Chapter One

1. Kidney Stone Disease

1.1. Background of the Disease

Nephrolithiasis, or urolithiasis, commonly known as kidney stones, is a common medical problem.[1] [2] Kidney stones can be described as pieces of solid material produced inside the kidney, in addition to normal urine constituents. Large stones may block the ureter, bladder, or urinary tract, thus potentially retarding urine excretion. [3] Stone formation is a variegated process comprising nucleation, growth of crystal, and aggregation. [4]

The epidemiology of urolithiasis varies according to the geographical area, age, and gender of the patients. [5]

The prevalence of kidney stones is 10% in males and 6% in females. [6] It increases with age, peaking in those aged 40 to 59 years. [7]

Kidney stones affect some 5 - 15% of the inhabitants worldwide [8] with higher incidences observed in Caucasian patients, followed by Hispanics, Africans, and Asians. [9]

1.2. Composition of stones

Approximately 80 % of all stones are made up of calcium oxalate (CaOx) and calcium phosphate (CaP). Urinary calcium concentrations that are 7-11 times higher than normal raise the risk of Ca-containing kidney stones. [10-14] Calcium phosphate (Cap) stones account for nearly 15% of all urinary stones with a noticeable preponderance in females. [15]

Although most kidney stones contain primarily calcium oxalate, up to 50% of these, contain calcium hydroxyl phosphate (10–20%), magnesium ammonium phosphate (struvite or triple phosphate), urate (5%), and 1–2% comprises cysteine. Ideally, a stone analysis should be performed via infrared spectroscopy or x-ray diffraction. [14, 16] A kidney stone may form when high levels of calcium, oxalate, uric acid, or cysteine are excreted in the urine. [14] Stones may also form if these compounds are present at normal levels, but urine flow is restricted. [13] Supersaturation of these substances leads to crystals, which may become anchored in the kidney and grow (crystal growth) to form a kidney stone. [17]

The prevalence of kidney stones in end-stage renal disease (ESRD) [7] is 5.2% in the United States. African-Americans, who are a minority (12.9%) make up > 30% of patients progressing to ESRD. [18] However, in general, this group has a three-fold lower prevalence of kidney stones than the rest of the US population. [19]

The black South African population also shows a lower overall prevalence of urinary stones than their white counterparts. [19, 20]

People have suffered from kidney and bladder stones for centuries. [21] Its prevalence is 12% in Canada, 5 - 9% in Europe, and 13 - 15% in the US. While it is only 1 - 5% in most Eastern countries, the risks are much higher in certain Asian countries. Saudi Arabia has an occurrence rate of 20.1%, with a lifetime repetition rate of up to 50 %. [14]

Stones produce without any symptoms or clinical signs until significant stone growth results in hematuria. Stone passage begins as mild uneasiness but progresses to extreme pain over 30–60 min. [14] If the stone blocks the ureteropelvic junction, the pain localises in the flank, and, as the stone shifts down the ureter, the pain transfers downward towards the anterior side. [22] Once the stone reaches the ureters vesicular junction, it may cause dysuria, and symptoms may be mistaken for those of infection. [14] Stones less than 5 mm in diameter have a greater chance of passage, those 5–7 mm in diameter have a moderate chance (60%) of passage, and those greater than 7 mm in diameter usually cannot pass on their own and require urological intervention. [16][14]

1.3. Mechanism of stone formation

Various studies have attempted to discern the mechanism of CaOx kidney stone formation.

Kidney stones are produced from the growing of crystals to stones, and the physical process of stone formation involves the following complex cascade of events and physicochemical processes:

Saturation → Supersaturation → Nucleation → Crystal aggregation

Crystal growth → Crystal retention → Stone formation

Supersaturation is essential for stone formation. [23]

The multifactorial aetiology of kidney stone formation and high rates of recurrence have resulted in a long-standing interest in the potential role of macromolecules in nephrolithiasis, particularly considering all human stones in the kidneys consist of a complex mixture of mineral and organic materials. [5]

The major types of stones and their mechanisms of formation are as follows.

1.3.1. Calcium oxalate (CaOx)

Calcium oxalate (CaOx) stones are of two types: the monohydrate, and the dihydrate. Calcium oxalate monohydrate (COM) is observed to recur in patients with normal urine calcium excretions; these crystals could arise because of an absence or deficiency of inhibitors thereby allowing crystals to form and pass spontaneously in the urine. In contrast, calcium oxalate dihydrate (COD) is found in patients with high urine calcium and no elevation in citrate excretion or urinary pH. [24] COD can also be found in combination with uric acid or calcium phosphate. CaOx stones grow in the papillary tip, on Randall's plaque, [12] [21] and so the core of the stones may be CaP (usually 5%) surrounded by CaOx (95%).

Hypercalciuria occurs when a pathological process produces excessive urinary calcium. [12, 25]

Hyperoxaluria is increased urinary excretion of oxalate. Two distinct forms of hyperoxaluria exist. Primary hyperoxaluria is a metabolic error, while secondary hyperoxaluria is a result of increased dietary ingestion of oxalate, oxalate precursors or changes in intestinal microflora. [26]

Hypocitraturia is defined as low citrate secretion. [27] Hypocitraturia may be associate with hypercalciuria or occurs as an abnormality. Potassium citrate can be used as therapy, but some patients are affected by gastrointestinal side-effects, particularly dyspepsia. [28]

1.3.2. Phosphate stones

Phosphate stone occure as carbonate-apatite, brushite, hydroxyapatite , whitlockite and struvite,or a mixture of these. [29, 30]

Hydroxyapatite make up 9.5 % of stones, brushite 2.1 % and struvite infection stones 14.6 %. Stones resulting from infection are 20-60 % struvite with the remaining part comprising hydroxyapatite and or calcium-deficient hydroxyapatite as the Ca/P ratio varies between 1.3 and 1.6. [24]

1.3.3. Brushite ($CaHPO_4 \cdot 2H_2O$) stones

Brushite is named after the American mineralogist George Jarvis Brush and is the dominant phase of the $CaHPO_4 \cdot 2H_2O$ system that precipitates between pH 2 and pH 6.5. [31] These stones have a Ca/P molar ratio that is close to unity. Brushite precipitates from urine containing 60 mg/L of magnesium at pH < 7.0. [32] While brushite is the principal component of brushite stones they may also contain as much as 10 % hydroxyapatite. Brushite stones contain numerous cavities, partially filled with organic matter and/or hydroxyapatite. [24] Nucleated crystals grow from supersaturated urine by depositing growth units. [32, 33] These formations are composed of individual crystals. [34]

1.3.4. Uric acid stones

Uric acid stones make up approximately 13% of human kidney stones. These stones can be categorised into two distinct subtypes depending on their structure:

Compact uric stones (type I) are mainly formed by crystalline growth of anhydrous uric acid (UAA) and may include small urine deposits; this kind could be further divided into two stone subgroups. [35]

Type II stones consist of stones formed usually by sedimentation and could be divided into two groups.

(1) IIa stones have a porous interior, which is filled with UAA, COM or organic matter. [35]

(2) IIb stones were initially uric acid dihydrate (UAD) which later changed to UAA. Their interior is either empty or partially filled with crystals or organic matter. [35]

Urinary stones may also be typified according to their position in the urinary system and may be located in the kidney, pelvis, urethra **or** bladder (Figure 1.1)

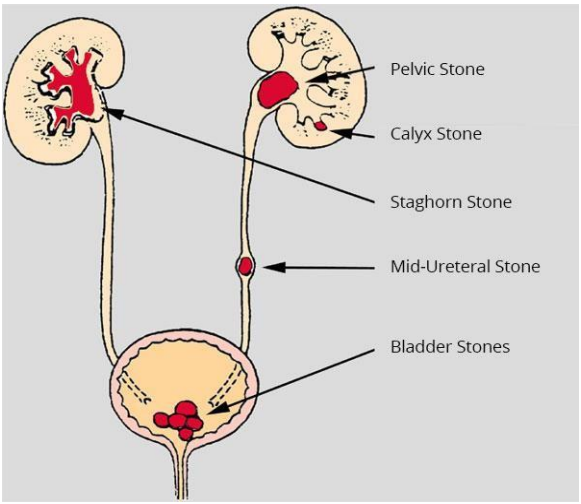

Figure 1.1. The major site of kidney stones according to the position in the urinary system. [36]

1.4. Kidney stone treatment

Kidney stone treatment and prevention consists of the following three approaches. [37]

1.4.1. Dietary recommendations

Adequate dietary calcium intake should be maintained, but dietary oxalate should be restricted because dietary oxalate may be significant in stone development and could be raise urinary oxalate secretion and predispose to the development of CaOx. [38-42]

Animal protein and salt consumption should be decreased because more than normal animal protein intake contributes to hyperuricosuria, a peril for calcium stones [43], while vegetables and fruits that are rich in potassium ought be increased. [44] Intake of fluids should be increased (>2 L per day). Various studies have been suggested that diets including fruits and greater intake of vegetables play a role in the prevention of kidney stones. [45]

1.4.2. Drug treatment

The following agents may be applied to thiazide diuretics, allopurinol, and potassium citrate. [37, 46]

1.4.3. Other therapeutic approaches

Unnatural risk factors for urinary stones such as infection should be identified and treated with appropriate antibiotics. Tests for secondary causes of nephrolithiasis, like cystinuria and hyperoxaluria, [37] should be performed.

1.5. Use of citrate

Citrate, whose structure resembles that of hydroxycitric acid (HCA) except for the presence of an additional OH group on the second carbon atom in HCA is shown in Figure 1.2.

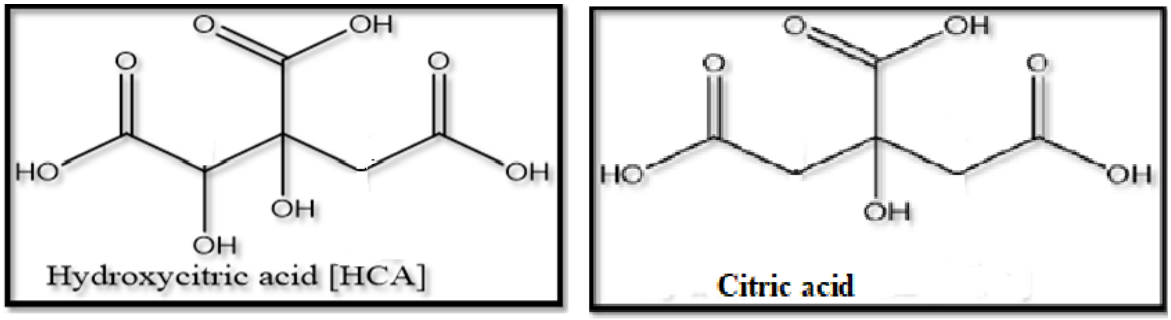

Figure 1.2. Structures for hydroxycitric acid and citric acid.

In vitro studies have shown that citrate prevents spontaneous nucleation of calcium oxalate and obstructs growth and agglomeration of preformed calcium oxalate crystals. [46, 47] Citrate has also been shown to be a potent inhibitor of the calcium phosphate crystals. [48]

Metastable supersaturation (MSL) is the condition in which the concentrations of solutes may significantly exceed their solubility. The mechanism by which inhibitor stone formers maintain supersaturation without precipitation of these salts is thought to be a result of crystal inhibitors. [49]

These inhibitors could be small organic molecules like citrate or larger macromolecules or ions which bind to the crystal surface thereby affecting crystal growth. [49] [8] [50]

Citrate forms a complex with calcium in urine, thereby directly reducing the saturation of calcium stone-forming salts. It is also an inhibitor of crystallization. [51] Coe *et al*. [52] reported that compounds of more substantial molecular weight, such as acidic glycoproteins, were the principal inhibitors of calcium oxalate stone formation. However, studies by Pak *et al.* [53] have suggested that citrate is also an inhibitor that increases the "permissible increment" of oxalate, such that

greater amounts of oxalate may be present in whole urine before spontaneous precipitation occurs. [54]

Citrate may be an altering factor for both calcium phosphate and calcium oxalate monohydrate crystallisation. [4]

Alkaline citrates have gained widespread importance in the remedy of kidney stones as these elevate urine pH as well as inhibit CaOx and calcium phosphate crystallization. [55] pH is very important as citrate excretion decreases with decreasing pH. Also the pKa of citrate means that, as the urine becomes more acidic, $[citrate]^{3-}$ is converted to $[citrate\ H]^{2-}$, which will affect the supersaturation of $[citrate]^{3-}$ salts. An increase in pH would have the opposite effect. [56, 57][58][59]

1.6. Hydroxycitric acid

Hydroxycitric acid (HCA) is one of the principal acids found in the fruit rind of several trees of the Garcinia family. [60, 61] One of these is Malabar tamarind, which is found in Southeast Asia. [62] The pulp and rind of the fruit are used for therapeutic purposes, as they contain the most amounts of HCA. The dried fruits contain nearly 25% HCA. HCA is isolated as the acid or as one of its salts. It can also be isolated in its lactone form. Natural tamarind extracts are presently marketed as the calcium or potassium salts of HCA. [67]

HCA has been added to a number of pharmaceuticals used to treat lipid abnormalities and heart disease. [63-66] It has been advocated to increase stamina and has been used for weight loss. HCA consist from two asymmetric centers, and two pairs of diastereoisomers making four dissimilar isomers (Figures 1.3). [67, 68]

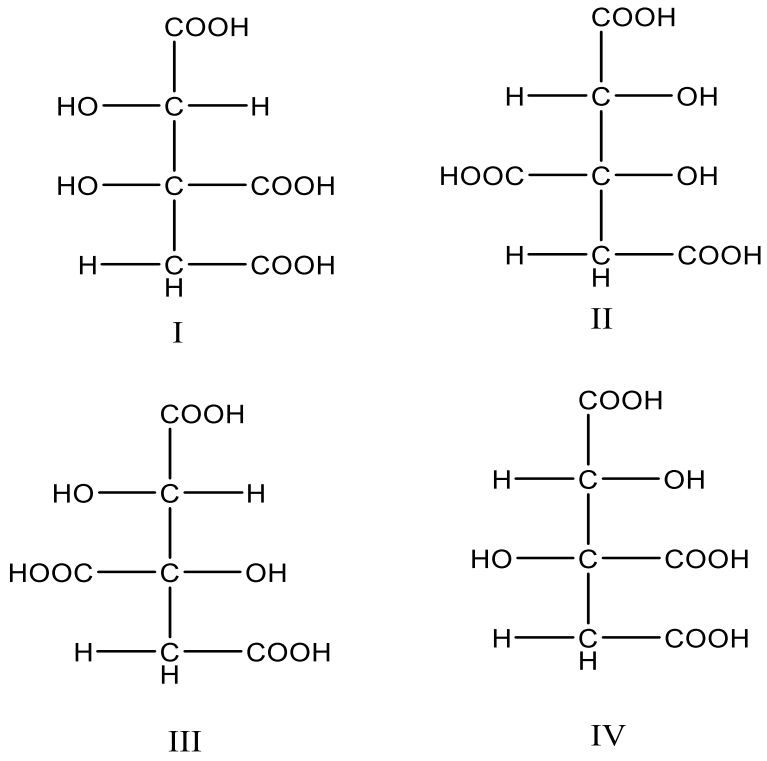

Figure 1.3. Isomer structures for hydroxycitric acid.

Since the discovery of HCA, its effects and bioactivities have been studied extensively. HCA is an important medicinal component with several health benefits in traditional Ayurveda medicine, and ailments such as rheumatism and bowel illnesses have been treated with a fruit rind decoction .[62,69-71] The rind is also used to treat certain mouth sicknesses in cattle. [62]

HCA is also useful as a strong inhibitor of ATP citrate lyase. The reaction of citrate is:

Citrate + ATP + CoA → acetyl - CoA + ADP + Pi + oxaloacetate

(ATP, adenosine triphosphate; CoA, co-enzyme A; ADP, adenosine diphosphate)

This restricts the formation of acetyl-CoA units. [72] Animal studies have also shown that HCA blocks fatty acid synthesis, lipogenesis, food intake,[67] and leads to weight loss.[62, 73] Soni *et al.* reported that in more than 10 years, almost 5 billion dosages of single HCA supplement had been sold without any bad side- effects being noted. [74]

Hydroxycitric acid is not a normal component find in human urine. However, studies have shown that orally ingested hydroxycitrate is excreted in the urine, making it potentially a very good candidate as a stone therapeutic. [75]

Various studies of HCA in humans have reported HCA to be well tolerated, with no important dangerous side- effects. [74] Given its molecular similarity to citrate and since it is well-tolerated, HCA is theoretically, a viable alternative to citrate as a kidney stone inhibitor. [75]

HCA is a potent inhibitor of CaOx monohydrate (COM) crystal formation. [52] Cody *et al*. [76] reported that at least two carboxylic acid groups are required for inhibitors to reduce the rate of COM crystallisation effectively. Thus, hypothetically HCA may be used instead of potassium citrate for the prevention of urinary stones. [77]

1.7. Role of HCA in kidney stones

HCA is more effective than citrate in counteracting the increased risk of calcium phosphate crystallisation associated with increased pH. [78] Increasing concentrations of HCA lead to a maximum of 60% inhibition of calcium oxalate monohydrate (COM) crystallization. [81] This net effect reflects the decrease of crystal growth rate as well as the potential inhibition of COM

nucleation. [77] Previous studies of HCA revealed it to be a strong inhibitor of COM crystal growth [82] as well as preventing crystal aggregation. [34] In 2019 Kim *et al.* [75] showed that HCA could melt crystal surfaces in supersaturated media (supersaturation ratio S = 4). This was the first observation of crystal dissolution in concentrated CaOx solutions. The formula of HCA highlights how a small change in molecular structure may markedly alter the influence of a compound on crystal growth. [77] [79] [80]

1.8. Aim

The aim of the present research was to establish whether hydroxy citrate affects and/or inhibits calcium oxalate crystallisation, and, if so, the extent to which it achieves this relative to citrate.

1.9. Objectives

1. To measure the equilibrium constants of HCA with H^+, Ca^{2+}, Mg^+ and Zn^+ using glass electrode potentiometry, so that thermodynamic calculations of speciation and supersaturation can be performed using these constants.
2. To determine the structure of metal-ligand complexes using ^{1}H-nuclear magnetic resonance (NMR) spectroscopy.
3. To model the influence of HCA on the speciation of urinary salts in artificial urine (AU) using the software program JESS. [83]
4. To calculate the theoretical supersaturation of stone-forming salts in AU as a function of HCA concentrations.

5. To experimentally determine the metasable limit (MSL) of CaOx in artificial urine (AU) with/without HCA, in order to empirically test the predictions of the theoretical modelling in this system.

6. To experimentally determine the effects of HCA on the kinetics of CaOx crystallisation using UV spectrophotometry.

References

1. Kamel KS, Shafiee MA, Cheema-Dhadli S, and Halperin ML, Studies to identify the basis for an alkaline urine pH in patients with calcium hydrogen phosphate renalstone . *Neph. Dial. Trans*, 2007, **22**(2), 424-31.

2. Johnson CM, Wilson DM, O'Fallon WM, Malek RS, and Kurland LT, Renal stone epidemiology: A 25-year study in Rochester Minnesota. *Kidney. Int*, 1979, **16**(5), 624-631.

3. Zarin F, Kazemi T, and Vakili P, A review of kidney stone and its risk factors along with diagnostic methods. *Res. J. Pharmaceutical*, 2015, **6**(2), 920-925.

4. Gupta M, Bhayana S, and Sikka SK, Role of urinary inhibitor and promotor in calcium oxalate crystallization. *Int .J. Res. Pharmacy. Chem*, 2011, **1**(4), 793-798.

5. Trinchieri A, M.D., Epidemiology of urolithiasis: an update. C*lin. Cases. Miner. Bone. Metab*, 2008, **5**(2), 101-106.

6. Aggarwal KP, Narula S, Kakkar M, and Tandon C, Nephrolithiasis: molecular mechanism of renal stone formation and the critical role played by modulators. *Bio. Med. Res. Int*, 2013, **63** (2003), 1817–1823.

7. Jones CA, Stamatelou KK, Francis ME, Nyberg LM, and Curhan GC, Time trends in reported prevalence of kidney stones in the United States. *Kidney. Int*, 2003, **63**(5), 1817-23.

8. Moe OW, Kidney stones pathophysiology and medicine management, *The Lancet*, 2006, **367**(9507), 333-344.

9. Shang W, Li L, Ren Y, Ku M, Ge S, Ge Q, and Xu G, History of kidney stones and risk chronic kidney disease: a meta-analysis. *Peer. J*, 2017, **5**, e 2907.

10. Han H, Segal AM, Seifter JL, and Dwyer JT, Nutritional management of kidney stones (Nephrolithiasis). *Clin. Nutr.Res,* 2015, **4**(3), 137-52.

11. Scholz D, Schwille PO, Ulbrich D, Bausch WM, and Sigel A, Composition of kidney stones and their frequency in stone clinic: Relationship to parameters: of mineral metabolism in serum and urine. *Urol. Res,* 1979, **7**, 161-170.

12. Pak CY, Poindexter JR, Adams-Huet B, and Pearle MS, Predictive value of kidney stone composition in the detection of metabolic abnormalities. *Am .J. Med*, 2003, **115**(1),26-32.

13. Elaine M.Worcester, MD, and Fredric L Coe, Calcium kidney stones. *J. Med*, 2010,**363**, 954-963.

14. Coe FL, Evan A, and Worcester E, Kidney stone disease. *J .Clin. Invest,* 2005, **115**(10), 2598-608.

15. Bushinsky DA, Parker WR, and Asplin JR, Calcium phosphate supersaturation regulate stone formation in genetic hypercalciuric stone-forming rats. *Kidney. In*, 2000, **57**(2), 550-60.

16. Deirdre MC, Michae J V, Robert CS, Relationship of spontaneous passe of ureteral calculi to stone size and location revealed unenhanced helical CT.2000,**178**,101-103.

17. Wesson JA, Worcester EM, Wiessner JH, Mandel NS, and Kleinman JG, Control of calcium oxalate crystal structure and cell adherence by urinary macromolecules. *Kidney. Int*, 1998, **53**(4), 952-957.

18. Am. J, The United States renal data system. *Kidney. Dis,* 2003, **42**, 1–230.

19. Lewandowski S, Rodgers A, Schloss I, The influence of a high-oxalate/low-calcium diet calcium oxalate kidney stone risk factors in non-stone-forming black and white South African subjects.*BJU. Int,* 2001, **87**, 307±311.

20. Stankus N, Hammes M, Gillen D, and Worcester E, African American patients have a high pre-dialysis prevalence kidney stones compared to NHANES III. *Urol. Res,* 2007, **35**(2), 83-7.

21. Lopez M, Hoppe B, History epidemiology and regional diversities of urolithiasis. *Pediatr. Nephrol*, 2010, **25**(1), 49-59.

22. Bultitude M, Rees J, Management of renal colic. *BMJ*, 2012, **345**, e5 499.

23. Chauhan CK, Growth and characterization of struvite and related crystals. *Thesis, PhD* 2011, University Saurashtra.

24. Grases F, Costa-Bauzá A, García-Ferragut L, Biopathological crystallisation: a general view about the mechanisms of renal stone formation. *Advances in Colloid and Interface Science, 1998*, **74** (1–3), 169-194.

25. Stephen W Leslie, MD, FACS, Chief, How are absorptive hypercalciuria types I and II differentiated hypercalciuria. *Med. Scape,* 2019.

26. Bhasin B, Ürekli HM., Atta MG, Primary and secondary hyperoxaluria: Understanding the enigma. *W .J. N*, 2015, **4**(2), 235-244.

27. Gates BC, MD, FASN, Chief, Hypocitraturia overview of potassium citrate and calcium citrate. *Am. So.Nephrol,* 2019.

28. Michael RC, Magee CN, Brenner BM, Pocket Companion to Brenner and Rector's. *The kidney.*Elsevier, Saunders, 2011, (pp 360-376).

29. Daudon M, Jungers P, Stone composition and morphology: A window on etiology. *Urolithiasis,* 2012, 113-140.

30. Daudon M, Traxer O, Jungers P, *et al*. Stone morphology suggestive of randall's plaque In: Evan AP, Lingeman JE, Williams JC Jr, editors. Renal stone disease. *Am. Institute .Phy. Conf. Proceed. Mel,* 2007, **900**, 26–34.

31. Miller MA, Kendall MR, Jain MK, Larson PR, Madden AS, Cuneyt TA, Testing of brushite (CaHPO4·2H2O)in synthetic biomineralization solutions and situ crystallization of brushite micro-granules. *J .Am. Ceramic. Soc*, 2012, **95**(7), 2178-2188.

32. Grases F, Sohnel O, Vilacampa AI, March JG, Phosphates precipitating from artificial urine and fine structure of renal phosphate calculi. *Clin. Chem. Acta, Elsevier*, 1996, **244**, 45-67.

33. Meyer JL, Bergert JH, and Smith LH, Epitaxial relationships in urolithiasis: the brushite-whewellite system. *Clin. Sci. Mol. Med,* 1977, **52**, 143-148.

34. Ratkalkar VN, Kleinman JG, Mechanisms of stone formation. *Clin. Rev.Bone.Miner Metab,* 2011, **9**(3-4), 187-197.

35. Grases F, Villacampa AI, Bauzá AC, and Söhnel O, Uric acid calculi. *Scan. Microsc,* 1999, **13** (2-3)**.** 223-234.

36. Evan AP, Physiopathology and etiology stone formation in the kidney and the urinary tract. *Pediatr. Nephrol,* 2010, **25**(5), 831-41.

37. Heilberg IP, and Schor N, Renal stone disease: Causes evaluation and medical treatment. *Arq.Bras. Endocrinol. Metab,* 2006, **50**,823-831.

38. Borghi L, Meschi T, Maggiore U, Prati B , Dietary therapy in idiopathic nephrolithiasis. *Nutr. Rev,* 2006, **64**,301–312.

39. Borghi L, Schianchi T, Meschi T, Guerra A, Allegri F, Maggiore U, Novarini comparison of two diets for the prevention of recurrent core in idiopathic hypercalciuria.. *N.Engl. J. Med,* 2002, **346**, 77–84.

40. Curhan GC, Curhan SG, Dietary factors and kidney stone formation. *Compr. Ther.* 1994, **20**,485–489.

41. Curhan GC, Taylor EN, Oxalate intake and the risk for nephrolithiasis. *J .Am. Soc. Nephrol,* 2007, **18**, 2198–2204.

42. Willett WC, Curhan GC, Rimm EB, Stampfer MJ. A prospective study dietary calcium and other nutrients and the risk of symptomatic kidney stones. *N.Engl. J .Med,* 1993, **328**,833–838.

43. Choi HK, Atkinson K, Karlson EW, Willett W, Curhan G, Purine-rich foods dairy and protein intake and the risk of gout in men. *N. Engl .J. Med,* 2004, **350** (11), 1093-1103.

44 Heilberg IP and Goldfarb DS, Advances in chronic kidney disease. *Elsevier,* 2013, **20** (2), 165-174.

45. Hajialyani M, Nirumand MC, Rahimi R, Farzaei MH, Zingue S, Nabavi SM, and Bishayee A, Dietary plants for the prevention and management kidney stones: Preclinical and clinical evidence and molecular mechanisms. *Int .J.Mole.Sci,* 2018, **19,** (765).

46. Goldberg H, Grass L, Vogl R, Rapoport A, Oreopoulos DG., MD, Urine citrate and renal stone disease. *CMAJ,* 1989, **141**, 217-221.

47. Biasz S, Felix R, Newman WF *et al.* Quantitative determination of inhibitors of calcium phosphate precipitation in whole urine. *Miner. Electrolyte.Metab,* 1978, **1**, 74-83.

48. Rodgers A, Jackson GE, Allie-Hamdulay S, Therapeutic action of citrate in urolithiasis explained by chemical speciation: increase in pH is the determinant factor. *Nephrol. Dial Trans,* 2006, **21**, 361–369.

49. Moe OW, Renal stones: pathophysiology and medical management. *The Lancet,* 2006, **367**(9507), 333-44.

50. Kok DJ, Papafoulos SE, Blomen LJMJ, and Bijvoet OLM, Modulation of calcium oxalate monohydrate crystallisation kinetics in vitro. *Kidney. Int,* 1988, **34**(3), 346-350.

51. Knauf F, Pfau A, Update on nephrolithiasis: Core curriculum 2016.*Am. J. Kidney. Dis,*

2016, **68**(6), 973-985.

52. Coe FL, Disorders of stone formation. *In Brenner BM. Rector*, 1986, 1403-1442.

53. Pak CY, Fuller C, BS, MD, Idiopathic hypocitraturia calcium-oxalate nephrolithiasis successfully treated with potassium citrate. *Ann. Int. Med*, 1986, **104**, 33-37.

54. Goldberg H, Grass L, Vogl R, Rapoport A, Oreopoulos DG, Urine citrate and renal stone disease. *CMAJ*, 1989, **141**, 217-221.

55. Fan J, Schwille PO, Schmiedl A, Gottlieb1 D, Manoharan M, Herrmann U, Calcium oxalate crystallisation in undiluted urine of healthy meals: *in vitro* and *in vivo* effects of various citrate compound. *Scan. Microsc*, 1999, **13** (2-3), 307-319.

56. Dedmon RE, Wrong O, The excretion of the organic anion in renal tubular acidosis with particular reference to citrate. *Clin. Sci*, 1962, **22**, 19–32.

57. Crawford MA, Minle MD, Scribner BH. The effects of changes in base -acid balance on urinary citrate in the rat. *J. Phy*, 1959, **149**, 413–423.

58. Jack M Zuckerman, BS and Dean G Assimos, MD, Hypocitraturia: Pathophysiology and medical management. *Rev Urol*, 2009, **11** (3), 134–144.

59. Hamm LL, Brennan S, Hering-Smith K, Effect of pH on citrate reabsorption in the proximal convoluted tubule. *Am.J. Phy*, 1988, **255**, F301–F306.

60. Sunny S, A review on the molecule: hydroxycitric acid. *Review Article. J. Pharmacy. Pharmaceutical*, 2018, **7**(2), 393-418.

61. Abidin HZ, The evaluation, production and derivatisation of the Garcinia acid in Garcinia Atroviridis. *MSc Thesis*, 2005, University Putra, Malaysia.

62. Jena BS, Jayaprakasha GK, Singh RP, Sakariah KK, Chemistry and biochemistry of (−)-hydroxycitric acid from Garcinia. *J. Agric. Food.Chem*, 2002, **50**, 10−22.

63. Lowenstein, J. M.U.S, Method of treating obesity. *Patent 3764692.* 1973.

64. Majeed MB, Badmaev V, Rajendran R, Potassium hydroxycitrate for the suppression of appetite and induction of weight loss. *U.S. Patent* 5783603, 1998.

65. Hastings CW, Barnes DJ, Weight loss composition for burning and reducing the synthesis of fats. *U.S. Patent* 5626849.1997.

66. Braswell A, Glenn A, Aftab J, Marina Del Ray, Method for controlling weight with hypericum perforatum and Garcinia cambogia. *U.S. Patent* 5911992, 1999.

67. Jena BS, Jayaprakasha GK, Singh RP, Sakariah KK, Chemistry and biochemistry of (−) - hydroxycitric Acid from Garcinia. *J. Agric.Food. Chem*, 2002, **50**, 10−12.

68. Ramachandran HD, Plant profile phytochemistry and pharmacology of Garcinia indica. A review. *Int. J. Pharm. Sci. Rev. Res*, 2014, **27** (2), 376-381.

69. Goudarzvand M, Afraei S, Yaslianifard S, Ghiasy S, Sadri Gh, Kalvandi M, Alinia T, Mohebbi A, Yazdani R, Azarian S K, Mirsha A, Azizi G, Hydroxycitric acid ameliorates inflammation and oxidative stress in mouse models of multiple sclerosis. *Res*, 2016, **11**(10), 610-1616.

70. Rasha HM, Salha A, Thanai A, and Zahar A, The biological importance of Garcinia cambogia. A review. *J. Nutri. Food Sci,* 2015.

71. Krishnamoorthy V, Nagappan P, Sereen AK, and Rajendran R, Preliminary phytochemical screening of the fruit rind of Garcinia cambogia and leaves of Bauhinia variegata a comparative study. *Int .J. Curr. Microbiol. Appl. Sci*, 2014, **3** (5), 479-486.

72. Watson JA, Lowenstein JM, Citrate and the conversion of carbohydrate into Fat. *J. Bio Chem*, 1970, **245**, 5993-6002.

73. Mozersky DO, Klonz K, Katz LM, The problem: Liver toxicity following consumption of the dietary supplement hydroxycut health hazard review board. *Food. Drug Administration*, 2009.

74. Soni MG, Burdock GA, Preuss HG, Ohia SE, Stohs SJ, Bagchi D, Safety assessment of (−)-hydroxycitric acid and super citrimax novel calcium/potassium salt. *Food. Chem. Toxicol* , 2004, **42**(9), 1513-1529.

75. Kim D, Rimer JD, and Asplin JR., Hydroxycitrate: a potential new therapy for calcium urolithiasis. *Urolithiasis*, 2019, **47**(4), 311-320.

76. Cody AM, Cody RD, Calcium oxalate trihydrate phase control by structurally-specific carboxylic acids. *J. Cryst. Growth*, 1994, **135**(1–2), 235-245.

77. Chung J, Granja I, Taylor MG, Mpourmpakis G, Asplin JR, and Rimer JD, Molecular modifiers reveal a mechanism of pathological crystal growth inhibition. *Nature*, 2016, **536**(7617), 446-450.

78. Denneberg T, Fjellstedt E, Jeppsson JO, Tiselius HG, A comparison of the effects of the potassium citrate and sodium bicarbonate in the alkalinisation of urine in homozygous cystinuria. *Urol.Res*, 2001, **29**(5), 295-302.

79. Li M, Zhang J, Wang L, Wang B, Putnis CV, Mechanisms of modulation of calcium phosphate pathological mineralisation by mobile and immobile small-molecule inhibitors. *J. Phys. Chem*, 2018, **122**(5), 1580-1587.

80. Taylor MG, Chung J, Mpourmpakis G, Asplin JR, Granja I, Rimer JD, Molecular modifiers reveal a mechanism of pathological crystal growth inhibition. *Nature*, 2016, **536**, 447-49.

81. Olafson KN, L.R., Alamani BG, Rimer JD, Engineering crystal modifiers: Bridging classical and nonclassical crystallization. *Chem Mater*, 2016, **28**(23), 8453–8465.

82. Chung J, Inhibition of calcium oxalate monohydrate crystallisation using organic growth modifiers. *Thesis, MSc*, 2013, University of Houston, 44-45.

83. Muray K, May PM, JESS, a joint expert speciation system-1. *Talanta*, 1991, **38**, 1409-1417.

Chapter Two

2. Potentiometry

2. 1. Introduction

Several studies have shown that HCA inhibits the crystallisation of Ca salts *in vitro* at low concentrations. [1, 2] The thermodynamic role for HCA as a Ca chelator which decreases the supersaturation of Ca-containing salts in the urine, has not been previously modelled-perhaps because of uncertainty regarding the nature of $[Ca(HCA)]^-$ complexes and a lack of reliable thermodynamic data under physiological conditions of urinary pH and ionic strength.

Determining formation constants [8] via potentiometry under these conditions would allow the modeling of HCA's effects on Ca salt supersaturation in urine and may provide insights into the clinical relevance of this mechanism.

Potentiometry is one of the methods used to investigate chemical interactions between acids and bases [3, 4] [9] in aqueous solutions. [5, 6] The glass electrode is one of the most reliable sensors currently available. [7]

In the study described in this chapter, potentiometry was used to investigate interactions between the ligand HCA ($C_6H_8O_8$) with H^+ and divalent metal ions, Ca^{2+}, Mg^{2+}, and Zn^{2+}.

2.1.1. Theory

The theory of stability constants was described in previous studies [10-13], and a generalized formation constant equation (2.1) is shown here

$$L + H \leftrightarrow LH \qquad (2.1)$$

where L is the ligand, H is a proton, and LH is the protonated ligand.

The thermodynamic pronation constant of the ligand may be expressed as:

$$^{T}K_1 = \frac{\{LH\}}{\{L\}\{H\}} \qquad (2.2)$$

{LH} is the activity of the single protonated ligand, {L} is the activity of the free ligand and {H} is the activity of the proton.

When the ionic strength is constant, the equilibrium constant may be expressed as

$$^{T}K_L = \frac{[\mathbf{LH}]}{[\boldsymbol{L}][\mathbf{H}]} \qquad (2.3)$$

where $^{T}K_L$ is the concentration equilibrium constant.

There are three stepwise protonation constants for the ligand of study, hydroxycitrat

$$L + H \leftrightarrow LH \qquad ^{T}K_{L1} = \frac{[\mathbf{LH}]}{[\mathbf{L}][\mathbf{H}]} \qquad (2.4)$$

$$LH + H \leftrightarrow LH_2 \qquad ^{T}K_{L2} = \frac{[\boldsymbol{LH_2}]}{[\mathbf{LH}][\mathbf{H}]} \qquad (2.5)$$

$LH_2 + H \leftrightarrow LH_3$ $\quad {}^{T}K_{L3} = \frac{[\boldsymbol{LH_3}]}{[\boldsymbol{LH_2}][\mathbf{H}]}$ (2.6)

Further, the following applies for a ligand with n protonation constants:

$LH_{n-1} + H \leftrightarrow LH_n$ $\quad {}^{T}K_{Ln} = \frac{\{LH_n\}}{\{LH_{n-1}\}\{H\}}$ (2.7)

Furthermore, the stepwise formation/stability constants (overall formation constant) β can be expressed as:

$L + H \leftrightarrow LH$ $\quad \beta_{L1} = K_{L1} = \frac{[LH]}{[L][H]}$ (2.8)

$LH + H \leftrightarrow LH_2$ $\quad \beta_{L2} = K_{L2} = K_{L1}K_{L2} = \frac{[LH_2]}{[L][H^2]}$ (2.9)

In a reaction between a ligand L with a metal M to give a complex ML, the stepwise stability constants can be expressed as:

$M + L \leftrightarrow ML$ $\quad K_{ML} = \frac{[ML]}{[M][L]}$ (2. 10)

$ML + L \leftrightarrow ML_2 \qquad K_{ML2} = \frac{[ML_2]}{[ML][L]}$ (2.11)

$ML_{n-1} + L \leftrightarrow ML_n \qquad K_{ML_n} = \frac{[ML_n]}{[ML_{n-1}][L]}$ (2. 12)

Consequently:

In the reaction between the proton and the metal ion for the ligand given by equation 2.13.

$ML_{n-1} + LH \leftrightarrow ML_n + H \qquad K_{LMn} = \frac{\{ML_n\}\{H\}}{\{MLn-1\}\{LH\}}$ (2.13)

The reaction of metal M with a ligand can be expressed as:

$M + L \leftrightarrow ML \qquad K_{ML1} = \frac{[ML]}{[M][L]}$ (2.14)

$ML + L \leftrightarrow ML_2 \qquad K_{ML1}K_{ML2} = \frac{[ML2]}{[ML][L]}$ (2.15)

$ML_2 + L \leftrightarrow ML_3 \qquad K_{ML1}K_{ML2}K_{ML3} = \frac{[ML3]}{[ML2[L]}$ (2.16)

The formation constant (β) of the protonated complex can be expressed as:

$pM + qL + rH \leftrightarrow \quad M_p L_q H_r$ (2.17)

where p indicates the coefficient of the metal, q is the stoichiometric coefficient of the ligand, and r is the stoichiometric coefficient of the proton.

The formation constant β can be expressed as:

$$\beta_{q\,p\,r} = \frac{M_p\, L_q\, H_r}{[M]^p[L]^q[H]^r} \qquad (2.18)$$

The concentrations from each titration point can be determined and at point *K*, the concentration is expressed as:

$$[M_p\, L_q\, H_r] = \beta_{pqr}\,[M]K^p\,[L]K^q\,[H]K^r \qquad (2.19)$$

Furthermore, the total concentration of the metal ion T_M at point $K = T_{KM}$ is expressed as:

$$T_{KM} = [M]_K + \sum_{i=1}^{N} p\,\beta_{pqr}[M]_K^p[L]_K^q\,[H]_K^r \qquad (2.20)$$

The total concentration of the ligand T_L at point $K = T_{KL}$ can be expressed as:

$$T_{KL} = [L]_K + \sum_{i=1}^{N} q\, \beta_{pqr} [M]_K^p [L]_K^q\, [H]_K^r \qquad (2.21)$$

The total concentration of the proton T_H at point $K = T_{KH}$ can be expressed as:

$$T_{KH} = [H]_K + \sum_{i=1}^{N} r\, \beta_{pqr} [M]_K^p [L]_K^q [H]_K^r \qquad (2.22)$$

If the coefficient of proton r = 1, the complex is protonated. If r < 0, the ligand has lost all protons, the complex is deprotonated, and/or a hydroxyl group (OH) has been added to the complex. [14- 17] M L is the mononuclear complex that is not protonated, and r = 0 indicates that no hydroxyl group is attached to the complex. MLH refers to a complex with one proton (protonation), and MLH_2 indicates that the complex has two protons.

The stability constant of a reaction depends on the temperature and this temperature dependence is given by the van't Hoff equation:

$$\frac{d\ln K}{dT} = \frac{\Delta H^{\circ}}{RT^2} \quad \text{or} \quad \frac{dInK}{d^1/_T} = \frac{-\Delta H^{\circ}}{R} \qquad (2.23)$$

where ΔH^o is the standard enthalpy change of the reaction (expressed in J mol^{-1}), T is the absolute temperature in *K*, and R is the universal gas constant in J K^{-1} mol^{-1}.

2.1.2. Instrumentation

The electrode cell is the centre of any potentiometric investigation. A typical cell for pH glass electrode potentiometry comprises a reference electrode (E_{re}), salt bridge (E_j), and analysis solution/glass electrode (Eg). E_{ref} has a known potential and maintains a constant potential regardless of the composition of the analyte solution [18]. The observed potential can be expressed as:

$$E_{cell} = E_{re} + E_j + E_g \qquad (2.24)$$

where E_j is the liquid junction potential dependent on the solution concentration.

Since the potential of the glass electrode, E_g, changes with the concentration of the analyte solution

E_{cell} can be written as:

$$E_{cell} = E_{ref} + E_j + E^{\emptyset}_g + \frac{RT}{F} \ln [H] \quad (2.25)$$

Considering $E^{\emptyset}_g$ is the standard electrode potential and [H] is the concentration of hydrogen ions, proton activity {H} can be expressed as:

$$\{H\} = H [H] \quad (2.26)$$

where is H the activity coefficient of the hydrogen ion and [H] is the concentration of the hydrogen ion.

Ionic strength I can be expressed as:

$$I = \frac{1}{2} \sum C_i Z_i^2 \quad (2.27)$$

where C_i is the concentration of the ionic species, and Z_i is the charge of the ion.

Where ionic strength is constant, the equation $E_{cell} = E_{ref} + E_j + E^{\emptyset}_g + \frac{RT}{F} \ln [H]$ can be rewritten as:

$$E_{cell} = E_{const} + \frac{RT}{F} \ln [H^+] \quad (2.28)$$

Moreover, the glass electrode potential depends on temperature, and the relationship between these two factors varies with the hydrogen ion activity, which can be expressed in terms of the slope factor *S*:

$$S = \frac{2.3RT}{F} \quad (2.29)$$

Substituting S into equation (2.28) yields the following:

$$E_{cell} = E_{constant} + S \log [H^+] \quad (2.30)$$

Calibration the system means determining both $E_{constant}$ and *S*.

2.2. Methods

2.2.1. Materials

All chemicals, materials and reagents were commercially available at analytical grade and were used without any more purification. Sodium hydroxide and the hydrochloric acid solutions (0.01M) were prepared from Merck ampoules (1.09959-Trisol). The ligand, HCA, ($C_6H_8O_8$) was salt from Finetech Industry Limited, web : www.finetechnology-ind.com ,and was 96% purity. The concentration of metal ions was measured via ethylenediaminetetraacetic acid (EDTA) titration. [20]

2.2.1. Solution preparation

All potentiometric titration were performed under an inert atmosphere of purified nitrogen at a constant ionic of strength of 0.15 mol·dm^{-3} NaCl at 25 °C. All solutions were prepared using boiled MilliQ water to avoid carbon dioxide contamination.

A hydrochloric acid solution (0.01 M) was prepared and standardized against sodium hydroxide solution (0.1 M) which itself was standardised versus potassium hydrogen phthalate (KHP) using the Gran plot analysis method. [19] The ligand (HCA) solution (0.01 M) was prepared by dissolving 0.322 g HCA (the ligand form was the potassium salt) into standardized hydrochloric acid (0.03 M). All ionic solutions were of 0.15 M ionic strength with (Cl^-) Na^+ as the background electrolyte. All metal solutions (0.01 M) were prepared by dissolving $CaCl_2$, $MgCl_2.6H_2O$, and $ZnCl_2$ (Merck) in boiled, distilled water and adding NaCl (0.12 M) to ensure a constant ionic strength of 0.15 mol·dm^3. These solutions were standardized against EDTA. [20] All titrations were performed in triplicate.

2.2.2. Potentiometric measurements

All potentiometric titrations were carried out at a constant temperature of 25 °C and constant ionic strength of 0.15 mol·dm^{-3} (NaCl). The slope of the glass electrode was determined using three different buffer solutions at pH 4, 7, and 9.

The value of the Nernstian slope varied from 407.76 to 410.88 mV over a pH range of 2 to 12. The intercept, $E_{Constant}$, was determined from strong acid (HCL)-strong base (NaOH) titrations. These titrations were also used to calculate pK_w, which was found to be 13.56 for ligand titrations. The metal to ligand molar ratios varied between 1:1 and 1:2 metal ion/ligand system was then titrated with standard solutions of NaOH (0.1M).

Potentiometric data were analyzed using an equilibrium simulation titration analysis (ESTA) software. [21] These data were used to forecast metal-ligand binding to produce models and determine the distribution of species in solution. The measurements were carried out using glass electrode potentiometry Figure 2.1 .

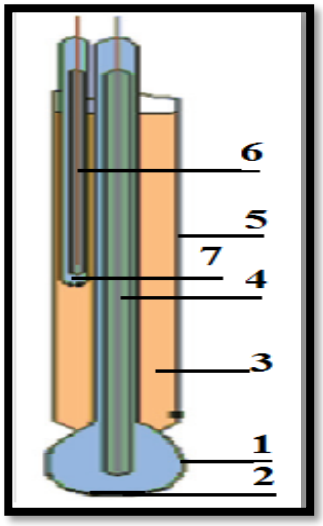

Figure 2.1. Glass electrode

1. sensing part of electrode.

2 .sometimes the electrode contains a small amount of AgCl precipitate inside the glass electrode

3 .internal solution, usually 0.1M HCl for pH electrodes

4. internal electrode, usually silver chloride electrode or calomel electrode

5. body of electrode, made from non-conductive glass or plastic.

6. reference electrode, usually the same type as 4

7. junction with studied solution.[42]

2.2.4. Data handling and calculations

The potentiometric data were analyzed using ESTA [14], a program that analyses potentiometric titration data and simulates the equilibrium distributions of chemical species. [22] ESTA has two program modules: ESTAl, a simulation module that can determine single values on a point-by-point basis for any titration parameter, and ESTA2, an optimization module that can determine the best values of the stability constants based on a least-square procedure over a whole system of titrations.[23]

In this study, three tasks from ESTA: Z-bar, Q-bar, and OBJE were employed. The Z-bar task uses the mass balance equation and distinguishes the system on a point-by-point basis. Furthermore, this task plots the Z_H-bar curve for the protonation of the ligand and the Z_M-bar function curve for the complex formation titrations .[24] The Z_H-bar function is plotted against pH and allows the estimation of p*K*a values.

Z_H-bar is expressed as:

$$Z_H\text{-bar} = \frac{T_H - [H + OH]}{T_{Lig}} \qquad (2.31)$$

where T_H is the total concentration of hydronium ions, T_{Lig} is the total concentration of the ligand H is the concentration of the hydronium ion, OH is the concentration of the hydroxide ion . It is possible to estimate p*K*a values from the half Z_H-bar values.

The function of metal-ligand Z_M-bar can be expressed as:

$$Z_M\text{-bar} = (T_L - [L](1+\sum n\beta_{LHn}H^n)/T_M \qquad (2.32)$$

where T_L means total concentration of the ligand, T_M is the total concentration of the metal, and [L] is the free ligand concentration, β_{LHn} is the formation constant of the protonated ligand with n protons

The Z_M-bar function is strictly only defined for simple stepwise complexation, where it rises monotonically to 1, 2 etc, as ML, ML_2, ML_3 are formed. Deviations from this stepwise behaviour are indicative of the formation of non-simple complexes. Thus, if MLH is one of the species in solution, the curve will split at high pL. The bending of the plots indicates the formation of hydroxo species. From the Z_M-bar graphs, the model of Zn(II)/ligand species Figure 2.10 shows that the formation of MLH_{-1} species begins to form at very low pH's, the curve fans back.

ESTA can also be used to calculate Z-bar residual:

$$Z\text{-}_{bar} \text{ residual} = Z^o\text{-}_{bar} - Z^C\text{-}_{bar} \qquad (2.33)$$

where Z^o-bar is the observed $Z\text{-}_{bar}$, and $Z^C\text{-}_{bar}$ is the calculated $Z\text{-}_{bar}$. A low $Z\text{-}_{bar}$ residual indicates a strong agreement between the observed and calculated $Z\text{-}_{bar}$ curves. If a ligand has two dissociable protons, Z_H-bar levels off at two.

The second ESTA task, Q-bar, reveals how many protons have been released upon complexation with a metal ion.

N-bar could be defined as the number of protons in the ligand before complexation. Q-bar is expressed as:

$$Q_M\text{-bar} = \frac{T_{*H} - T_H}{T_M} \qquad (2.34)$$

where T_H is the total proton concentration and $T*_H$ is the total concentration of protons in the system calculated at the observed pH in the absence of metal ion, or when no complexation took place, i.e.

when p = 0 and $OH = \frac{K_W}{T}$

The mass balance equations for $T*_H$ and T_L are written as:

$$T^*_H = H\text{-}OH + \sum_{j=1}^{Nj} r \{M_p L_q H_r\} \qquad (2.35)$$

$$T_L = L + OH + \sum_{j=1}^{Nj} q \{M_p L_q H_r\} \qquad (2.36)$$

where the N_j refers to the total number of titration points.

ESTA plots Q_M-bar and n-bar on the same graph against pH.

The formation function for a ligand, $n\text{-}_{bar}$, can be expressed as:

$$\text{n-bar} = \frac{T^{*}_{H} - H + OH}{T^{r}_{L}} \qquad (2.37)$$

The average number of dissociable protons in a complex can be expressed as:

$$F = q_{n\ bar} - Q_{\ barp} \qquad (2.38)$$

where p is the potentiometric coefficient of the metal, and q is the potentiometric coefficient of the ligand. n-bar is the average number of protons which would be bound to the ligand in the absence of metal complexation.

The agreement between the experimental and theoretical graphs indicates the validity of the chemical model.

The third task, OBJE, [25] [26] was used to optimise the titration parameters and equilibrium constants. The Gauss-Newton method is used to minimise the objective function U_{obj}, which is expressed as:

$$U_{obj} = \left(N - n_p\right)^{-1} \sum_{n=1}^{N} {n_e}^{-1} \sum_{q=1}^{ne} W_{nq} \left(Y_{nq}^{obs} - Y_{nq}^{calc}\right)^{2} \qquad (2.39)$$

where N is the total number of experimental titration points, n_p is the total number of parameters optimised, n_e is the total number of electrodes, W_{nq} is the weight of the q^{th} residual at the Y_{nq}^{obs} titration, Y_{nq}^{calc} is the calculated variable of the q^{th} the residual at the n^{th} titration point, and

is the observed variable of the q[th] residual at the n[th] titration point.

OBJE also calculates the Hamilton factor R_F^H to ensure the model is accurate. R_F^H is expressed as:

$$R_F^H = \left(\frac{U_{obj}}{\sum n_e^{-1} \sum(W_{nq})(Y_{nq}^{obs})_2}\right)^{1/2} \quad (2.40)$$

where the R-factor depends on random errors and the number of variables optimised. R^H is determined according to value-based variables, and R^H_{Lim} can be expressed as:

$$R_{Lim}^H = \left(\frac{N}{\sum n_e^{-1} \sum(W_{nq})(Y_{nq}^{obs})_2}\right)^{1/2} \quad (2.41)$$

The model is as precise as statistically possible if $R^H < R^H_{Lim}$. [27]

2.3. Results

All experiments were performed using NaCl as the background electrolyte, at a stable of temperature of 25 °C, and an ionic strength of 0.15 mol dm^{-3} under an atmosphere of purified nitrogen. The electrode slope varied from 56.30 to 57.91, pK_W was -13.56, and E^0 range between 410.88 to 407.76 mV.

2.3.1. HCA protonation

The protonation constants for HCA are listed in Table 2.1.

The Z_H-bar function is shown in Figure 2.2, with the blue signs representing the experimental data points while the red line is calculated based on the model given in Table 2. 1. A bove pH 7,

Z_H-bar is 0, and the ligand is fully deprotonated. Below pH 7, Z_H-bar rises, and ligand protonation starts. At pH 4.6, Z_H-bar ~ 1, indicating that one proton has been added to the ligand. From pH 3.7 to 2.4, Z_H-bar ~ 2.55, which indicates three protons are being added to HCA, The addition of the 3rd proton is not complete and will only happen below pH 2. No distinct steps (plateau regions) indicate that the three protonation steps overlap and are not well separated.

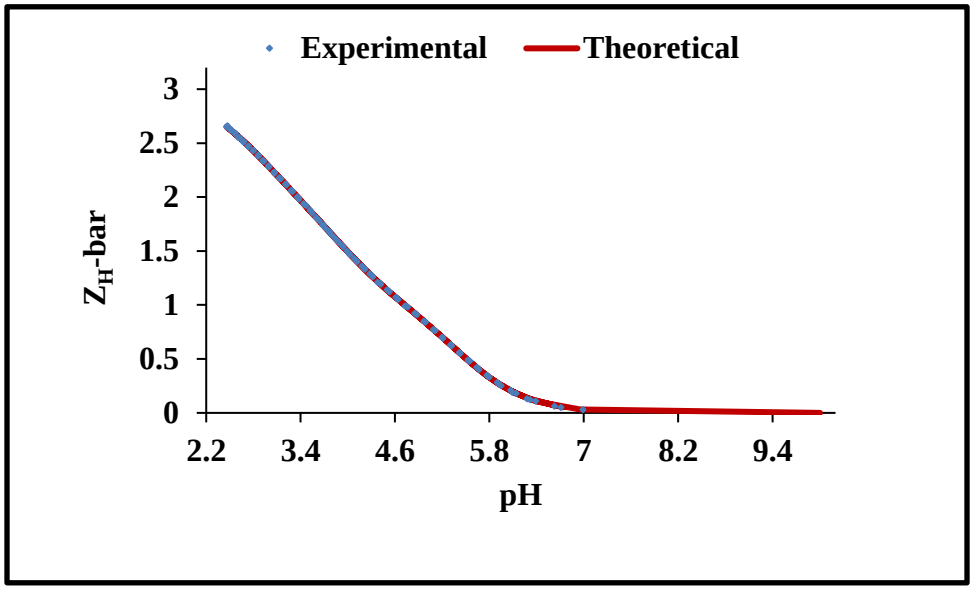

Figure 2.2. Z_H-bar for protonation of hydroxycitric acid (HCA).

Table 2.1. Stability constants ($\log\beta_{pqr}$) for hydroxycitric acid (HCA) $\beta_{pqr} = [M_pL_qH_r]/[M]^p[L]^q[_H]^r$, I = 0.15 mol dm^{-3} (NaCl), T = 25 ºC. S. dev, standard deviation in $\log \beta_{pqr}$; R_f^H, Hamilton R-factor and R_{lim}^H its Hamilton R-factor limit.

Model			**$\log\beta_{pqr}$**	**S. dev**	**R_f^H**	**R_{Lim}^H**	**n_t (n_p)**
p	**q**	**r**					
0	1	1	5.47	0.002	0.001	0.003	3 (129)
0	1	2	9.43	0.004			
0	1	3	12.20	0.009			

The analysis of the data gave the model shown in Table 2.1. The excellent agreement between the experimental data points and curves calculated based on the model given in Table 2.1, the low standard deviations, and the fact that $R^H_f < R^H_{Lim}$ indicates the validity of these results.

The HCA protonation speciation is shown in Figure 2.3 as a function of pH. Between pH 3.78 and pH 7.54, the predominant species is L. At pH 5.15, LH was most common, followed by LH_2 at pH 3.90, and LH_3 between pH 2 and 4.70.

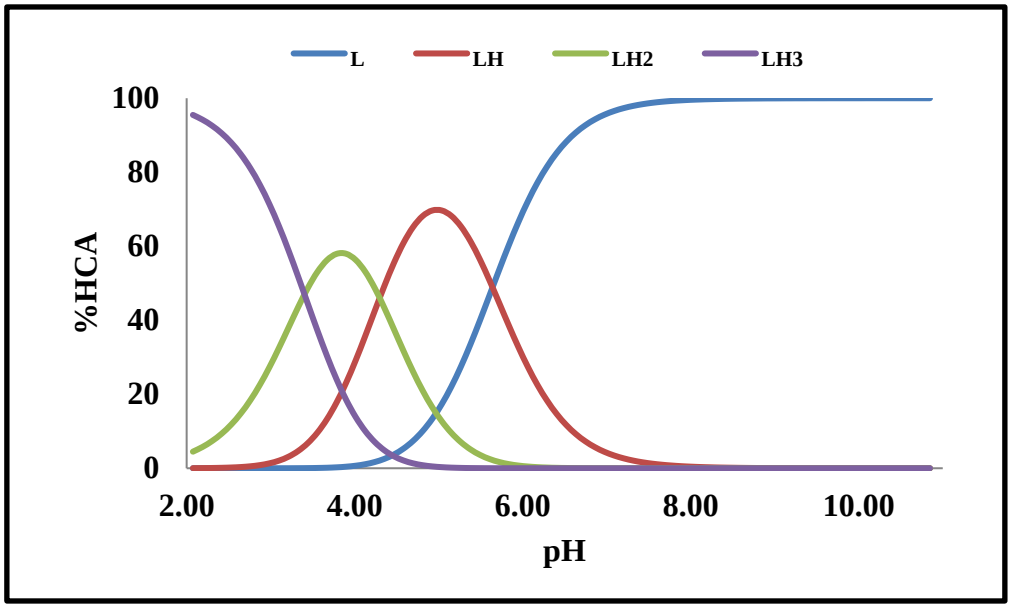

Figure 2.3. Speciation curve for hydroxycitric acid (HCA).

A previous study on citric acid protonation revealed the following pK_a values: pK_{a1} = 5.83, pK_{a2} = 4.44, and pK_{a3} = 3.11. [28] However, the measurement conditions, including pH, temperature, ionic strength, among others, varied, and the agreement between the various results, were poor. [29] The log K_{exp} values listed in Table 2.2. were compared to the log K_{lit} which were reported by Martell *et al*. [30] for HCA and showed excellent agreement .

Table 2.2. Literature and experimental protonation constants of hydroxycitric acid. [30]

Model **p q r**	**logβ_{pqr}**	**R_f^H**	**R_{Lim}^H**	**n_t (n_p)**	**logK_{exp}**	**logK_{lit}**
0 1 1	5.47	0.001	0.003	3(129)	5.47	5.64
0 1 2	9.43				4.51	4.29
0 1 3	12.200				3.32	3.41

2.3.2. Complex formation titrations

As metal ions are present with the ligand, the number of hydrogen ions set free by complex formation is different from titrations of the ligand on its own.[31] The equilibrium constants ($\log\beta_{pqr}$) for the 1:1 , 1:2 and 1:3 the metal-ligand complexes were calculated using the ESTA suite of programs and used to determine Z_M-bar, Q_M-bar [32],[33, 34] and to plot species distribution functions.

2.3.2.1. Ca (II)-HCA complexation

Ca-HCA complex formation is shown in Figure 2.4. At the titration start (pH 2.7), the Z_M-bar is approximately 0.02 (greater than 0), indicating that complexation has already started. The Z_M-bar curves are not superimposable at dissimilar metal: ligand ratios [1:1, 1:2 and 1:3 metal: ligand ratio] indicating that protonated species are forming. Table 2.3 lists the model calculated for this system. The standard deviations are small indicating the accuracy of the model.

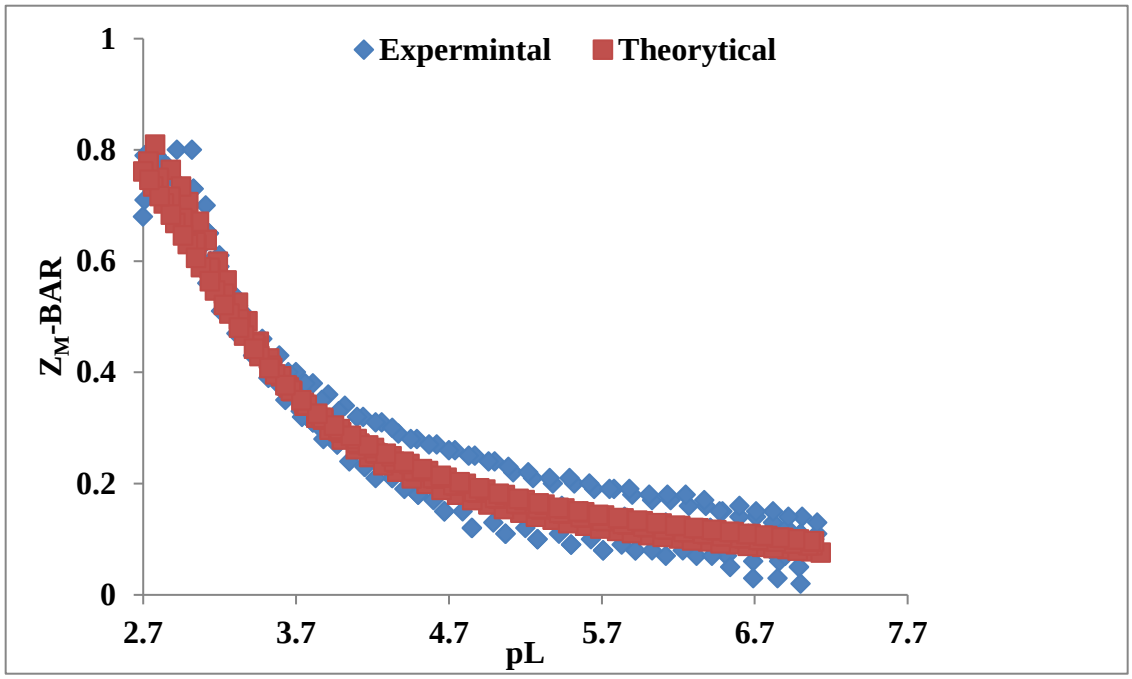

Figure 2.4. Z_M-bar as a function of pL for the Ca(II)-HCA system.

Table 2.3. Stability constants ($\log\beta_{pqr}$) for Ca^{2+} and hydroxycitric acid (HCA) complexes.

$\beta_{pqr} = [M_p L_q H_r]/[M]^p [L]^q [H]^r$,T = 25 ºC, I = 0.15 mol dm^{-3} (NaCl), St. dev, standard deviation in $\log\beta_{pqr}$, R_f^H, Hamilton R-factor and R_{lim}^H its Hamilton R-factor limit.

Model			**$\log\beta_{pqr}$**	**St. dev**	**R_f^H**	**R_{Lim}^H**	**n_t (n_p)**
p	**q**	**r**					
1	1	2	11.76	0.02	0.005	0.002	6 (249)
1	1	1	8.44	0.01			
1	1	0	3.93	0.01			

The Q_M-bar function is plotted in Figure 2.5. The n-bar function indicates the number of dissociable protons on the ligand at each pH in the absence of metal complexation. Q_M-bar is the total number of protons released by the ligand due complexation. Thus, the difference in these two curves indicates the stoichiometry of the species formed. At pH 3, the Q_M-bar curve is > 0, indicating that complexation has already commenced. The Q_M -bar increases steadily, and MLH_2, MLH species are evident between pH 3.24 and 4.5. Between pH 5.35 and 6.21, Q_M -bar corresponds with n-bar, indicating no more complexation takes place over this pH range. There is an good agreement between the experimental and theoretical curves.

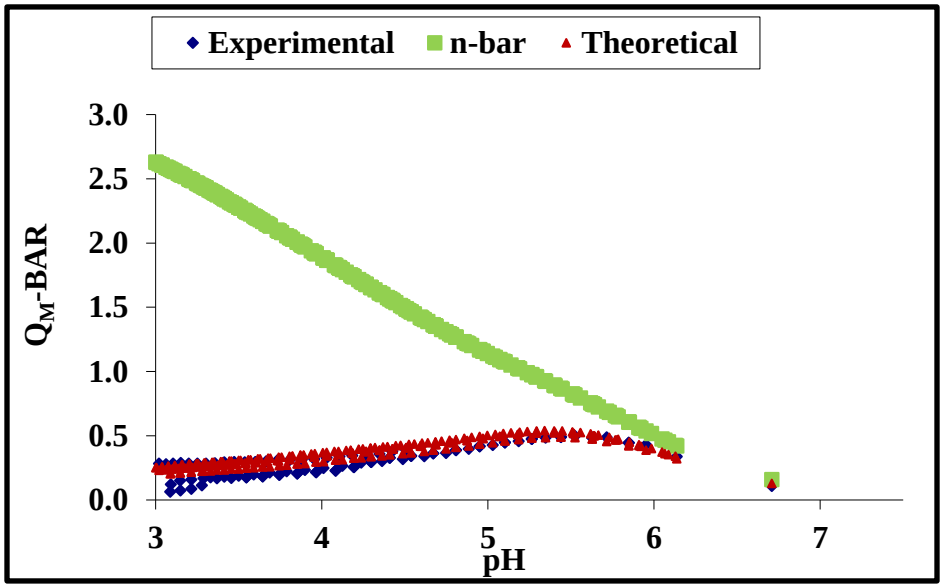

Figure 2.5. Q_M-bar for Ca(II)-HCA system.

The species distribution for the Ca(II)-HCA system is shown in Figure 2.6. ML is the predominant metal complex between pH 3.2 and 7.87 and reaches 99.37%. Between pH 2.15 and 6.22, MLH is most common, and this species reaches 61.50%, whereas MLH_2 forms 58.65% of species at pH 2.75.

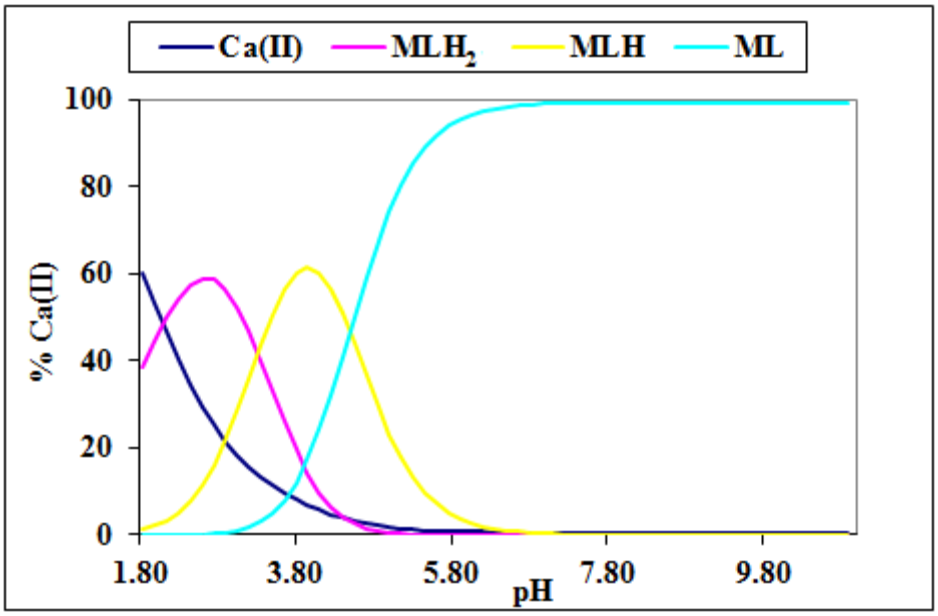

Figure 2.6. Speciation curve for Ca^{2+} with hydroxycitric acid (HCA).

The stability constants are summarized in Table 2.4. There is general agreement between the experimental results, and the literature for citric acid with calcium. [35] Also the protonation constants of HCA obtained in the present study were comparable to those reported in the literature [30], thus lending confidence to our results.

The formation constants of HCA complexes obtained in the present study were used to model Ca-HCA speciation in urine using the program JESS .[36]

Table 2.4. Literature stability constants of citric acid with calcium and experimental stability constants of hydroxycitric acid with calcium.[35]

Model **p q r**	**log β_{pqr}**	**R_f^H**	**R_{Lim}^H**	**n_t (n_p)**	**logK_{exp}**	**logK_{lit}**
1 1 0	3.93	0.005	0.002	6 (249)	3.93	3.39
1 1 1	8.44				4.51	4.25
1 1 2	11.76				3.32	3.36

2.3.2.2. Mg (II)-HCA complexation

Z_M- bar curve of the Mg(II)-HCA complexes are shown in Figure 2.7. The Z_M-bar curve levels off at approximately 0.57 indicating that the ML species is not the only species present in solution. There is a strong agreement between the experimental and theoretical curves.

The log β_{pqr} value for the Mg (II)-HCA complexes are listed in Table 2.5. The standard deviation is low indicating the validity of the model.

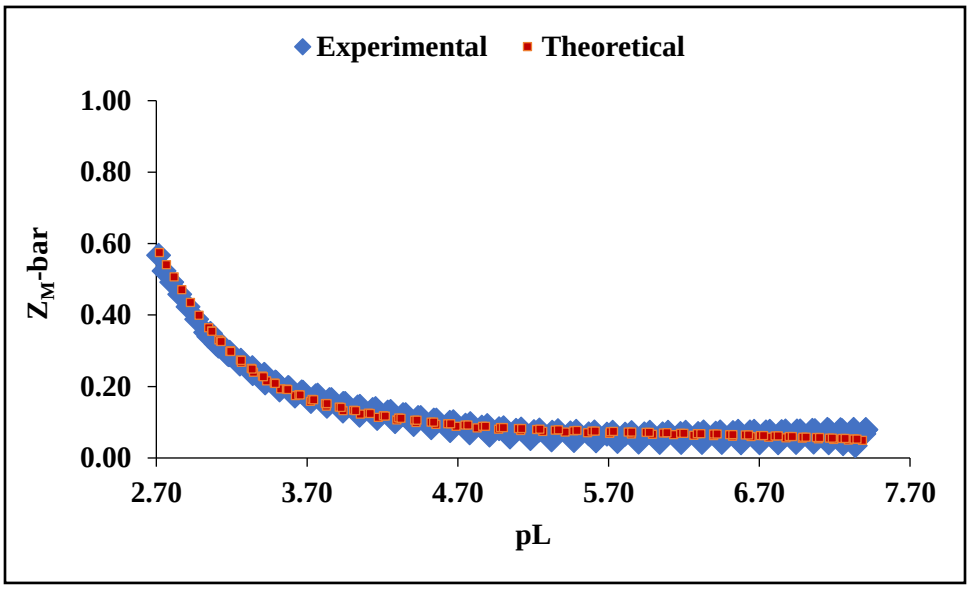

Figure.2.7. Z_M-bar for Mg^{2+} and hydroxycitric acid (HCA).

Table 2.5. Stability constants ($\log\beta_{p\,q\,r}$) for Mg^{2+} and hydroxycitric acid (HCA) complexes.

$\beta_{pqr} = [M_p\,L_q\,H_r]/[M]^p[L]^q[H]^r$, I = 0.15 mol dm^{-3} (NaCl), T = 25 ºC, St.dev, standard deviation in $\log\beta_{pqr}$; R_f^H, Hamilton R-factor; R_{lim}^H, Hamilton R-factor limit.

Model			**$\log\beta_{pqr}$**	**St. dev**	**R_f^H**	**R_{Lim}^H**	**n_t (n_p)**
p	**q**	**r**					
1	1	2	11.55	0.01	0.004	0.001	3 (133)
1	1	1	7.97	0.01			
1	1	0	3.28	0.008			

The Q_M-bar for the Mg(II)/HCA titration is shown in Figure 2.8. The n-bar curve levels off at approximately 2.5, which indicates the ligand has three dissociable protons. The Q_M-bar curve begins at values greater than 0, indicating that complexation has already started, and between pH 5 and pH 6, the n-bar and Q_M-bar are parallel and show no further complexation occurs in that pH range.

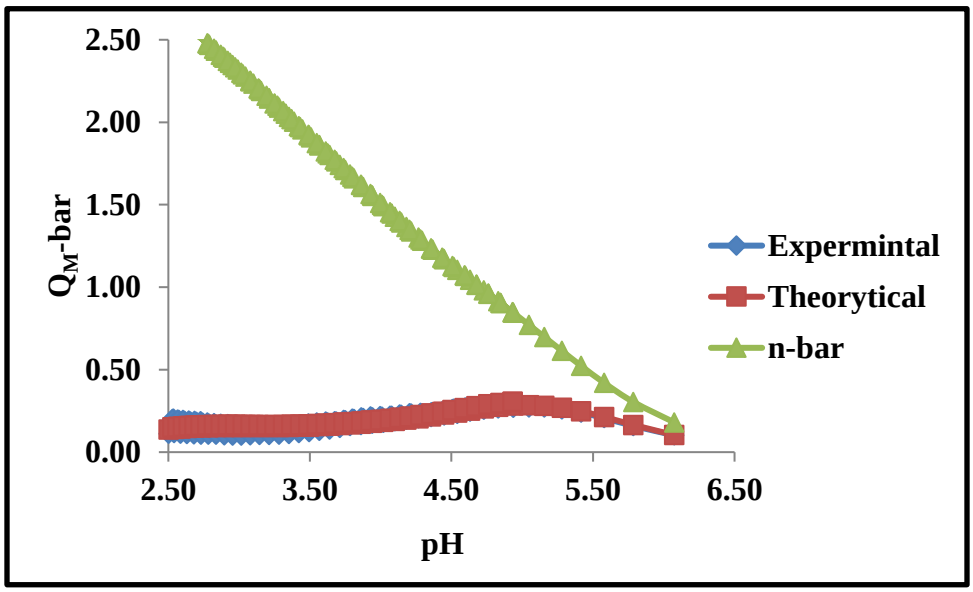

Figure 2.8. Q_M-bar for Mg^{2+} and hydroxycitric acid (HCA).

The distribution curves for the Mg(II)-HCA complexes are shown in Figure 2.9. The predominant species was ML produced from pH 3.35, with MLH and MLH_2 present at 59.5% (pH 4.26) and 69.1% (pH 2.75), respectively.

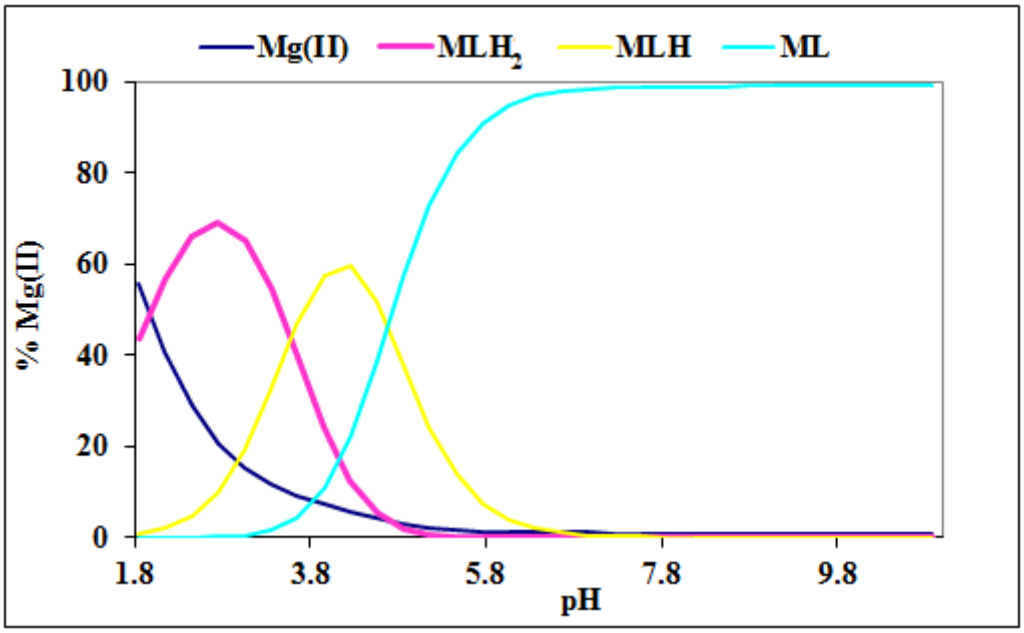

Figure 2.9. Speciation diagram for Mg^{2+} and hydroxycitric acid (HCA).

The stability constants of the Mg(II)-HCA complexes were compared with those of Mg(II)-citric acid. [37] Table 2.6 showed that the log *K* values did not differ significantly from the literature values.

Table 2.6. Literature stability constants of citric acid with magnesium and experimental stability constants of hydroxycitric acid with magnesium. [37]

Model **p q r**	**logβ_{pqr}**	**R_f^H**	**R_{Lim}^H**	**n_t (n_p)**	**log K_{exp}**	**logK_{lit}**
1 1 0	3.28	0.004	0.001	3 (133)	3.28	3.31
1 1 1	7.97				4.69	4.09
1 1 2	11.55				3.58	3.43

2.3.2.3. Zn (II)-hydroxycitric acid complexation

The stability constants ($\log\beta_{pqr}$) for the Zn(II)-HCA complexes were calculated using the ESTA suite of programs and used to calculate the model Z_M-bar, Q_M-bar, and the species distribution functions. The Z_M-bar curve for the Zn(II)-HCA complexes (Figure 2.10) levels off at ~0.8. This indicates that the formation of the ML species. Since the Z_M-bar function deviates from its normal shape when varying the metal to ligand ratio (1:2, 1:3), the formation of other species in solution is indicated. In this case protonated and hydroxy species are suggested.

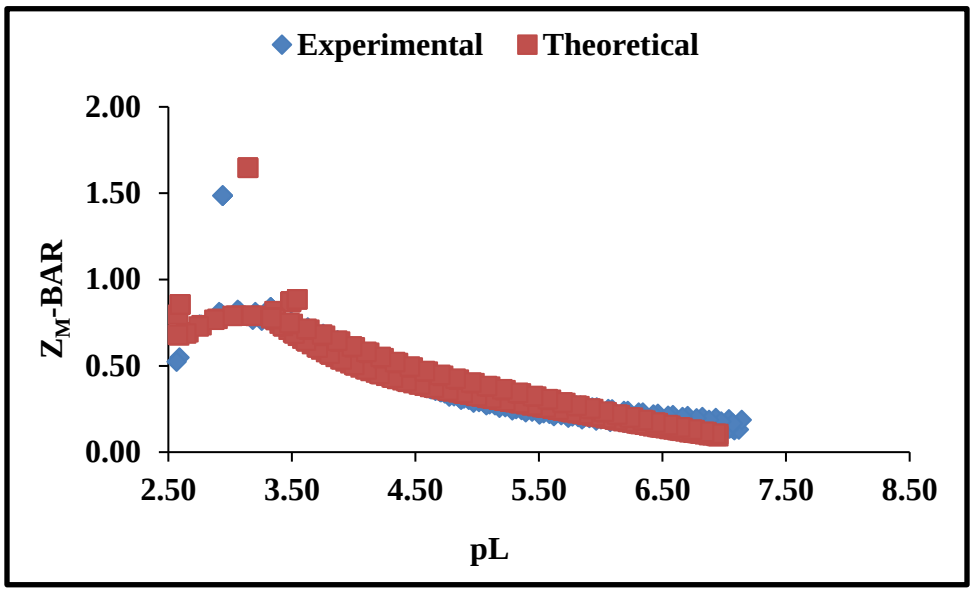

Figure 2.10. Z_M-bar for Zn^{2+} and hydroxycitric acid (HCA).

Results of the potentiometric data analysis using the ESTA suite [38] of programs are listed in Table 2.7 and show low standard deviations and Hamilton R-factors. This indicates the accuracy of the model.

Table 2.7. Stability constants ($\log \beta_{pqr}$) for the Zn^{2+} hydroxycitric acid (HCA) complexes.

$\beta_{pqr} = [M_p L_q H_r]/[M]^p [L]^q [H]^r$, I = 0.15 mol dm^{-3} (NaCl), T = 25 ºC,St. dev, standard deviation in $\log\beta_{pqr}$; R_f^H, Hamilton R-factor R_{Lim}^HHamilton R-factor limit.

Model			$\log\beta_{pqr}$	St. dev	R_f^H	R_{Lim}^H	n_t (n_p)
p	q	r					
1	2	1	12.43	0.06	0.01	0.001	4 (228)
1	1	1	8.83	0.02			
1	1	0	4.59	0.04			
1	1	-1	-3.01	0.08			

The Q_M-bar function (Figure 2.11) is > 0 at pH 2.3, indicating complex formation, and the curve increases slowly before intersecting the n-bar curve between pH 5.48 and 7.51.

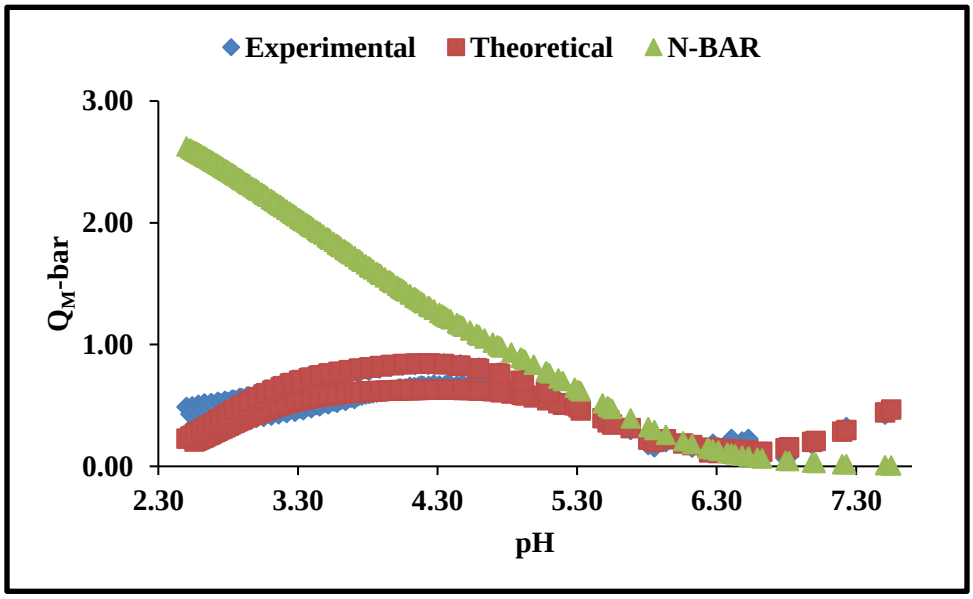

Figure 2.11. Q_M-bar for Zn^{+2} and hydroxycitric acid (HCA).

The speciation of Zn(II)-HCA is shown in Figure 2.12 and indicates the start of complexation at pH 2.15. The solution shows a mixture with 50% ZnLH at pH 3.66, 89% ZnL at pH 6.37, and 99% $ZnLH_{-1}$ at pH 10.89.

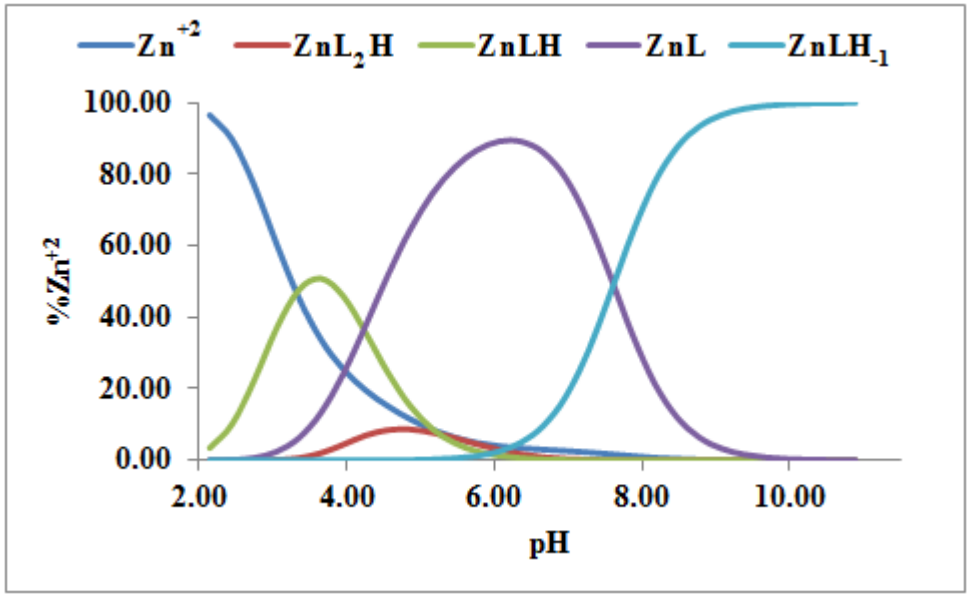

Figure 2.12. Speciation curves for the Zn^{+2} hydroxycitric acid (HCA) system.

2.4. Discussion

The focus of this chapter was the measurement of the stability constants of HCA complexes with the bivalent metal ions Ca^{2+}, Mg^{2+}, and Zn^{2+}. The present investigator used the complexation of HCA with these divalent metals as a proxy for that of citric acid, as citric acid is identical except for an OH-group on the second carbon atom. Citrate anions are well known to form complexes with alkali mineral cations,[39] which is reflected in the different apparent values for logβ for citrate with metal. In 1975, Field *et al.* studied [31] metal complexes in solutions of citric acid with Ca, Mg, and Zn. The stability constants are MLH and ML are 8.02, 3.5 respectively. The values for ML species for calcium citrate complexes concur with those reported by Campi *et al*. [29] and Pearce, but are greater than those reported by Li *et al*.[40] The values for MLH species were in agreement with Pearce's but were higher than those reported by Campi *et al*. This discrepancy with regard to MLH and MLH_2 species is related to the inability to characterise MLH_2 as a discrete species. [31] The results of the present study show three species ML, MLH, and MLH_2. The stability constants for Ca(II)-HCA (ML = 3.93, MLH = 4.51, and MLH_2 = 3.32) are higher than the stability constant of citric acid reported by Field. *et al*. [31] The percentage Ca uncomplexed in the Ca(II)-HCA complex is 60.27% in the present study, and 50.7% in the Ca(II)-citric acid complex reported by Field *et al.* [31] A summary of the results of stability constant of Ca(II)-HCA compression with calcium citrate is shown in Table 2.8 for easy reference by the reader.

Table 2.8. Summary of stability constant for calcium citrates [31] and HCA with calcium.

	Calcium	
	$\log\beta_{111}$	**$\log\beta_{101}$**
Citrate	8.2	3.50
HCA	8.44	3.93

For the Mg-citrate species, Field *et al*. [31] reported $\log\beta_{111}$ = 7.66 and $\log\beta_{101}$ = 3.38, which is in agreement with the values reported by Campi *et al* [41] and Pearce *et al*.[29] Covington *et al.* in 2009[37] reported different stability constants: $\log\beta_{110}$ = 3.31, $\log\beta_{111}$ = 7.40, and $\log\beta_{112}$ = 10.83. These values are analogous to those of the present study ($\log\beta_{110}$ = 3.28, $\log\beta_{111}$ = 7.97, and $\log\beta_{112}$ = 11.55). A summary of the results of stability constant of Mg(II)-HCA compression with magnesium citrate is shown in Table 2.9 for quick and easy reference by the reader.

Table 2.9. Summary of stability constant for magnesium citrates and HCA with magnesium.

	Magnesium	Magnesium	Reference
	$\log\beta_{111}$	**$\log\beta_{101}$**	
Citrate	7.66	3.38	[31]
	7.40	3.31	[37]
HCA	7.97	3.28	

The stability constant for the Zn(II)-citrate complexes reported by Field *et al*. [31] namely $\log\beta_{101}$ = 5.10, log β_{111} = 8.98, concur with those reported by Campi *et al.*[41] The results in the present study differ $\log\beta_{101}$ = 4.5, $\log\beta_{111}$ = 4.24, $\log\beta_{121}$= 3.6, and $\log\beta_{11\text{-}1}$ = -3.01. Furthermore, the value of ML for the present study was less than that reported by Field . *et al*.[31]

References

1. Chung J, Granja I, Taylor MG, Mpourmpakis G, Asplin JR, Rimer JD, Molecular modifiers reveal a mechanism pathological crystal growth inhibition. *Nature*, 2016, **536**,446-450.

2. Chung J, Inhibition of calcium oxalate monohydrate crystallization using organic growth modifiers. *Thesis, PhD,* 2013, University of Houston.

3. Zakharova EA, Moskaleva ML, AkeneevYuA, Moiseeva ES, Slepchenko GB, Pikula NP,Potentiometric determination of the total acidity and concentration for citric acid in wines. *J. Anal.Chem,* 2011, **66**(9), 848-853.

4. Jansen DR, The study for the complexation of Sn(II)-APDDMP and Sn(IV)-PEIMP considered as potential therapeutic agents of bone metastases. *Thesis, PhD,* 2005, University of Cape Town.

5. Meinrath G, Kufelnicki A, and Świątek M, Approach to accuracy assessment of the glass-electrode potentiometric determination of acid-base properties. *Accreditation and Quality Assurance*, 2005, **10**(9), 494-500.

6. Akhtar M, Method of analysis and assay: Potentiometry. *Pharmaceutical Analysis*, 2007, 2-19.

7. Kreuer KD, Solid potentiometric pH electrode, *Elsevier B.V,* 1990, **1**, 286-292.

8. Reijenga J, van Hoof A, van Loon A, and Teunissen B, Development of methods for the determination of *pKa* values. *Anal. Chem. Insights*, 2013, **8**, 53-71.

9. Burton JO, Matheson H, and Acree SF, Glass electrode potentiometer system for the determination of the PH value of weakly buffered solution such as natural and treated waters. *RP634*, 1934, **12**, 67-71.

10. pletnev I, Popov K, Wanner H, vendilo A Hans wanner and Andrey vendilo, Stability constant data sources reliability a goithn and a soft war the data verification. *PT Conf*, 2007.

11. Nagypal I, Beck MT, chemistry of complex equilibria. *New York*, 1990.

12. Martell AE and Motekaitis RJ, Determination and use of Stability Constants. *VCH. New York*, 1988.

13. Liptay W, The determination of stability constants and other equilibrium constants in solution. *Zeitschrift für Elektrochemie. Berichte der Bunsengesellschaft für Physikalische Chemie.* 1962, **66**(3), 280-280.

14. Odisitse S, and Jackson GE, Potentiometric and blood plasma simulation studies of Nickel (II) complexes of poly (amino) amido pentadentate ligands: computer-aided metal-based drug design. *Bioinorg.Chem, Appl*, **2014**, 2014, 863612.

15. Murray K, May PM, Equilibrium simulation for titration analysis; version 1.1. University of Wales Institute Scienceand Technology Chemistry. *Appl. Chem*, **1**, 1984.

16. Liyanag JA, Chemical speciation of nickel - glycinate complexation. *J Sci. Univ. Kelaniya*, **1,** 2003, 1-13.

17. Jackson GE, Zvimba JN, Copper chelating anti-inflammatory agents; N 1-(2-aminoethyl)-N2-(pyridin-2-ylmethyl)-ethane-1,2-diamineandN-aminoethyl amino)ethyl) picolinamide: An *in vitro* and *in vivo* study. *J .Inorg .Biochem*, 2007, **101**, 148-158.

18. Santini AO, Pezza HR, Oliveira JEd, Pezza L, Braz, Development of a potentiometric flufenamate ISE and its application to pharmaceutical and clinical analyses. *J. Braz. Chem. Soc*, 2008, **19**, 162–168.

19. Gran G, Analyst. 1952, **77**, 661–671.

20. Nakani BS, Jackson GE, A potentiometric and spectroscopic study of copper(II) diaminodioxime complexes. *Chem. Soc. Dalton. Trans*, 1996, 1373–1377.

21. May PM. Murray K, JESS,a joint expert speciation system-1. *Talanta*, **38**, 1991, 1409-1417.

22. Elmagbari FMA, Synthesis and Design of ligand Copper Complexes as Anti-Inflammatory Drugs. *Thesis*, *PhD*, University of Cape Town, 2015.

23. Jackson GE, Nomkoko ET, Nakani BS, and Bourne SA, Computer simulation of nickel in blood-plasma following the in vitro investigations of complex formation chemistry with polyamine (amide) ligand.*Dalton. Trans*, 2004, **12**, 1789–1796.

24. Findlow JA, Duffield JR, and Williams DR, The chemical speciation of aluminium in milk. *Chemical Speciation & Bioavailability*, 2015, **2**(1), 3-32.

25. May PM, Murray K, Williams DR, The use of glass electrodes for the determination of formation constants—III Optimization of titration data: The esta library of computer programs. *Talanta,* 1988, **35**, 825–830.

26. Murray K, May PM, The use of glass electrodes for the determination of formation constants—IV Matters of weight. *Talanta,* 1988, **35** (12), 927-932.

27. Sabatini A, Vacca A, and Gristina MA, Computational methods for the determination of formation constants. *Chem. Rev,* 1972, **8**, 45–53.

28. Mufti AT, KHANZADA AWK, Saeeduddin, Dissociation constant studies of citric acid at different temperatures in different organic -water solvent systems. *J.chem.soc,* 1996, **18**, 82-87.

29. Pearce K, Formation constants for magnesium and calcium citrate complexes. *Aust. J.Chem,* 1980, **33**, 1511-1517.

30. Martell EA and. Motekaits JR, The determination and use of stability constant. *VCH publishers. INC. New York,* 1988.

31. Field TB, Coburn J, McCourt JL, McBryde WAE, Composition and stability of some metal citrate and diglycolate complexes in aqueous solution. *Analytica Chimica Acta,* 1975, **74**, 101-106.

32. Odisitse S, Jackson GE, In vitro and in vivo studies of N, N, bis[2(2-pyridyl)-methyl]pyridine-2,6-dicarboxamide-copper(II) and rheumatoid arthritis. *Polyhedron*, 2008, **27**, 453–464.

33. Jackson GE, Nomkoko TE, Nakani BS, Louw WKA, Zeevaart JR, Thermodynamic and biodistribution studies of Zn(II), Ca(II), Gd(III) and Cu(II) complexes of 3,3,9,9-tetramethyl- 4,8-diazaundecane-2,10-dione dioxime . *Dalton. Trans*, 2004, **5**,741–749.

34. Jackson GE, Odisitse S, Govender T, Kruger HG, and Singh A, Chemical speciation of copper(II) diamine diamide derivative of pentacycloundecane—a potential anti-inflammatory agent. *Dalton. Trans*, 2007, **11**, 1140–1149.

35. Pettit LD and powell HKJ, Stability constant database. Otley. *NewYork,* **212**, 1993.

36. May PM, K. M, JESS, a joint expert speciation system-1. *Talanta*, 1991, **38**, 1409-1415.

37. Covington AK, and Danish EY, Measurement of magnesium stability constants of biologically relevant ligands by simultaneous use of pH and ion-selective electrodes. *J .Solution.Chem*, 2009, **38**, 1449-1462.

38. Murray K, May PM, ESTA (Equilibrium Simulation for Titration Analysis) Manual Version 3, 1989.

39. Zamochnick SB, Rechnitz GA, Application of cation-sensitive glass electrodes to the study of alkali metal complexes. *Talanta*, 1964, **11**, 1061-1065.

40. Lindenbaum A, Li NC, White JM, Some metal complexes of citric and tricarballylic Acids. *J. Inorg. Nucl. Chem,* 1959, **12**,122-128.

41. Campi E, Ostacoli G, Meirone M, Saini G, Stability of the complexes of tricarballylic and citric acids with bivalent metal ions in aqueous solution. *J. Inorg. Nucl. Chem,* 1964, **26**, 553-564.

42. KOPECKÝ, F., et al., Laboratory manual for physical chemistry, Farmaceutical faculty of Comenius University in Bratislava,Report, (1996).Manual edited by: RNDr. Alexander Búcsi, PhD., Ing. Jarmila Oremusová,CSc. and doc. RNDr. Daniela Uhríková, CSc.

Chapter Three

3. ^{1}H-NMR spectroscopy

3.1 Introduction

^{1}H-nuclear magnetic resonance (NMR) spectroscopy is a technique used to investigate a compound's unique structure. [1-3] The technique is flexible, has many applications, and provides information regarding chemical bonding, electronic structure, and local site dynamics. [4, 5]

In recent years, the implementation of NMR has been extended to medicine [6] through magnetic resonance imaging (MRI) [7] and also biology. [6]

In this study, ^{1}H-NMR was used to gain insight into the site of metal coordination upon complexation of HCA with Ca^{2+}, Mg^{2+}, and Zn^{2+} ions. [8] The presence of metal ions is expected to cause a shift in the signals arising from protons attached to carbons near the site of coordination. [9, 10]

3.2. Experimental

A solution of 0.01 M HCA was prepared in D_2O at 25 ℃. Tert-butanol was added as the internal reference, and the pD of the solutions was adjusted using concentrated DCI and NaOD. The spectra were recorded at predetermined pH values from pH 2 to 6, and ^{1}H-NMR signal broadening and shifting were analysed. [11]

An Acrison micro pH meter and a Metrohm glass electrode were used to measure pH, and corrections were made by using Equation 3.1 described by Popov [12] and Glasoe.[13]

$$pH = pD - 0.044 \qquad (3.1)$$

For the metal complexation reactions, the pH values were selected to reflect the maximum concentration of a single species according to the species distribution diagrams, and the pH of each solution was monitored and kept constant during each experiment.

Solutions of $CaCl_2.2H_2O$, $MgCl_2.6H_2O$, and $ZnCl_2$ (0.01 M) were prepared in D_2O. These solutions were titrated into the 0.01 M HCA solution.

^{1}H-NMR spectra were recorded on a Bruker DRX600 MHz spectrometer and data processed using the software Mestrenova.

3.3. Results

Figure 3.1 shows the proton numbering for HCA, and the ^{1}H-NMR spectra of HCA, as a function of pH (pH 2 to 6), are shown in Figure 3.2.

Between pH 3 and 6, the signals for **Ha1**, **Ha2**, and Hb shifted to a lower frequency. This shift (in signals) is due to a change in the shielding of the protons as the HCA becomes deprotonated.

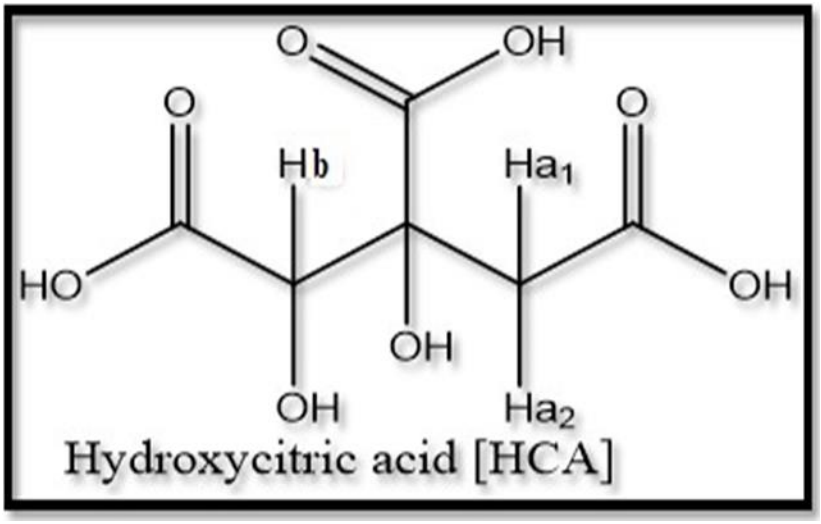

Figure 3.1. Structure of hydroxycitric acid (HCA). Proton labels are shown in Figure 3.2.

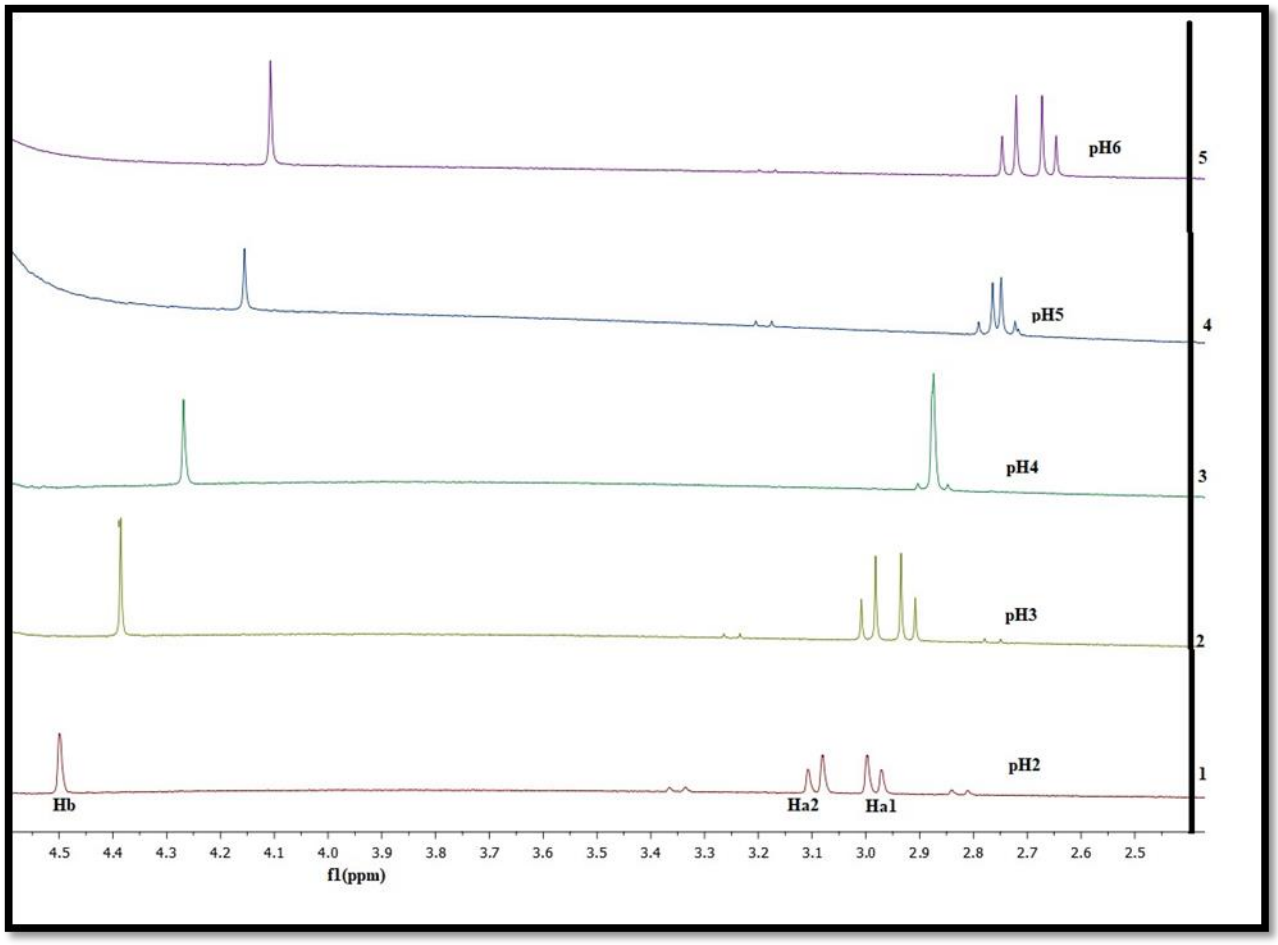

Figure 3.2: ^{1}H-NMR spectra of hydroxycitric acid (HCA) as a function of pH.

Proton chemical shifts were plotted against pH and shown in Figure 3.3. Several authors have previously used shifts in chemical shifts with pH to estimate pKa. [14, 15] In the case of HCA, all three protons shift at the same time, so these results could not be used to assign protonation sites. The fact that all the protons shift at the same time indicates that all sites are being protonated at

the same time. This means that several microstates, with very similar protonation constants, exist simultaneously [16] these possible microstates are shown in Figure 3.4. Figure 2.2 showed that the same phenonium, the protonation steps were not well separated and the formation curves did not show distinct steps.

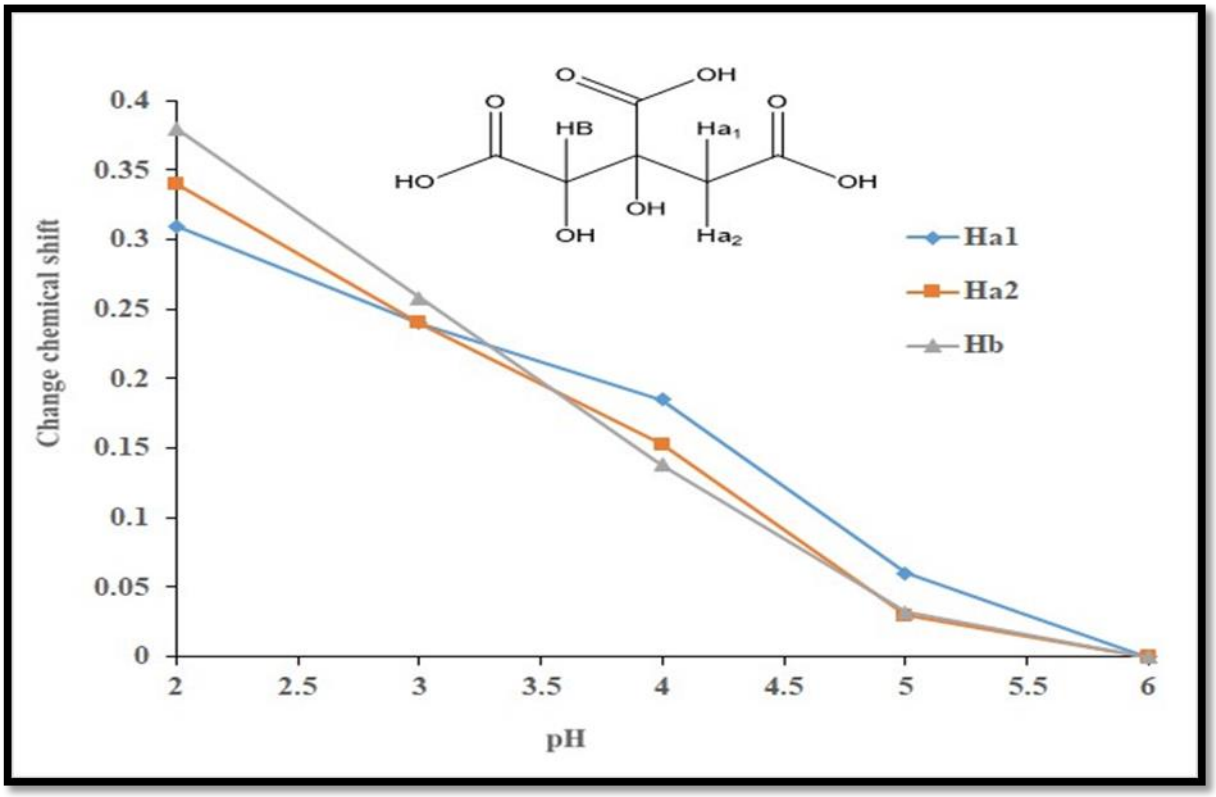

Figure 3.3. Change in chemical shift of selected hydroxycitric acid (HCA) protons as a function of pH.

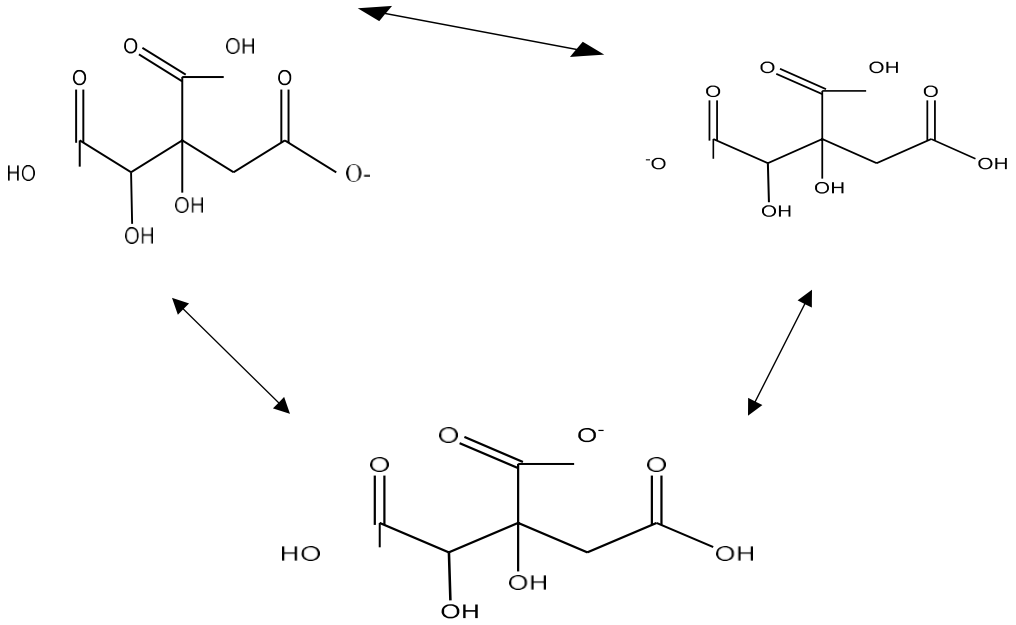

Figure 3.4. The effect of microstates on the p*Ka* values of hydroxycitric acid (HCA).

At pH 4, unusual signals were observed for **Ha1** and **Ha2** (see Figure 3.2). As the signals were different from those observed at other pH values, this spectrum was repeated on the same day and 5 days later (Figure 3.5). The results obtained indicate the formation of HCA-lactone. The coupling constants of **a1** and **a2** in Figure 3.5 agree with those of a previous study. [17]

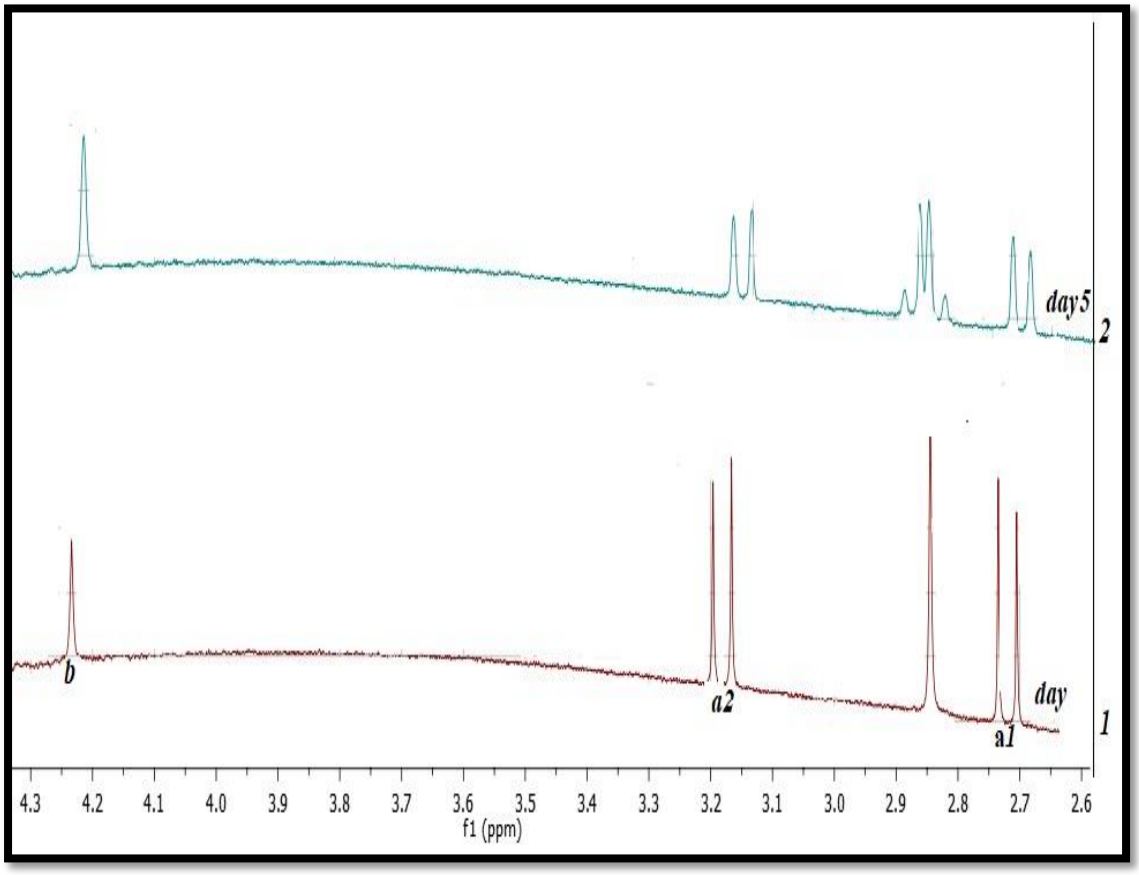

Figure 3.5. ^{1}H-NMR spectra of hydroxycitric acid (HCA) at pH 4.

HCA has two asymmetric centers; it has two pairs of diastereoisomers or four different isomers are possible, as shown in Figure 3.6. Each of these diastereomers may form a lactone ring. [17, 18]

Free (-)-HCA is unstable and is usually converted to the (-)-HCA lactone through concentration (drying) and evaporation. The configurations of the hydroxycitric acid lactone were determined to be (2S,3R)- and (2S,3S). [17, 18]

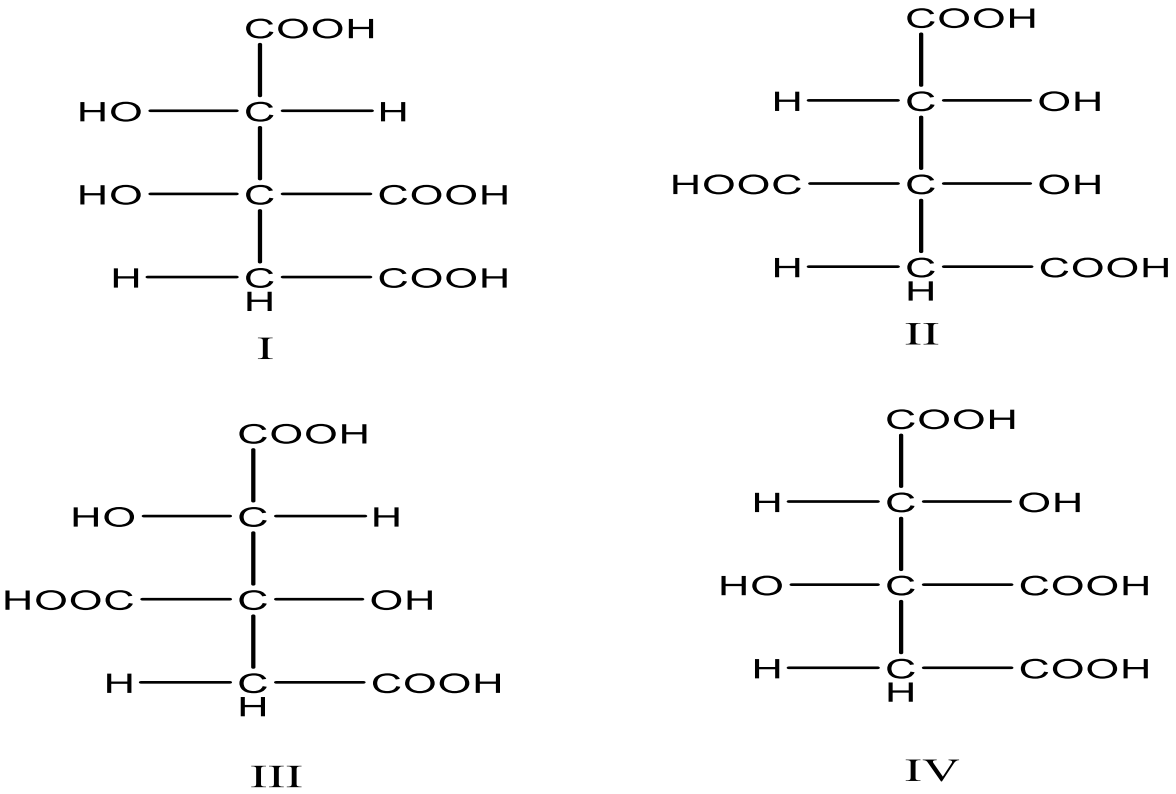

Figure 3.6. Isomer structures of hydroxycitric acid.

The structure of lactone formation is shown in Figure 3.7.

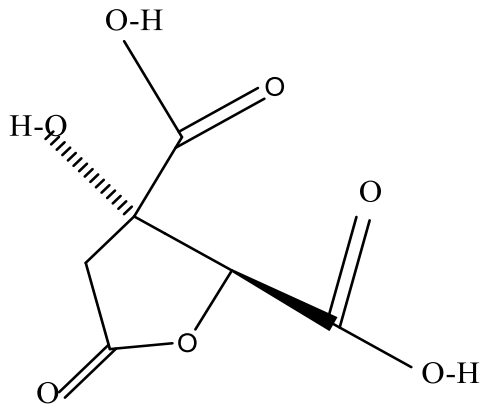

Figure 3.7. Structure of (2S,3S)- hydroxycitric acid lactone (HCA-lactone).

3.3.1. Ca (II)-HCA complexes

^{1}H-NMR results for the complexation of HCA with Ca(II) are shown in Figure 3.8.

According to the potentiometric studies reported, in Chapter 2, complexation starts at pH 1.8, and therefore a change in NMR signals was expected at pH 2. At this pH, all peaks shifted to a high frequency. This shift indicates that Ca(II) coordinates to HCA.

At pH 4, both HCA and HCA-lactone exist in solution. For HCA, the peaks were slightly shifted and broadened. This broadening may indicate that several different structures coexist in solution with a rapid exchange between them. For HCA-lactone, the signals Ha1, Ha2 were broadened, indicating that the Ca(II) coordinated to the lactone.

At pH 7, not all the peaks broadened to the same extent. The **Hb** peak broadened more than that of **Ha1,** and **Ha1** broadened more than **Ha2.**

The broadening in **Hb** and **Ha1** means complexation between Ca(II) and HCA is occurring. From potentiometry studies, at this pH, the ML species is most abundant. The broadened peaks indicate that there is an exchange between structures but not at the slow exchange limit, or separate signals would be seen for each structure. In fact, two signals can be seen for **Hb**.

From the potentiometric study, the metal is not monodentate – the equilibrium constant is too high. This means that the metal will bind to several sites at the same time to form five or six-membered rings. Four possible structures for $[Ca(HCA)]^-$ are shown in Figure 3.9. The intermediate exchange between these isomers would result in line broadening. If the central hydroxyl group was coordinated, a structure similar to that found for aluminium(III) with citrate would be formed. [19]

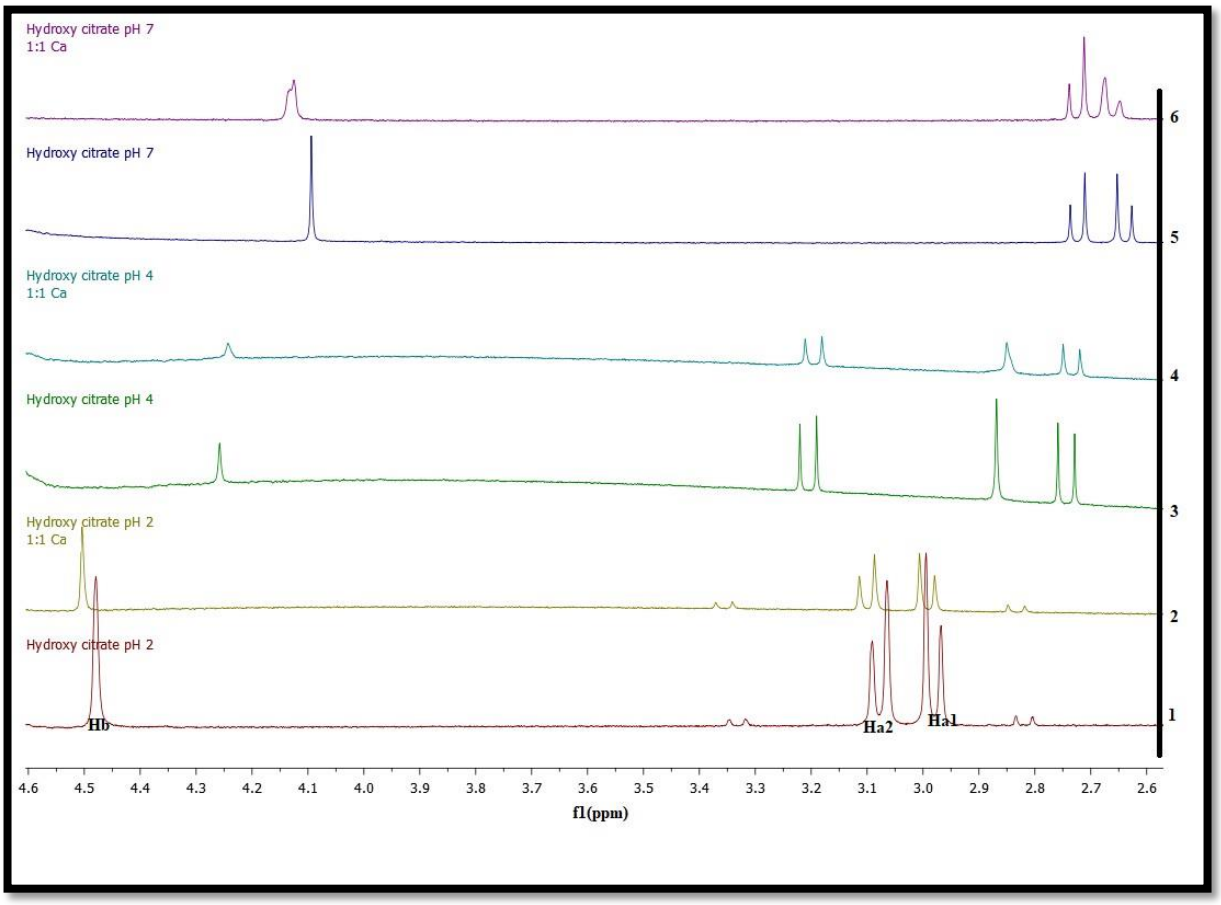

Figure 3.8. ^{1}H-NMR spectra of hydroxycitric acid (HCA)-Ca(II) complexes in D_2O.

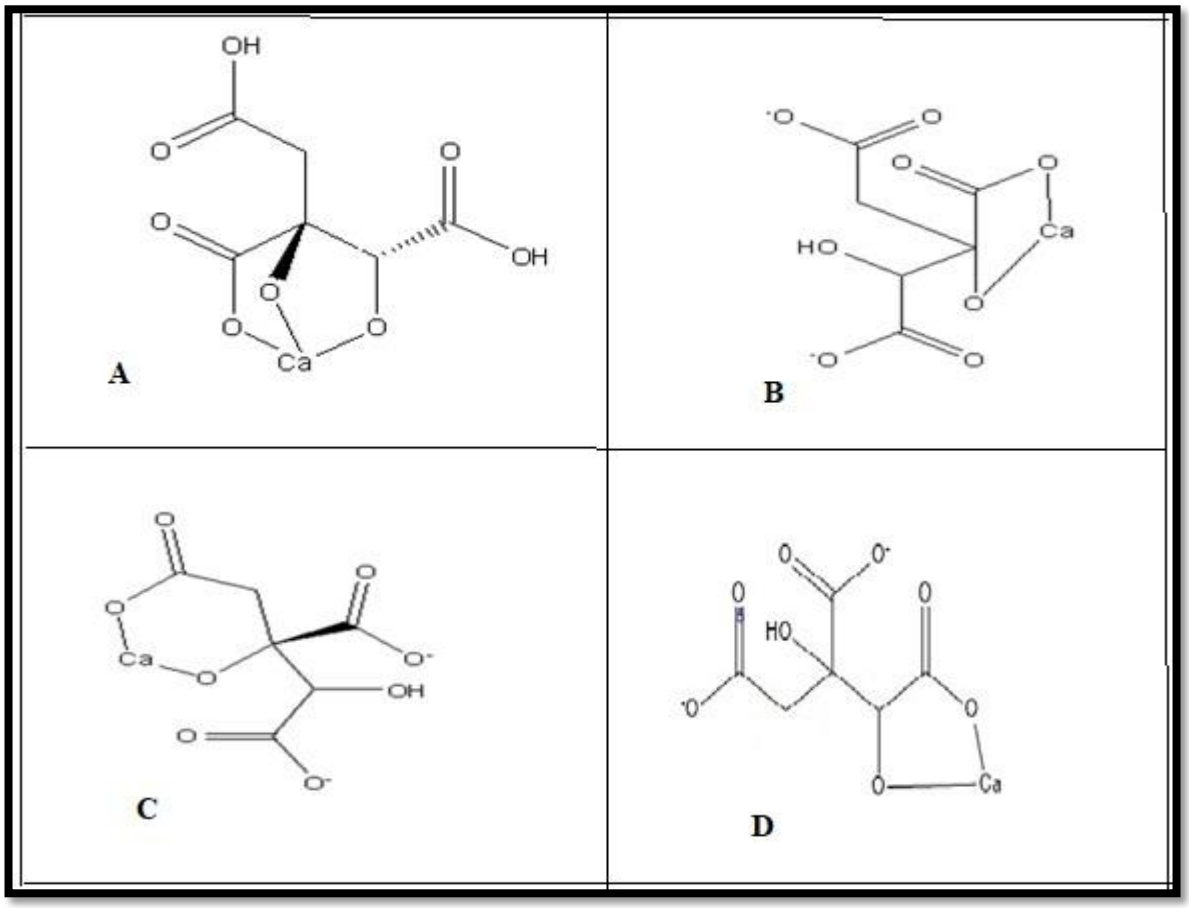

Figure 3.9. Four possible structures for $[Ca\text{-}(HCA)]^{-}$.

3.3.2. Mg (II)-HCA complexes

The ^{1}H-NMR spectra of the HCA - Mg(II) complexes at pH 2.8, 3.67, and 9.38 are shown in Figure 3.10. There is very little difference between the spectra with and without Mg(II). Here it is not possible to say anything about the structure of the complexes formed in solution from these results.

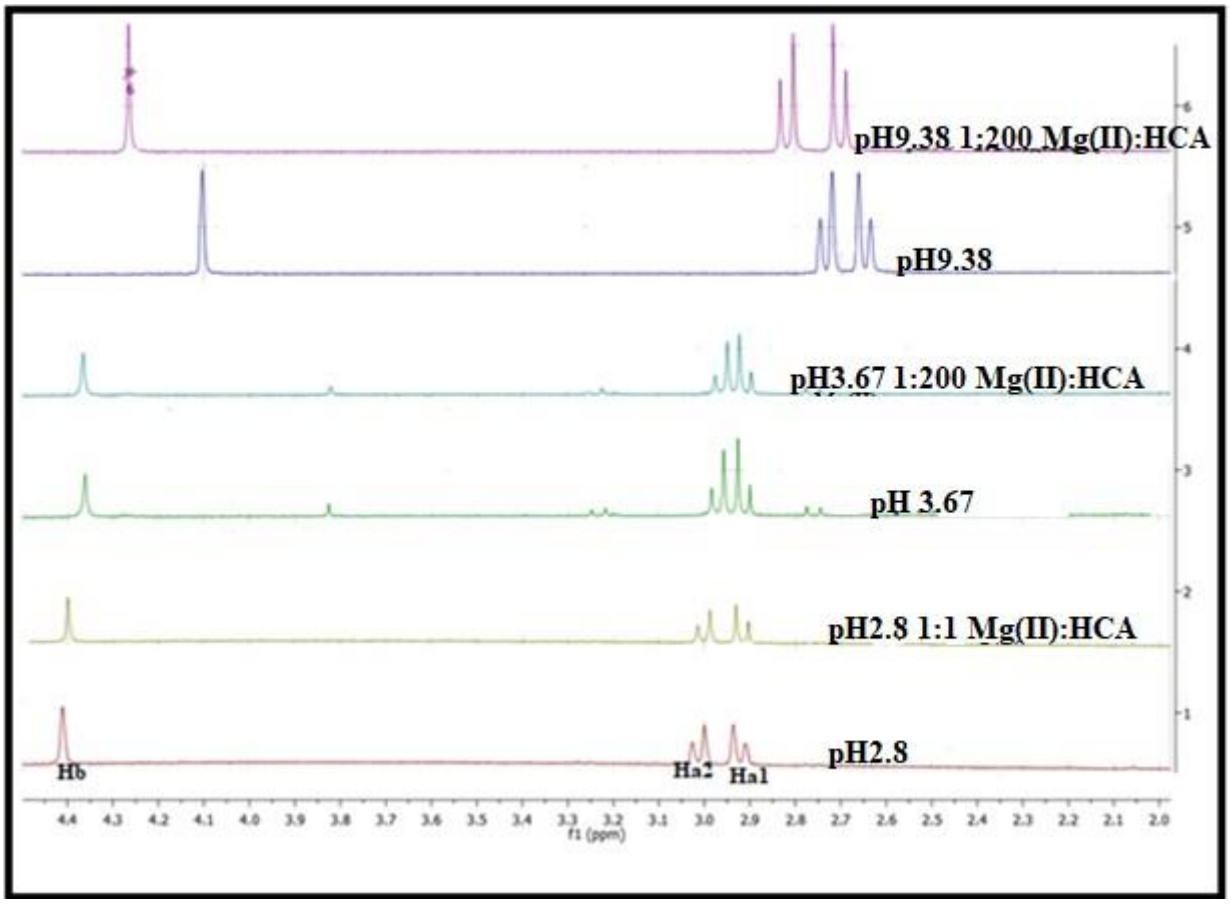

Figure 3.10. ^{1}H-NMR spectra of hydroxycitric acid (HCA) -Mg(II) complexes in D_2O.

3.3.3. Zn(II)-HCA complexes

^{1}H-NMR spectra for the complexation of HCA with Zn(II) are shown in Figure 3.11.

At pH 3.05, all the peaks **a1, a2,** and **b** were broadened, indicating that the Zn(II) was complexing to the HCA. The MLH species is assumed to predominate at this pH.

At pH 4.27, the HCA-lactone was formed. The lactone peaks are shifted relative to theirposition in the absence of Zn(II), and so the present investigator concludes that the metal is coordinated. However, the mode of complexation of these species could not be determined.

At pH 6.67, all peaks shifted to a higher frequency, and peak **b** is split into two. The dominant species at this pH is ML. Once again, there must be an exchange between different structural isomers of the complex.

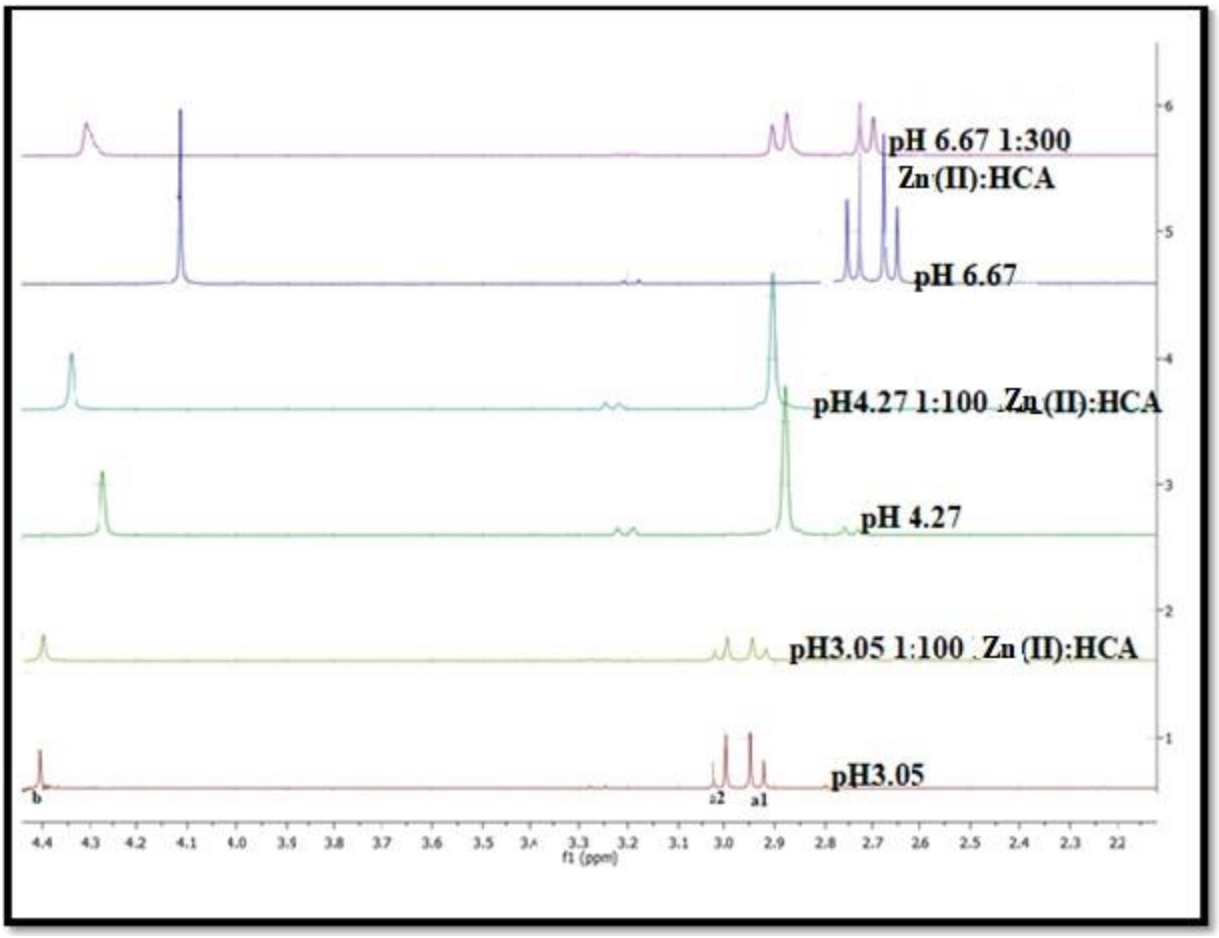

Figure 3.11. ^{1}H-NMR titration for complexation of hydroxycitric acid (HCA) with Zn(II) in D_2O.

3.4. Discussion

The spectra were recorded at different pH values at which the maximum concentrations of the various species were observed, as deduced from the speciation diagrams.

For HCA alone, all the protons in ^{1}H-NMR spectra shifted in response to changes in pH. A plot showing the chemical shift against pH revealed that when a proton was added, all the signals shifted. Thus, these data could not be used to estimate the pK_a values of HCA or to assign

protonation sites to individual pK_a's. HCA has three protonation sites, whose pK_a values are too close to resolve. In solution, an equilibrium exists between several microstates with a rapid exchange between them.

The results obtained at pH 4 were surprising and showed the reversible formation of a lactone.

The solution structures of the metal (Ca^{2+}, Mg^{2+}, and Zn^{2+})-HCA complexes were also investigated by using ^{1}H-NMR. The idea was that those protons closest to the coordination site would be most affected. On addition of the metal ion, however, all the peaks shifted and/or broadened. Shifting of the proton signals is due to the inductive effect of the metal ion. None of the metal ions is paramagnetic, and so the broadening must be exchange broadening. That is, several different structural isomers of a species must exist in solution, at the same time. Since the chemical shifts of the different isomers will be different, rapid or intermediate (on the NMR time-scale) exchange between them will lead to signal broadening. Thus, the NMR results were inconclusive or showed that even for the metal complexes, several microstates co-exist in solution.

References

1. Gauglitz G. and Dinh -TVo., Handbook of spectroscopy. *WILEY-VCH Verlag GmbH & Co.KGaA, Weinheim.Germany.* 2003. **1**.

2. Bloch F, The principle of nuclear induction nobel lecture. *John Wiley & Sons*, 1952.

3. Pandya A, Howard MJ, Zloh M, Dalby PA, An evaluation of the potential of NMR spectroscopy and computational modelling methods to inform biopharmaceutical formulations. *Pharmaceutics*, 2018, **10**(4).

4. Grant DM, Harris R K, Encyclopedia of nuclear magnetic resonance eds. *John Wiley & Sons.Chichester*, 1996.

5. Abragam A, The principles of nuclear magnetism, *Oxford University Press. Oxford* 1961.

6. Gerothanassis Ioannis P, Troganis A, Exarchou V, and Barbarossou K, Nuclear magnetic resonance (NMR) spectroscopy: basic principles and phenomena and their application to chemistry biology and medicine. *Chem. Educ. Res.Pract.Eur* , 2002, **3**(2), 229-252.

7. Macomber RS, A complete introduction to modern NMR spectroscopy. *John. Wiley and Sons. Inc*, 1998.

8. Günther H, Selected topics from recent NMR studies of organolithium compounds. *J .Braz. Chem. Soc*, 1999, **10** (4), 241-262.

9. Lammers H, der Heijden AM, Van Bekkum H, Geraldes CFGC, Peters JA, potentiometric and NMR spectroscopic study of protonations and amide hydrogen exchange rates of DTPA-bis(butylamide)DTPA-bis(glucamide) and their lanthanide(III) complexes. *Inorg.Chim. Acta,* 1998, **277** (2), 193-201.

10. Pregosin PS, Ed, Transition metal nuclear magnetic resonance studies in inorganic chemistry. *Elsevier*, 1991, **13**, 362.

11. Wells MA, Jelinska C, Hosszu L LP, Craven J, Clarke AR, Collinge J, Waltho JP, and Jackson GS, Multiple forms of copper (II) Co-ordination occure through the disordered N-terminal region of the prion proteinat pH 7.4. *J. Bio. Chem,* 2006, **400**(3), 501-510.

12. Popov, Rönkkömäki K, and Lajunen H, Lauri H J, Guidelines for NMR measurements for determination of high and low p*K*a. *Pure. Appl.Chem,* 2006, **78**(3), 663-675.

13. Glasoe PK and Long FA, Use of glass electrode to measure acidities in deuterium oxide11,2. *J. Phys. Chem,* 1960, **64**,188-190.

14. Sokolov FD, Babashkina MG, Safin DA, Rakhmatullin AI, Fayon F, Zabirov NG, Bolte M, Brusko VV, Galezowska J, and Kozlowski H, Complexes of N-thiophosphorylthioureas (HL) with copper(I). Crystal structures of [Cu3L3] and [Cu(PPh3)2L] chelates. *Dalton. Trans,* 2007(**41**), 4693–700.

15. Mohajane M, Development of copper-based anti-inflammatory drugs: histidine derivatives. *MSc .Thesis,* University of Cape Town 2010.

16. Ullmann GM, and Bombarda E, pK(a) values and redox potentials of proteins. What do they mean?. *Biol.Chem*, 2013, **394**(5), 611-9.

17. Hida H, Yamada T, and Yamada Y, Production of hydroxycitric acid by microorganisms. *Biosci Biotechnol Biochem*, 2005, **69**(8), 1555-1561.

18. Sunny S, A review on the molecule: hydroxycitric acid. *J. Pharm. Pharmaceutical Sci*,2018, **7** (2), 393-418.

19. Le Roux A, Hard hard and soft soft coordination in complexes of group 6 and group 10 and 11 metal respectively. *MSc .Thesis*, 2008, Stellenbosch.

Chapter Four

4. *Effect of HCA on chemical speciation and supersaturation of stone-forming salts in artificial urine: theoretical modelling*

4.1. Introduction

Chemical speciation is essential in understanding the form of chemicals of interest in natural systems. [1] The International Union of Pure and Applied Chemistry (IUPAC) has defined speciation as the specific form of a chemical element in reference to its molecular, electronic, or nuclear structure. [2] According to IUPAC "speciation" denotes the distribution of an element amongst defined chemical species in a system. [2, 3] Chemical speciation is essential for gaining insights into the biological availability and possible toxicity of chemical complexes and holds significance concerning the potential of biosensors in investigating metal pollution. [4] Chemical speciation has caught the notice of many investigators in the fields of risk analysis, dental care, total parenteral nutrition, metallurgical operations, and environmental protection. [5, 6] It is, therefore, useful to determine the speciation of calcium and other elements, which in turn contribute to the supersaturation (SS) of stone-forming salts. As mentioned in **Chapter 2**, HCA contains three carboxy groups and two hydroxyl groups (OH), thus allowing HCA to form complexes with Ca in urine.

If calcium is complexed to HCA, less is available for binding to free oxalate (or phosphate). The SS of (Ca-phosphate) CaP and (calcium oxalate) CaOx, therefore, is lower, thereby decreasing the risk of crystallization of these substances. The extent to which this occurs is contingent on the chemical composition of urine. Thus, HCA could, be potentially used as a curative agent against the formation of kidney stones, specifically those compose of CaOx and CaP.

In the present study,the theoretical effect of HCA on the speciation of calcium was modelled by using the speciation program JESS. [7, 8] JESS is extensively used to model metal-ligand equilibria in biological systems. This program comprises an extensive database of thermodynamic constants for one or multiple binary, tertiary, and quaternary complexes that may form at equilibrium. It also takes into account changes in ionic strength and the formation of solid phases. The JESS database system provides a powerful and versatile means of storing and retrieving thermodynamic data associated with chemical reactions. [7, 8] In recent years, Jess has also been used to model the chemical speciation of various elements in blood plasma [9] and urine. [10-14]

4.2. Methods

4.2.1. Model

The chemical speciation was evaluated in a solution of chemical composition typical of urine (Table 4.1) in the absence of HCA ("control") and the presence of 1 mM HCA. [15, 16] Previous studies by Chung and *et al.* [30] showed that the concentration of HCA in urine after supplementation was 0.7 mM. An elevated concentration of 1 mM HCA was used for modelling

in the present study to highlight Ca-HCA interactions. The JESS software set was used to calculate the speciation. In order to achieve this, the JESS database was expanded to include the thermodynamic binding constants for HCA with H^+, Ca^{2+}, and Mg^{2+}, which were determined experimentally as part of the current study (**Chapter 2**).

Equilibrium constants and species formation are dependent on temperature and ionic strength. [18] Accordingly, the temperature for the urine model was set at 37 °C (physiological temperature). The ionic strength was calculated by JESS.

Table 4.1. Urinary concentrations used in JESS modelling.

Urinary parameters	Concentration / mM
pH	6
Calcium	1.89
Magnesium	3.24
Hydroxy citrate	0.00 [control], 1.00 [test]
Potassium	41.05
Sodium	160
Citric	2.13
Phosphate	24.43
Oxalate	0. 15
Chloride	60
Urate	3.2

4.3. Speciation

4.3.1. HCA speciation

The percentage distribution of each HCA species in urine with 1 mM HCA is shown in Figure 4.1, while the percentages and concentrations for each species are provided in Table 4.2.

At 1 mM concentration, most of the HCA is complexed to Ca in the form of $[Ca(HCA)]^-$ (65%). The other major species is free HCA^{-3} (28%). Thus, HCA does affect the speciation of Ca and may play a role in lessening the supersaturation of Ca salts.

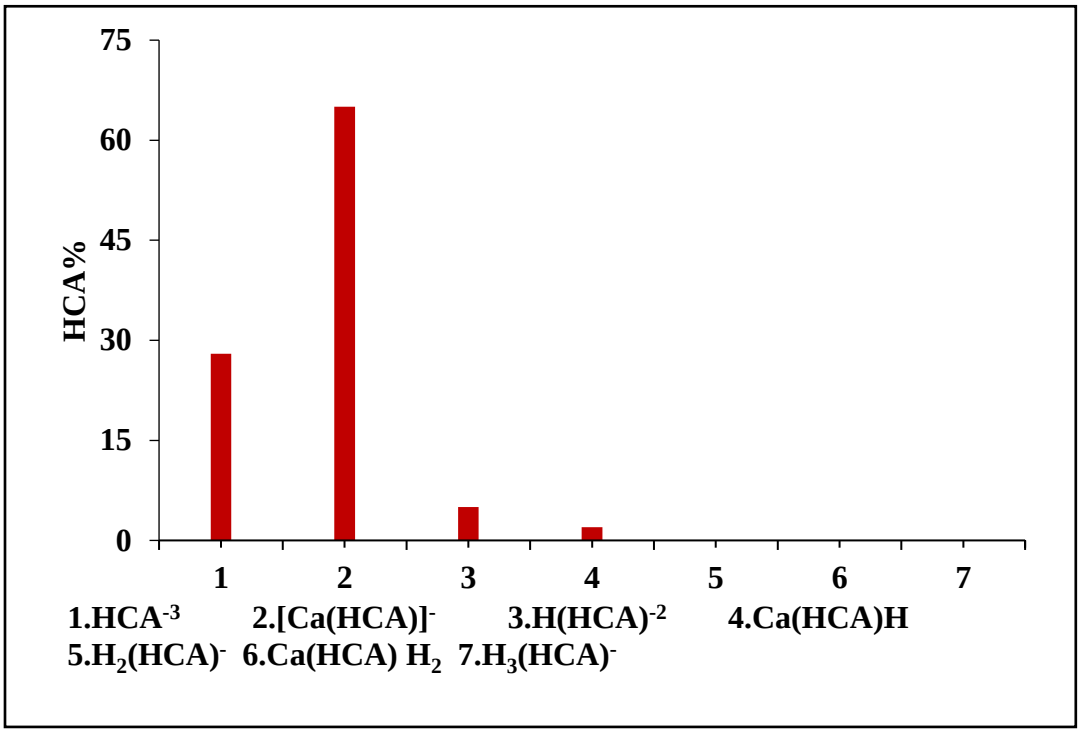

Figure 4.1. Percentage distribution of HCA^{-3} species in urine containing 1 mM HCA.

Table 4.2. Percentage distribution of HCA species in urine

Species	**% HCA**	**[HCA] mol/L**
HCA^{-3}	28	0.0002786
$[Ca(HCA)]^{2-}$	65	0.0006518
$H(HCA)^{2-}$	5	5.07E-05
$[Ca(HCA)H]^{-}$	2	1.86E-05
$H_2(HCA)^{-}$	0	3.73E-07
$]Ca(HCA)H_2]$	0	3.89E-08
$H_3(HCA)$	0	1.98E-10

4.3.2. Calcium speciation

The percentage distribution of Ca^{+2} species in urine and urine containing 1 mM HCA is shown in Figure 4.2. Percentages and concentrations for each species are listed in Table 4.3.

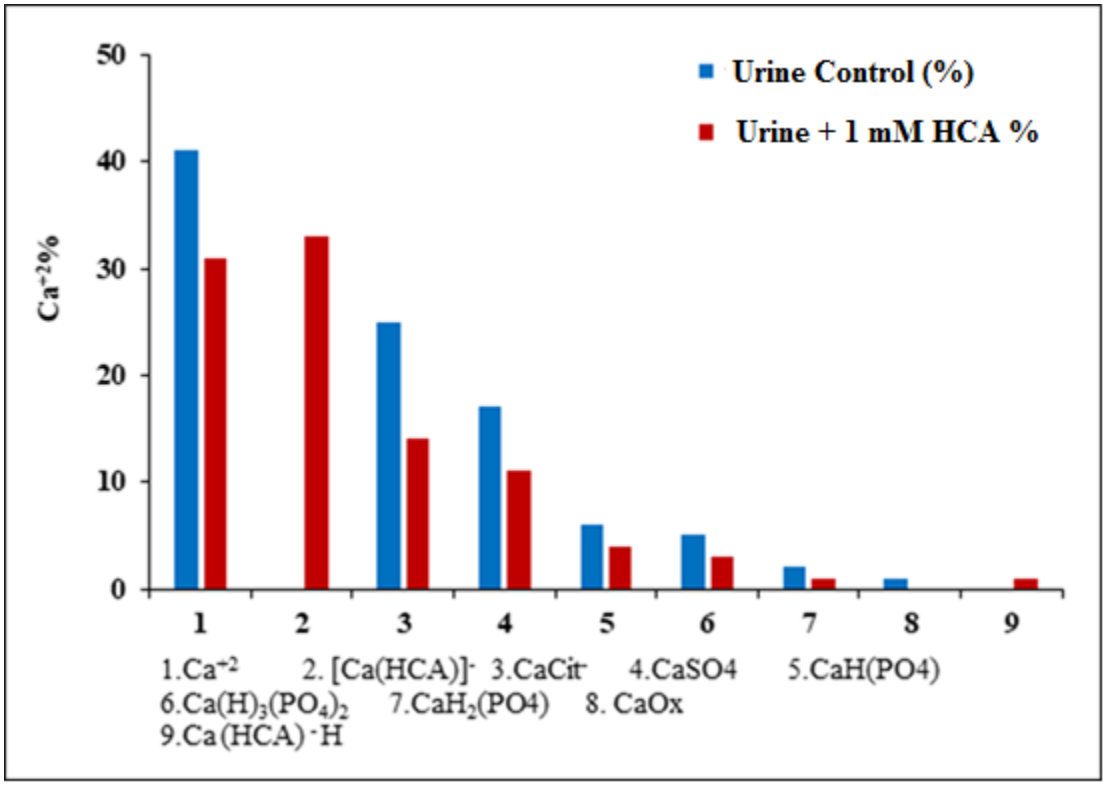

Figure 4.2. Percentage distribution of calcium species in urine and urine containing 1 mM HCA.

Table 4.3. Calcium species in urine and urine containing 1 mM HCA

Species	**Urine Control**		**Urine Control + 1mM HCA**	
	Concentration mol/l	(%)	Concentration mol/l	(%)
Ca^{+2}	0.0008062	41	0.0006038	31
$[Ca(HCA)]^{-}$	0.000	0	0.0006518	33
$CaCit^{-}$	0.0004915	25	0.0002840	14
$CaSO_4$	0.0003438	17	0.0002188	11
$CaH(PO_4)$	0.0001198	6	7.177E-5	4
$CaH_3(PO_4)_2$	9.212E-5	5	5.010E-5	3
$CaH_2(PO_4)$	3.745E-5	2	2.038E-5	1
CaOX	1.168E-5	1	8.378E-6	0
$Ca\ (HCA)^{-}H$	0.000	0	1.8566E-5	1

As expected, the Ca urinary speciation is significantly affected by 1 mM HCA. There is a 10% drop in the free Ca^{2+} concentration, which affects the concentration of other Ca species. In order to see if this change is sufficient to affect the supersaturation of calcium oxalate monohydrate (COM) or calcium dihydrogen phosphate (brushite), it is necessary to calculate the relative supersaturation of these two solids (see section 4.4).

4.3.3. Oxalate speciation

The percentage distribution of oxalate species in urine and urine containing 1 mM HCA is shown in Figure 4.3. Percentages and concentrations are listed in Table 4.4.

On addition of HCA, the free Ox^{-2} concentration increased. At the same time, the concentration of MgOx and CaOx decreased. These decreases mean that less free oxalate has been utilized, thereby explaining the increase in $[Ox]^{2-}$. The decrease in CaOx concentration is understandable because free Ca^{2+} has decreased. The change in MgOx concentration is counter-intuitive, however, as the free Mg^{2+} has increased (see later). This illustrates the interconnectedness of the speciation and why it is so difficult to predict. The 4% decrease in MgOx in urine containing 1 mM HCA may be due to a reduction in its formation constant as a result of ionic strength changes.

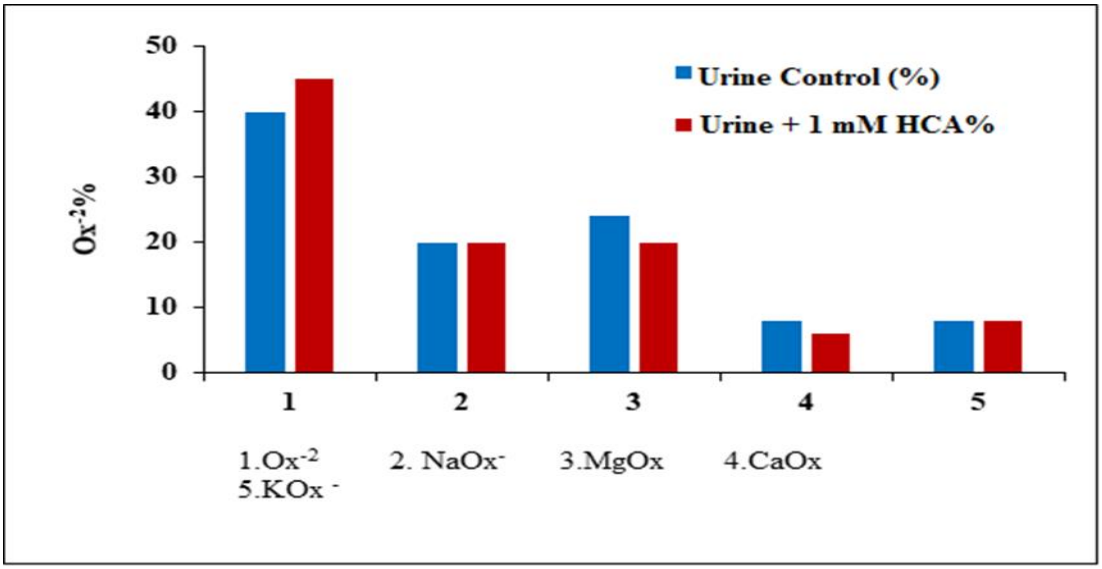

Figure 4.3. Percentage distribution of oxalate species in urine and urine containing 1mM HCA.

Table 4.4. Oxalate speciation in urine and urine + 1 mM HCA.

Species	**Urine Control**		**Urine Control + 1 mM HCA**	
	Concentration mol/l	%	Concentration mol/l	%
Ox^{-2}	5.942E-5	40	6.698E-5	45
$NaOx^{-}$	2.962E-5	20	3.060E-5	20
MgOx	3.564E-5	24	2.999E-5	20
CaOx	1.168E-5	8	8.378E-6	6
KOx^{-}	1.211E-5	8	1.246E-5	8

4.3.4. Phosphate speciation

The percentage distribution of phosphate species is shown in Figure 4.4. Percentages and concentrations are listed in Table 4.5.

The result showed a decrease in 3% of the species H_2PO^{4-} [species number 1, Figure 4.4] in the attendance of 1 mM HCA in urine; this is accompanied by rise in 2% HPO_4^{-2} which forms upon the deprotonation for the former species.

HPO_4^{-2} is a precursor to the creation of CaP.[13] Thus, an increase in HPO_4^{-2} is expected to lead to an increase in the supersaturation of CaP salt; however, the opposite happened because the upsurge in HPO_4^{-2} is outweighed by the reduction in Ca^{+2} (Table 4.3). The same observation has been reported in the literature for other exogenous ligands. [13]

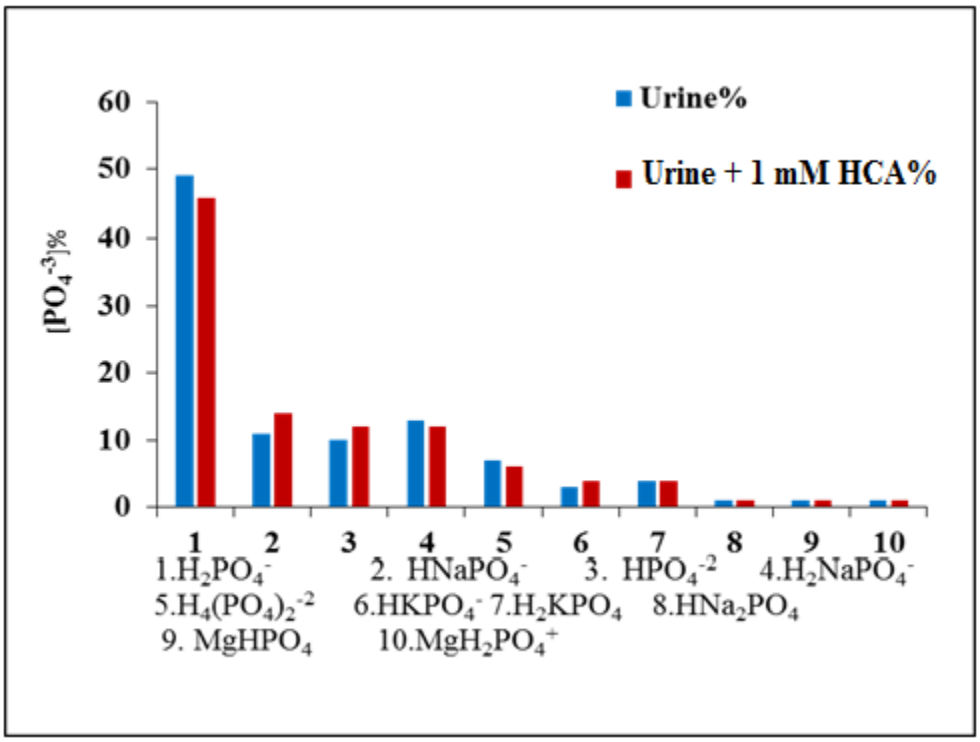

Figure 4.4. Percentage distribution of phosphate species in urine and urine containing 1 mM HCA.

Table 4.5. Phosphate species in urine and urine containing 1 mM HCA

Species	**Urine Control**		**Urine Control + 1 mM HCA**	
	Concentration mol/l	(%)	Concentration mol/l	(%)
$H2PO_4^-$	0.01191	49	0.01121	46
$HNaPO_4^-$	0.002674	11	0.003357	14
$HPO4^{-2}$	0.002513	10	0.003046	12
H_2NaPO_4	0.003079	13	0.002951	12
$H_4(PO_4)_2^{-2}$	0.001791	7	0.001525	6
$HKPO_4^-$	0.0008055	3	0.0009425	4
H_2KPO_4	0.0009876	4	0.0009169	4
HNa_2PO_4	0.0002251	1	0.0002058	1
$MgHPO_4$	0.0002313	1	0.0001943	1
$MgH_2PO_4^+$	0.0002107	1	0.0001654	1

4.3.5. Citrate speciation

The percentage distribution of citrate species is shown in Figure 4.5. Percentages and concentrations are listed in Table 4.6.

In the presence of HCA in urine, the Cit^{-3} distribution increased by 5 %. At the same time, $CaCit^-$ concentration decreased by 10% and $CaH_2Cit_2^{-2}$ by 1%. This is because of the formation of $[Ca(HCA)]^-$ (Table 4.3, species number 2), which utilises a large amount of Ca^{+2} and leads to a decreased free Ca^{+2}.

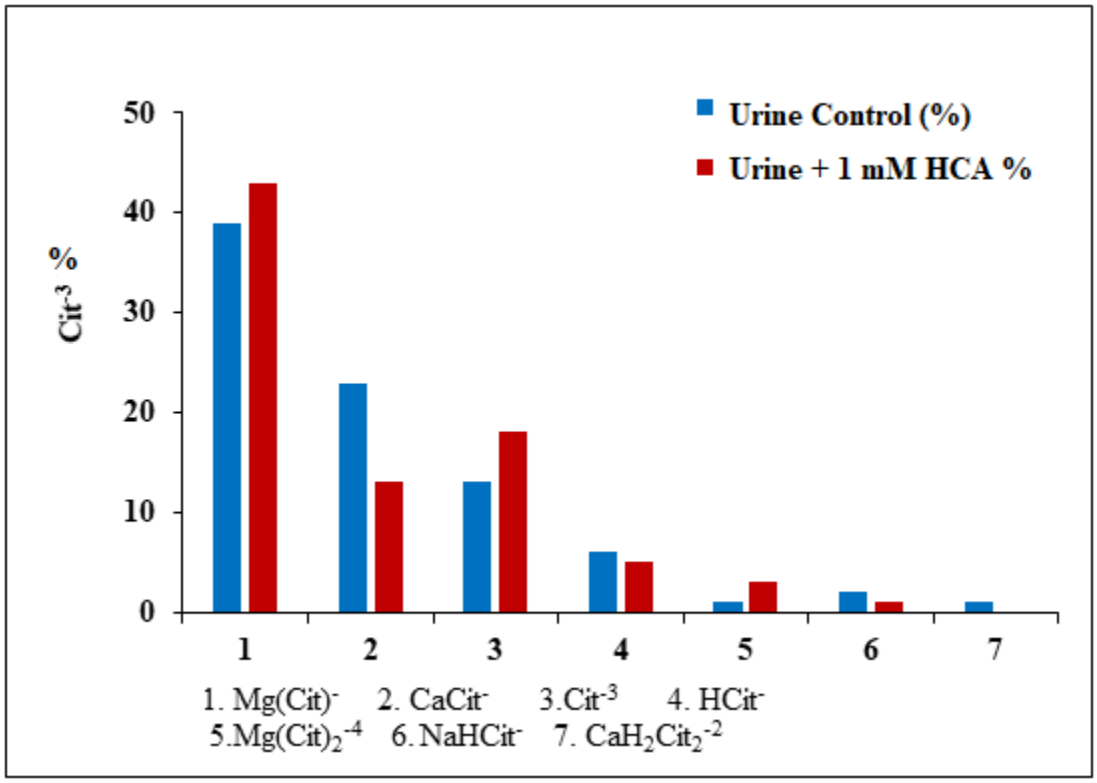

Figure 4.5. Percentage distribution of Cit^{-3} species in urine and urine containing 1 mM HCA.

Table 4.6. Cit^{-3} species in urine and urine containing 1 mM HCA

Species	**Urine Control**		**Urine Control + 1 mM HCA**	
	Concentration mol/l	(%)	Concentration mol/l	(%)
$Mg(Cit)^-$	0.0008381	39	0.0009292	43
$CaCit^-$	0.0004915	23	0.0002840	13
Cit^{-3}	0.0002861	13	0.0003915	18
$HCit^{-2}$	0.0001175	6	0.0001099	5
$MgCit_2^{-4}$	2.957E-5	1	5.961E-5	3
$HNaCit^-$	3.770E-5	2	3.203E-5	1
$CaH_2Cit_2^{-2}$	1.519E-5	1	6.784E-6	0

4.3.6. Magnesium speciation

The percentage distribution of magnesium is shown in Figure 4.6. Percentages and concentrations are listed in Table 4.7.

The presence of HCA leads to a rise in the concentration of Mg^{2+} and $MgCit^{-}$. This increase in $MgCit^{-}$ leads to decreases in MgOx concentration (see Figure 4.3) and in $MgH_2(PO_4)_2$ (see Figure 4.6).

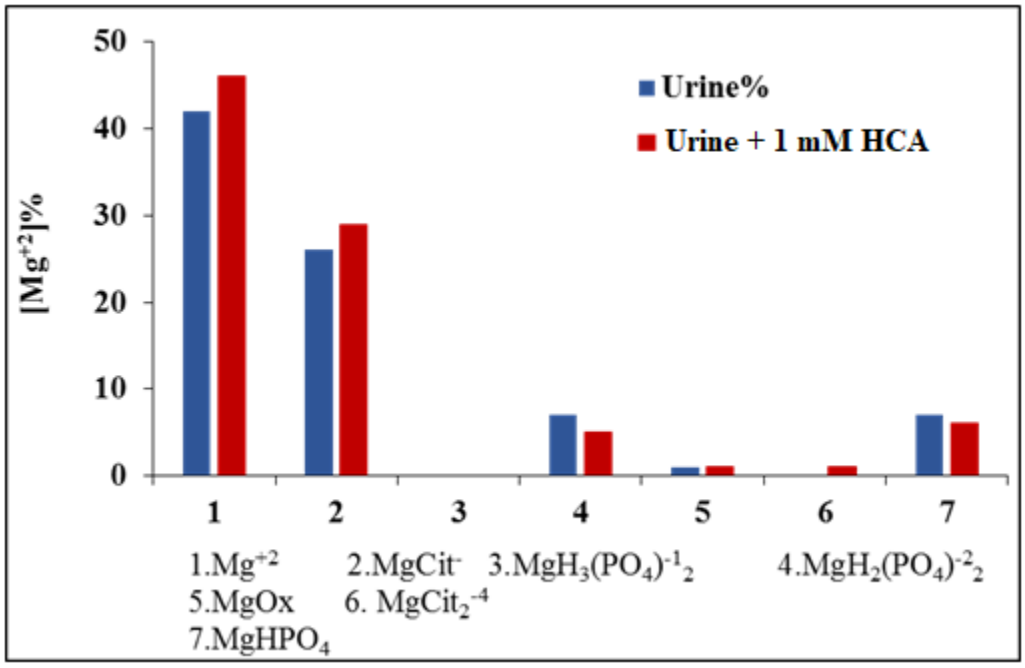

Figure 4.6. Percentage distribution of Mg^{+2} species in urine and urine containing 1 mM HCA.

Table 4.7. Mg^{+2} species in urine and urine containing 1 mM HCA

Species	Urine Control		Urine Control + 1 mM HCA	
	Concentration mol/l	(%)	Concentration mol/l	(%)
Mg^{+2}	0.001365	42	0.001496	46
$MgCit^{-}$	0.0008381	26	0.0009292	29
$MgH_3(PO_4)_2^{-1}$	1.434E-5	0	1.089E-5	0
$MgH_2(PO_4)_2^{-2}$	0.0002107	7	0.0001654	5
MgOx	3.564E-5	1	2.999E-5	1
$MgCit_2^{-4}$	1.479-5	0	2.980E-5	1
$MgHPO_4$	0.0002313	7	0.0001943	6

4.4. Effect of HCA on supersaturation in urine

Supersaturation refers to the force driving the formation of stones in urine. [19, 20] It is often expressed as relative supersaturation (RS). In this study, the influence of varying the concentration of HCA in urine on the RS of calcium salts was investigated.

Kidney stones are made up of different minerals. The most common component is calcium oxalate (CaOx), which accounts approximately 70% of all kidney stones. CaOx can be found as the monohydrate (crystal name: whewellite) or dihydrate (crystal name: weddellite) forms. [21] It can also be found in combination with uric acid or calcium phosphate because calcium oxalate stones typically grow on

Randall's plaque on the papillary tip [22] [23] Calcium phosphate is found in about 15% of kidney stones and can be present in combination with calcium oxalate or struvite. Because of differences in pH urine at which the two minerals precipitate, calcium phosphate is not found mixed with uric acid. The two types of CaP include apatite (sometimes reported as carbonate apatite), which is the crystal kind found in bone, or calcium hydrogen phosphate (brushite); the frequency of apatite is more than brushite. Calcium phosphate crystals in the urine sediment are typically dark and amorphous. [21]

A kidney stone may form when substances such as calcium, oxalate, or uric acid are present at high levels in the urine. [24] Stones may also form if these substances are present at normal levels, especially if the amount of urine produced each day is low. [25] Once crystals form, they may become anchored in the kidney and gradually increase in size (crystal growth) to form a kidney stone. [26] In order for a mineral to precipitate, it must exceed its solubility product. Thus, an important parameter used to evaluate the risk of kidney stone formation is the relative supersaturation of the salt. In this study, the RS of various salts was calculated by determining the saturation index (SI), using the program JESS. [7]

The SI of different calcium salts as a function of HCA concentration are shown in Figures 4.7 to 4.9, and data at the various concentrations of HCA vs SI are reported in Appendix from Tables 4.8 to 4.10.

Increasing the concentration of HCA decreased the SI of COM, hydroxyapatite, and brushite. At an HCA concentration of 0.002 M, the urine was no longer supersaturated in COM. This 2 mM HCA is double the amount used in our JESS modelling but is clinically easily achievable.

Various trials of HCA in humans have reported HCA to be well tolerated, with no significant adverse events. [27-17]

A much higher concentration of HCA (10 mM) is needed to achieve a SI of 1 for apatite.

The result in the present study showed that a concentration 1 mM HCA significantly decreases the RS of COM, hydroxyapatite, and brushite salts in the urine.

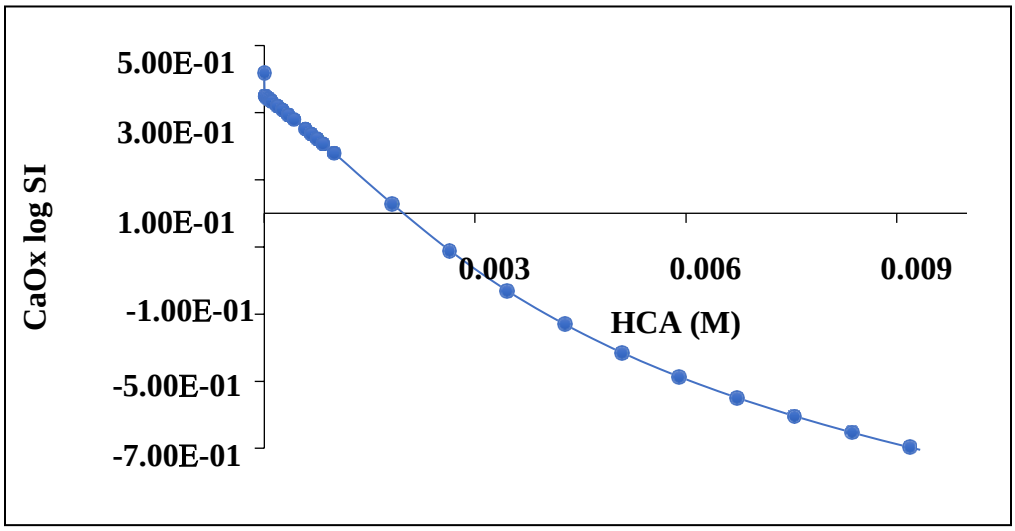

Figure 4.7. CaOx log SI versus HCA concentrations.

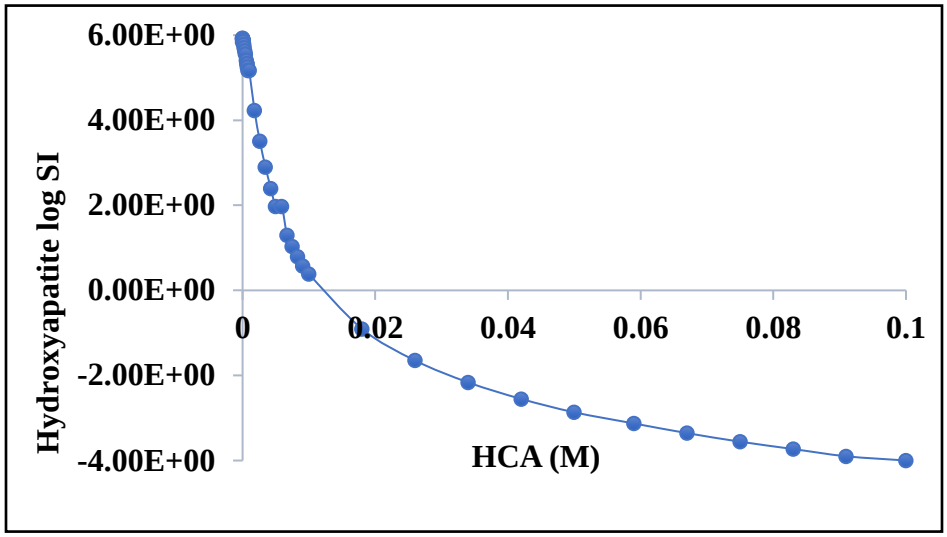

Figure 4.8. Hydroxyapatite log SI versus HCA concentrations.

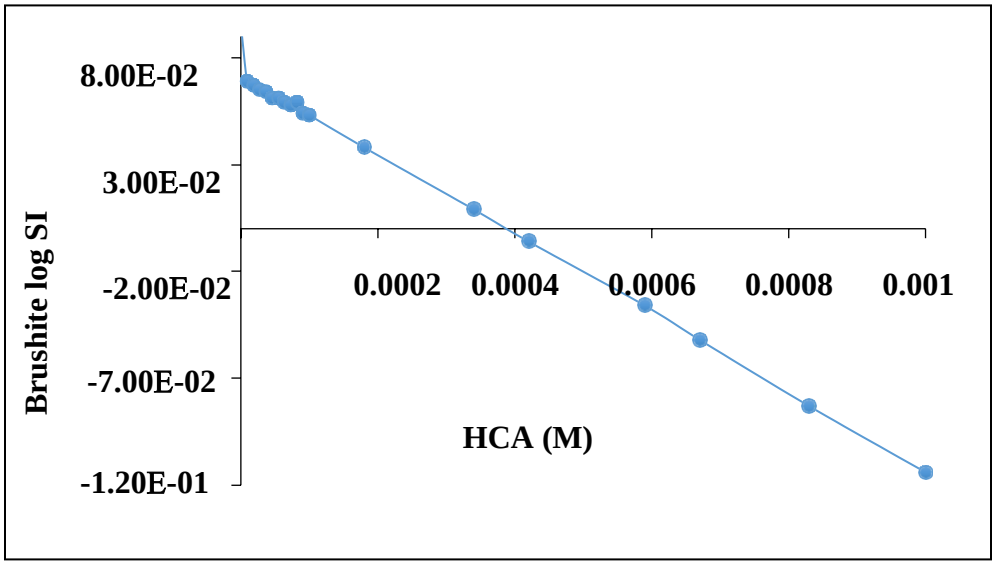

Figure 4.9. Brushite log SI versus HCA concentration.

4.5. Conclusion

It has been reported/suggested that HCA can be used to decrease the risk of CaOx kidney stone formation. [31] Studies at the University of Houston [17] reported HCA is capable of dissolving COM crystals. These *in vitro* studies established that an increased number of hydroxyl and carboxyl groups play a crucial role in specific COM crystal surfaces.

In 2019, Kim *et.al.* showed that HCA could melt crystal surfaces in supersaturated media (supersaturation ratio S = 4). This study was the first observation of crystal dissolution in a concentrated CaOx solution .[31] The study described in the present chapter aimed to investigate the theoretical role that HCA may play in controlling the thermodynamic crystallisation of calcium stone-forming salts in artificial urine role.

Speciation calculations showed that at a moderate concentration of 1 mM, HCA significantly affects the *in vitro* speciation of calcium. At this concentration, in ideal urine, 33% of the calcium is in the form of $[Ca(HCA)]^-$. A result of this complexation of Ca^{2+} is that the free calcium concentration decreased. Having established that HCA affected calcium speciation, the question arises, is this sufficient to change the SI of important kidney stone minerals. Here it has been shown that, indeed, HCA decreased the SI of COM and brushite. HCA also reduced the SI of apatite but to a lesser extent.

In conclusion, it has been shown that HCA has a thermodynamic effect on the risk of kidney stone formation. However, the possibility exists that it may also affect the kinetics of CaOx crystal formation. This is described in the next chapter.

Appendix

Table 4.8. Hydroxyapatite log SI and HCA concentrations.

log SI	HCA (mM)
5.837	0
5.93	0.000009
5.922	0.000018
5.914	0.000027
5.906	0.000036
5.891	0.000054
5.883	0.0000636
5.875	0.0000727
5.867	0.0000818
5.859	0.0000909
5.851	0.0001
5.779	0.00018
5.706	0.000263
5.631	0.000345
5.557	0.000427
5.405	0.00059
5.328	0.00067
5.328	0.00067
5.25	0.00075
5.172	0.00083
5.172	0.001
4.229	0.0018
3.511	0.0026
2.901	0.00345
2.394	0.00427
1.97	0.005
1.97	0.0059
1.3	0.0067
1.03	0.0075
0.791	0.0083
0.577	0.0091
0.384	0.01
-0.905	0.018

-1.648	0.026
-2.162	0.034
-2.552	0.042
-2.866	0.05
-3.129	0.059
-3.3556	0.067
-3.557	0.075
-3.73	0.083
-3.9	0.091

Table 4.9. Brushite log SI and HCA concentrations

log SI	HCA (mM)
0.095	0
0.069	0.000009
0.067	0.000018
0.065	0.000027
0.064	0.000036
0.061	0.000045
0.061	0.0000545
0.059	0.000063
0.058	0.0000727
0.059	0.0000818
0.054	0.00009
0.053	0.0001
0.038	0.00018
0.009	0.00034
-0.006	0.00042
-0.036	0.00059
-0.052	0.00067
-0.083	0.00083
-0.114	0.001

Table 4.10. log SI COM vs HCA concentrations. (COM: Calcium oxalate monohydrate)

log SI	HCA (mM)
0.344	0
0.276	0.000009
0.274	0.000018
0.273	0.0000272
.271	0.000036
0.27	0.000045
0.268	0.000054
0.267	0.000063
0.266	0.000072
0.264	0.0000818
0.263	0.00009
0.261	0.0001
0.248	0.00018
0.235	0.00026
0.221	0.00034
0.207	0.00042
0.179	0.00059
0.164	0.00067
0.15	0.00075
0.135	0.00083
0.106	0.001
-0.044	0.00181
-0.183	0.0026
-0.303	0.00345
-0.403	0.0042

-0.488	0.005
-0.56	0.0059
-0.622	0.0067
-0.677	0.007
-0.72	0.0083
-0.77	0.009
-0.81	0.01

References

1. Briesen JMV, Small M, Weber Ch, and Wilson J, Modelling chemical speciation: Thermodynamics kinetics and uncertainty. *ILM. Pub.* 2010.134-149.

2. Templeton DM, Ariese F, Cornelis R, Danielsson LG, Muntau H, Leeuwen HVP, Lobinski R, Guidelines for terms related to chemical speciation and fractionation of elements definitions structural,aspects, and methodological approaches (IUPAC Recommendations 2000). *Pure. Appl. Chem,* 2000, **72**(8), 1453–1470.

3. Cornelis RC, Crews HN, Caruso JA, and Heumann KG, Introduction. In Cornelis, R.C., Crews, H.N., Caruso, J.A., and Heumann, K.G., Handbook of elemental speciation: Techniques and methodology. *John.Wiley. Sons.Chichester,* 2003, 1-5.

4. Azeez PA, Prusty BAKumar and Jagadeesh EP, Chemical speciation of metals in the environment its relevancy to ecotoxicological studies and the need for biosensor development. *J. Food.Agr. Envir,* 2006, **4** (3&4), 235-239.

5. Michalke B, Element speciation definitions, analytical methodology and some examples ecotoxicology. *Envir.Safety, 2003,* **56**, 122- 139.

6. Berthon E, Matuchansky C, and May PM, Computer simulation of metal ion equilibria in biofluids Part.3. *J. Inorg. Biochem,* 1980, **13**(1), 63-73.

7. May PM, Muray K, JESS, a joint expert speciation system-1. *Talanta,* 1991, **38**, 1409-17.

8. May PM, Muray K, Jess, a joint expert speciation system-II. The thermodynamic database.

Talanta, 1991, **38**(12), 1419-26.

9. Jackson GE, Byrne MJ, Metal ion speciation in blood plasma: gallium-67- citrate and MRI contrast agents. *J.Nucl. Med*, 1996, **37** (2), 379-86.

10. Darn SM, Sodi R, Ranganath LR, Roberts NB, and Duffield JR, Experimental and computer modelling speciation studies of the effect of pH and phosphate on the precipitation of calcium and magnesium salts in urine. *Clin. Chem. Lab. Med*, 2006, **44** (2), 185-91.

11. Gogwana P, investigation of the beneficial effects of supplemental polyunsaturated fatty acids and glycosaminoglycans on the risk factors for calcium oxalate kidney stone formation using theoretical experimental and human models. *Thesis,PhD*, 2014, University of Cape Town.

12. Rodgers A, Allie-Hamdulay S, Jackson GE, Therapeutic action of citrate in urolithiasis explained by chemical speciation: Increase in pH is the determinant factor. *Neph.Dial.Trans*, 2006, **21** (2), 361- 369.

13. Fakier S, The effect of inositol-hexakisphosphate (phytate) on urinary risk factors for calcium oxalate urolithiasis in South African population groups with different kidney stone risk profiles: theoretical modelling, in vitro crystallisation experiments and in vivo human studies. *Thesis, PhD*, 2015, University of Cape Town.

14. Grases F, Costa-Bauza A, Königsberger E, and Königsberger LC, Kinetic versus thermodynamic factors in calcium renal lithiasis. *Int. Urol. Nephrol*, 2000, **32**, 19-27.

15. Walton RC, Kavanagh JP, Rao PN, Heywood BR, The association of different urinary proteins with calcium oxalate hydromorphs. Evidence for non-specific interactions. *Biochim, Biophys. Acta,* 2005, **1723** (1-3), 175-83.

16. Grases F, Kroupa M, Costa-Bauza A, Studies on calcium oxalate monohydrate crystallization: influence of inhibitors. *Springer-Verlag,* 1994, **22**, 39-43.

17. Chung J, Inhibition of calcium oxalate monohydrate crystallization using organic growth modifiers. *MSc Thesis,* 2013, University of Houston.

18. Rodgers A, Allie-Hamdulay S, Jackson GE, Durbach I, Theoretical modelling of the urinary supersaturation of calcium salts in healthy individuals and kidney stone patients: Precursors, speciation, and therapeutic protocols for decreasing its value. *J. Crys. Growth,* 2013, **382**, 67-74.

19. Finlayson B, Physicochemical aspects of urolithiasis. *Kidney. Int,* 1978, **13**,344-360.

20. Kavanagh JP, Supersaturation and renal precipitation: the key to stone formation*? Urol. Res*, 2006, **34**(2), 81–85.

21. Curhan GC, MD, ScD, Interpretation of kidney stone composition analysis *.up to date,* 2019.

22. Miller N, Williams Jr JC, Evan AP, Bledsoe SB, Coe FL, Worcester EM, Munch LC, Lingeman JE, Handa SE, In idiopathic calcium oxalate stone-formers, unattached stones show evidence of having originated as attached stones on Randall's plaque. *BJU. wiley online library* ,2010,**105** (2), 242-5.

23. Miller N, Gillen DL, Williams JC Jr, Evan AP, Bledsoe SB, Coe FL, Worcester EM, Matlaga BR, Munch LC, Lingeman JE, A formal test of the hypothesis that idiopathic calcium oxalate stones grow on Randall's plaque. *BJU. Int*, 2009, **103** (7), 966-71.

24. Coe FL, Evan A, Worcester E, Kidney stone disease. *J. Clin. Invest*, 2005, **115**(10), 2598-608.

25. Worcester EM, Coe FL, Calcium kidney stones. *J. Med*, 2010,**363**, 954-963.

26. Wesson JA, Worcester E M, Wiessner JH, Mandel NS, Kleinman JG, Control of calcium oxalate crystal structure and cell adherence by urinary macromolecules. *Kidney. Int,* 1998, **53**(4), 952-957.

27. Soni MG, Burdock GA, Preuss HG, Stohs SJ, Ohia SE, Bagchi D, Safety assessment of (–)-hydroxycitric acid and Super CitriMax a novel calcium/potassium salt. *Food. Chem. Toxicol,* 2004, **42**(9), 1513–1529.

28. Van L LJ, Van RJJ, Niesen B, Verhagen H, Saris WH, Wagenmakers AJ, Effects of acute (–)-hydroxycitrate supplementation on substrate metabolism at rest and during exercise in humans. *Am. J. Clin. Nutr,* 2000, **72** (6), 1445–1450.

29. Schwarz JM, Loe YC, Bergeron N, Rodriguez N, Gas chromatography/mass spectrometry method to quantify blood hydroxycitrate concentration. *Anal. Biochem*, 2001, **292** (1), 148–154.

30. Chung J, Granja I, Taylor MG, Mpourmpakis G, Asplin JR, Rimer JD, Molecular modifiers reveal a mechanism of pathological crystal growth inhibition. *Nature,* 2016,**536** (7617), 446.

31. Kim D, Rimer JD, Asplin JR, Hydroxycitrate: a potential new therapy for calcium urolithiasis. *Urolithiasis,* 2019, **47**(4), 311-320.

Chapter Five

5. In vitro study of the effect of hydroxycitric acid (HCA) on calcium oxalate (CaOx) crystallisation

5.1. Introduction

The crystallisation capacity of urine may be used as an estimate of the risk to form kidney stones. [1] *In vitro* crystallisation studies in both artificial urine and real urine remain of fundamental importance in kidney stone research.

Many different methods have been used to mimic the physiological aspects of the urinary system to differentiate between processes of crystallisation, such as nucleation, aggregation, and growth. [2, 3] These methods may be classified in terms of technique, or in terms of supersaturation levels in the kidney. [4]

As previously described in Chapter 4, modelling showed the presence of the $[Ca(HCA)]^-$ complex led to decreased CaOx concentrations in urine, and concomitant decreases in the supersaturation of COM and brushite under physiological conditions.

In the present study, artificial urine (AU) was prepared according to the method described by Walton and *et al.* [5]

HCA is not a component of human urine. Primary studies have shown that orally ingested hydroxy citrate is secreted in the urine. [6]

Various trials of HCA in humans have reported HCA to be well tolerated, with no significant danger to health. [7] Thus, in the context of the present study, it is an excellent candidate as a potential therapeutic agent for crystal and stone formation.

Regarding its effect on crystallisation, Chung [8] showed that HCA inhibits CaOx crystallisation to a greater extent than citric acid. In 2019, Kim *et al.* reported that HCA could melt crystals surfaces in supersaturated media; this was the first observation of crystal dissolution in concentrated CaOx solution. [6]

The purpose of the study described in the present chapter was to determine the effect of HCA on the **metasable** limit (MSL) and total CaOx crystallisation kinetics.

The objectives of the experiments described in this chapter were to:

1. measure the CaOx metasable limit (MSL) and CaOx crystallisation kinetics in AU.
2. measure the CaOx metasable limit (MSL) in AU containing HCA instead of citrate
3. measure the metasable limit (MSL) in AU containing citrate and HCA at a ratio of 1:1.
4. measure the metasable limit (MSL) and crystallisation kinetics in AU containing HCA at different concentrations and compare these results with that obtained for the control AU (zero HCA).

5.2. Preparation of artificial urine

Artificial urine (AU) was made according to the method reported by Walton *et al.* [5] A stock solution of AU was prepared from 320 mM NaCl, 50 mM NaH_2PO_4, 6.52 mM $MgCl_2$, 164.2 mM

KCl, 4.34 mM K_3 citrate, 43.8 mM $(NH_4)_2SO_4$, and 7.0 mM NH_4Cl. and an appropriate volume (1000 ml) of distilled water. The pH was adjusted to pH 6 using 5 M NaOH.

Solutions of 50 mM Na_2Ox and 120 mM $CaCl_2$ were prepared separately and filtered.

Next, 16.7 mL $CaCl_2$ and 3 mL Na_2Ox were added to 480.3 mL AU stock solution and diluted to a volume of 1000 mL using MilliQ water. The solution was stored at 4℃ for 24 h until it was ready to be used. Immediately before use, the solution was heated to 37℃ and filtered. The final concentrations of calcium and oxalate were, therefore, 2.0 mM and 0.15 mM, respectively.

5.3. Measurement of CaOx metastable limits

The CaOx MSL is a measure of the ability of a solution to resist spontaneous crystallisation of CaOx. [9, 10] The protocol described by Ryall was used to determine this parameter in AU. [10]

In this method, 10 mL samples of AU (x 13) were incubated at 37°C. Each sample was dosed with increasing concentrations of Na_2Ox to obtain final concentrations of oxalate in the range 0.15-1.95 mM. Dosing was performed at 1-minute intervals.

After an incubation period of 30 min, the absorbance of each sample was measured in a glass cuvette at 620 nm. The MSL was determined by plotting the absorbance against Na_2Ox concentration.

The concentration at which a sudden increase in absorbance occurred was recorded as the MSL. All experiments were repeated three times, and the average CaOx MSL was determined.

Five MSL experiments were conducted:

(i) AU (control).

(ii) AU containing HCA instead of citrate (concentration 4.34 mM).

(iii) AU containing HCA and citrate (1:1) (Concentration HCA = concentration Cit = 2.17 mM).

(iv) AU control + 0.5 mM HCA.

(v) AU control + 1 mM HCA.

5.3.1.Results

Experiment (I): AU (Control)

As a control, the MSL of CaOx was measured in AU. The averaged plot for absorbance vs Na_2Ox concentration is shown in Figure 5.1. The MSL of 0.75 mM Na_2Ox is indicated as the point (concentration) at which the absorbance of the solution increases. This is the concentration at which spontaneous crystallisation occurs.

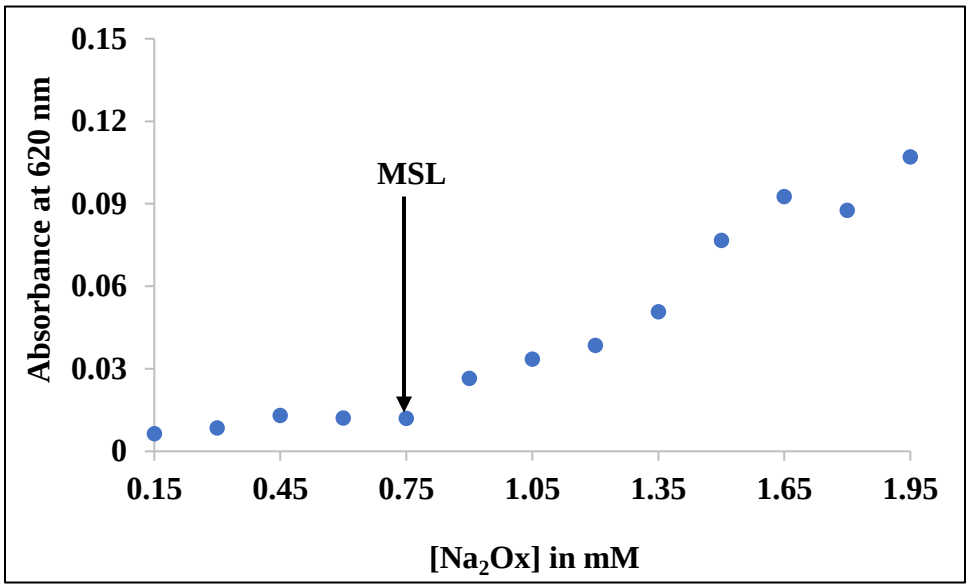

Figure 5.1. Mean absorbance as a function of Na_2Ox concentration in AU.

Experiment (II). AU containing HCA instead of citrate

In this experiment, the concentration of citrate was zero, while that of HCA was 4.34 mM. The averaged result is shown in Figure 5.2. It can be seen that the MSL is 1.35 mM.

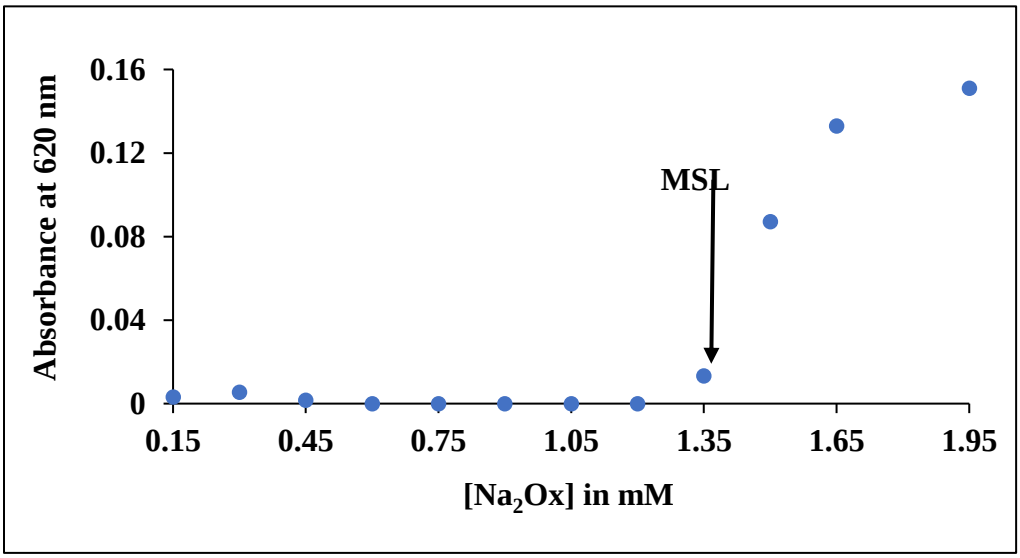

Figure 5.2. Mean absorbance as a function of Na_2Ox concentration in AU containing HCA instead of citrate.

Experiment (III). AU containing HCA and citrate (1:1)

In order to see at what concentration HCA affects CaOx MSL, different concentrations of HCA were tried. In this particular experiment, the concentrations of HCA and citrate in the AU were each 2.17 mM. The result is shown in Figure 5.3. It can be seen that the CaOx MSL is now 1.20 mM. This result is intriguing as it demonstrates that HCA alone (experiment #2, MSL 1.35 mM) has a stronger effect on the MSL than when it is present in combination with citrate (experiment #3, MSL 1.20 mM).

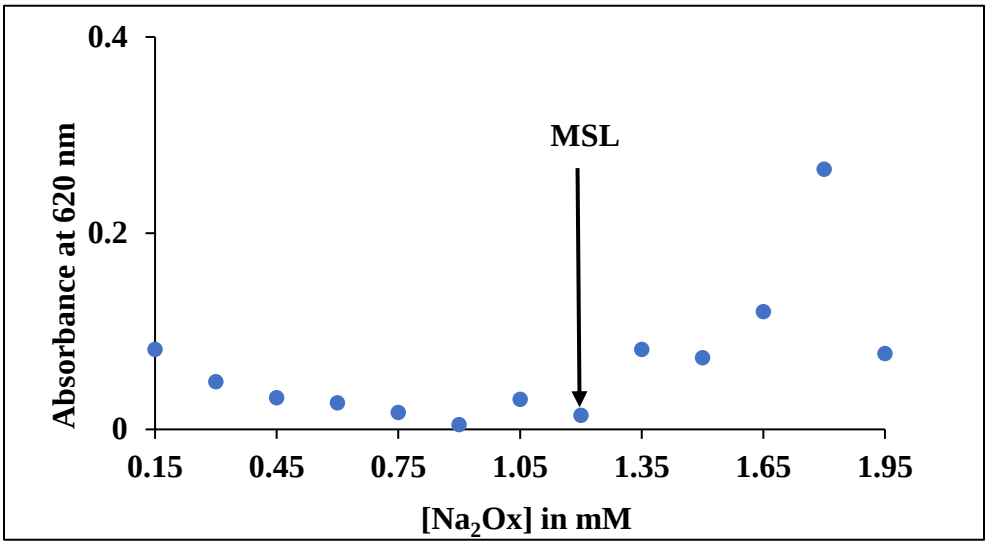

Figure 5.3. Mean absorbance versus Na_2Ox concentration in AU containing 1:1 citrate: HCA.

Experiment (IV). AU control + 0.5 mM HCA

The result is shown in Figure 5.4. It can be seen that the MSL of AU containing 0.5 mM HCA decreased to 0.75 mM Na_2Ox, indicating that 0.5 mM HCA had no effect on CaOx crystallisation in AU.

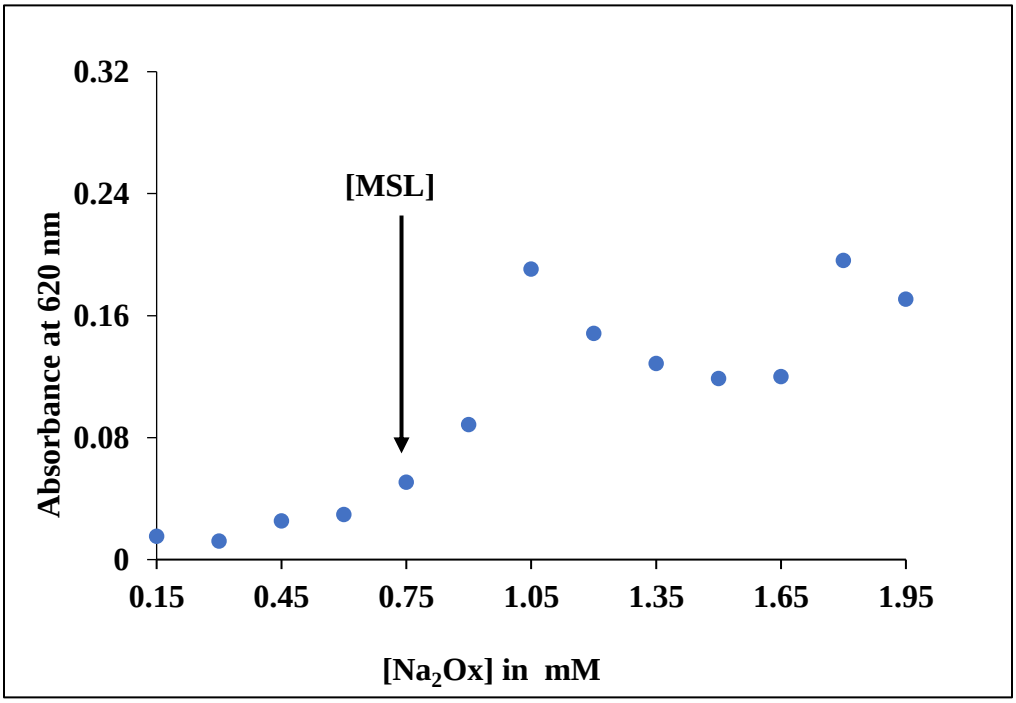

Figure 5.4. Mean absorbance as a function of Na_2Ox concentrations in AU containing 0.5 mM HCA.

Experiment (V). AU control + 1 mM HCA

The results are shown in Figure 5.5. It can be seen that the MSL is 1.20 mM.

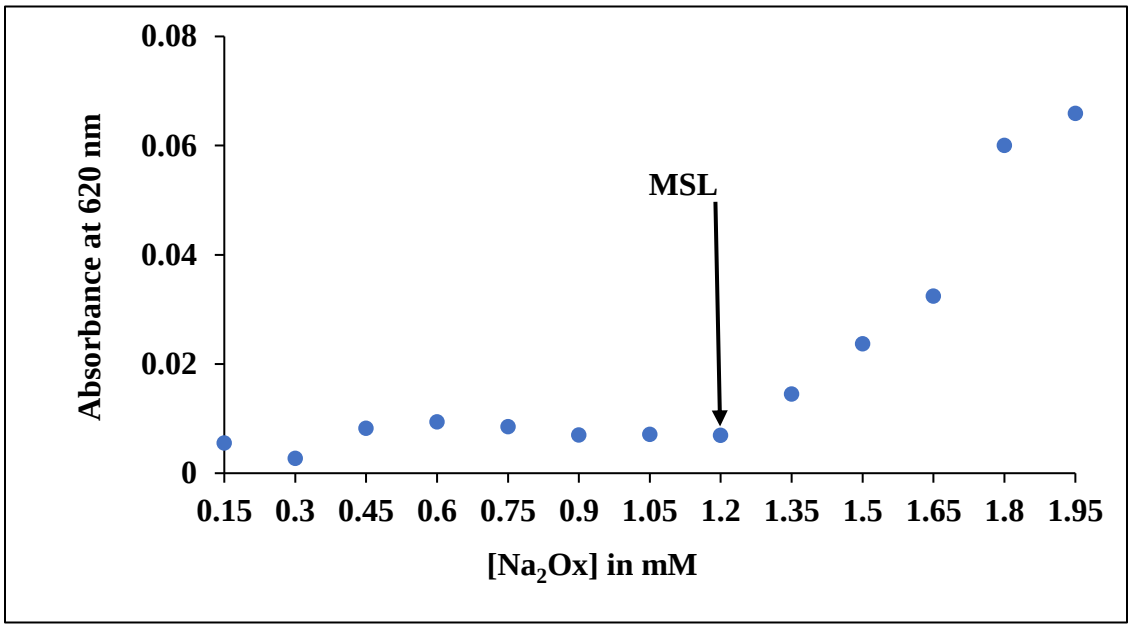

Figure 5.5. Mean absorbance as a function of Na_2Ox concentrations in AU containing 1 mM HCA.

5.3.2. Comments

A summary of the results of the CaOx MSL experiments is shown in Table 5.1 for quick and easy reference by the reader.

Table 5.1. Summary of CaOx MSL values in AU containing various concentrations of Cit and HCA.

Experiments	Experiment 1 Control [conc Cit = 4.34 mM, conc HCA = 0]	Experiment 2 AU– Cit + HCA [conc Cit = 0, conc HCA = 4.34 mM]	Experiment 3 Cit: HCA: 1:1 [conc Cit = conc HCA = 2.17 mM]	Experiment 4 Control + 0.5 mM HCA [conc Cit = 4.34 mM, conc HCA = 0.5 mM]	Experiment 5 Control + 1.0 mM HCA [conc Cit = 4.34 mM, conc HCA = 1.0 mM]
MSL (mM Na_2Ox)	0.75	1.35	1.20	0.75	1.20

Comparison of experiments 1 and 2 shows that when citrate is replaced by HCA, the CaOx MSL increases from 0.75 to 1.35 mM Na_2Ox. This means that HCA has a more powerful effect on the MSL than citrate. This can be accounted for by the higher value of the thermodynamic binding constant for Ca(II)-HCA = 3.93 compared to Ca(II)-Cit = 3.5.

Comparison of experiments 1 and 3 shows that when the concentrations of HCA and Cit are equal, the MSL increases from 0.75 to 1.20 mM Na_2Ox, indicating the inhibitory effect of HCA, but the

change in the MSL compared to experiment 2 is not as great. Thus, HCA alone has a bigger effect on the MSL than when Cit is present too.

Comparison of experiments 1 and 4 shows that the addition of 0.5 mM HCA to the control urine has no effect on the MSL. However, when the concentration of HCA is increased to 1.0 mM (experiment 5), the MSL increases to 1.20. This indicates that the effective concentration of HCA for retarding crystallisation is 1.0 mM.

Comparison of the MSL in experiment 1 with the MSL in experiments 2, 3, 4, and 5 shows that the biggest change in the CaOx MSL occurred when HCA was present in the absence of Cit (experiment 1 vs experiment 2).

From these results, it is clear that HCA is stronger than Cit at preventing CaOx crystallisation, and that a concentration of at least 1 mM HCA is needed for it to be effective. These results are expected as the potentiometric results show that HCA is a better chelator of Ca(II) than citrate. Thus, one would expect it to lower the concentration of free Ca(II) in AU, which in turn would increase the CaOx MSL. These results confirm the literature findings that HCA is more effective than citrate in preventing crystallisation [5,7,10] and demonstrate a thermodynamic role for HCA in retarding CaOx crystallisation.

5.4. Measurement of CaOx crystallisation kinetics

5.4.1. Methods

Total crystallisation kinetics was determined in samples by adding Na_2Ox (1 ml per 10 ml samples) at a concentration of 0.15 mM above the previously determined MSL (thus inducing crystallisation). In this method, 10 ml of each AU sample was incubated in a water bath with shaking at 37°C. The absorbance at 620 nm was measured at time zero and every 10 minutes over 120 minutes.

CaOx crystals kinetics were determined by plotting the absorbance against time. The rate of CaOx crystallisation was determined from the slope of the curve. [11] Gradients were determined for the time periods during which the curve showed a constant linear increase, as this is indicative of steady crystallisation.

In addition to the rate of crystallisation, a second parameter, the crystallisation induction time, was also measured. This corresponds to the time taken for crystallisation to be detected (sudden increase in absorbance) after the addition of Na_2Ox.

CaOx crystallisation kinetics and induction times were determined in three experiments involving the following solutions:

(I) AU control.

(II) AU control + 0.5 mM HCA.

(III) AU control + 1.0 mM HCA.

Experiment (I) was performed in duplicate while experiments (II) and (III) were performed in triplicate.

5.4.2.Results

Experiment (I). Artificial urine (Control)

The absorbance vs time graph is shown in Figure 5.6. Absorbance (i.e., crystallisation) increased after 50 minutes. The gradient was determined for the time period 50-120 min because the graph showed a linear increase (corresponding to a steady increase in crystallisation rate) during this time. AU1 and AU2 show good repeatability for the duplicated experiments.

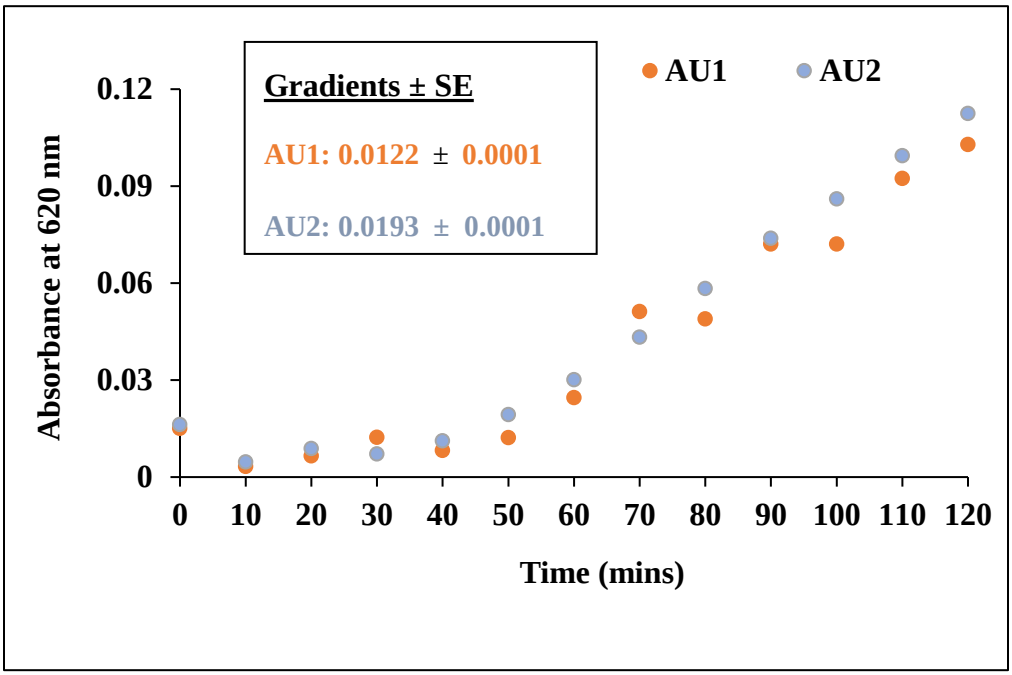

Figure 5.6. Absorbance versus time for CaOx crystallisation kinetics in AU.

Experiment (ii). AU + 0.5 mM HCA

The kinetic plots for the triplicate experiments in AU containing 0.5 mM HCA are shown in Figure 5.7. Absorbance (i.e. crystallisation) increased immediately (induction time = 0). Gradients were determined during the period 0–70 min. The results show excellent repeatability for the experiments performed in triplicate.

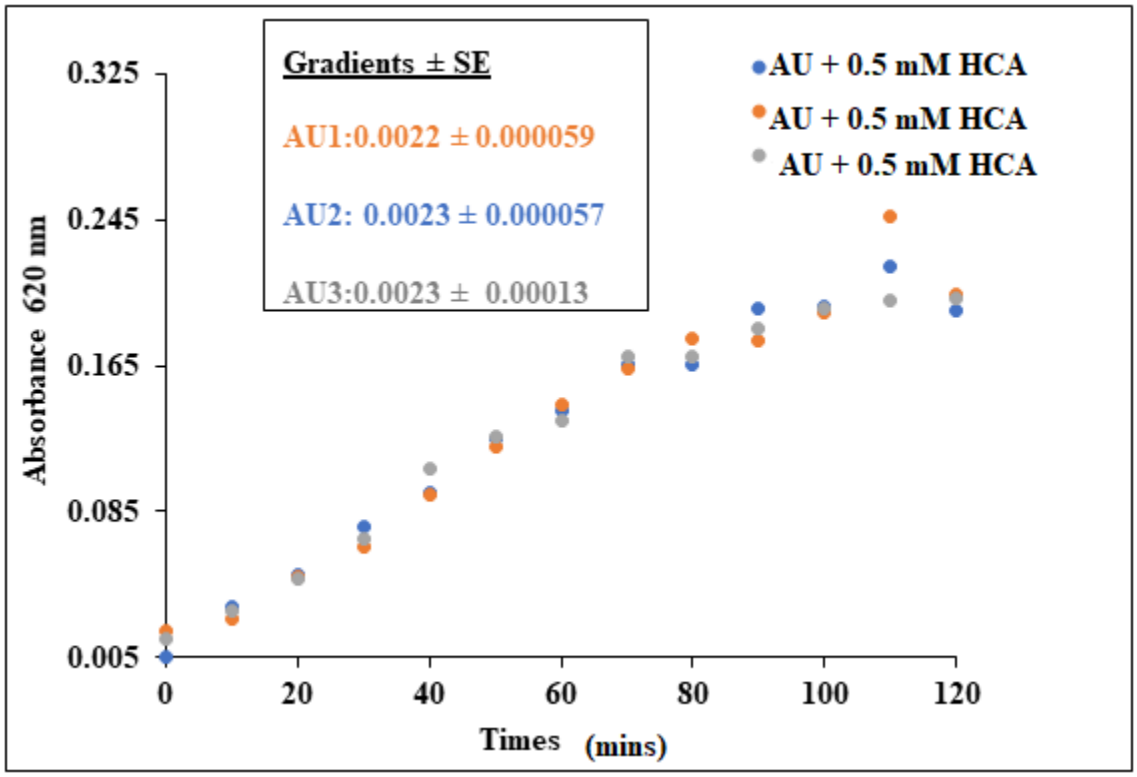

Figure 5.7. Absorbance versus time for CaOx crystallisation kinetics in AU containing 0.5 mM HCA.

Experiment (iii). AU + 1.0 mM HCA

The kinetic plots for the triplicate experiments in AU containing 1 mM HCA are shown in Figure 5.8. Absorbance (i.e. crystallisation) increased after an induction time of 10 minutes in each sample. Gradients were determined during the period 20–70 min. The results show excellent repeatability for the experiments performed in triplicate.

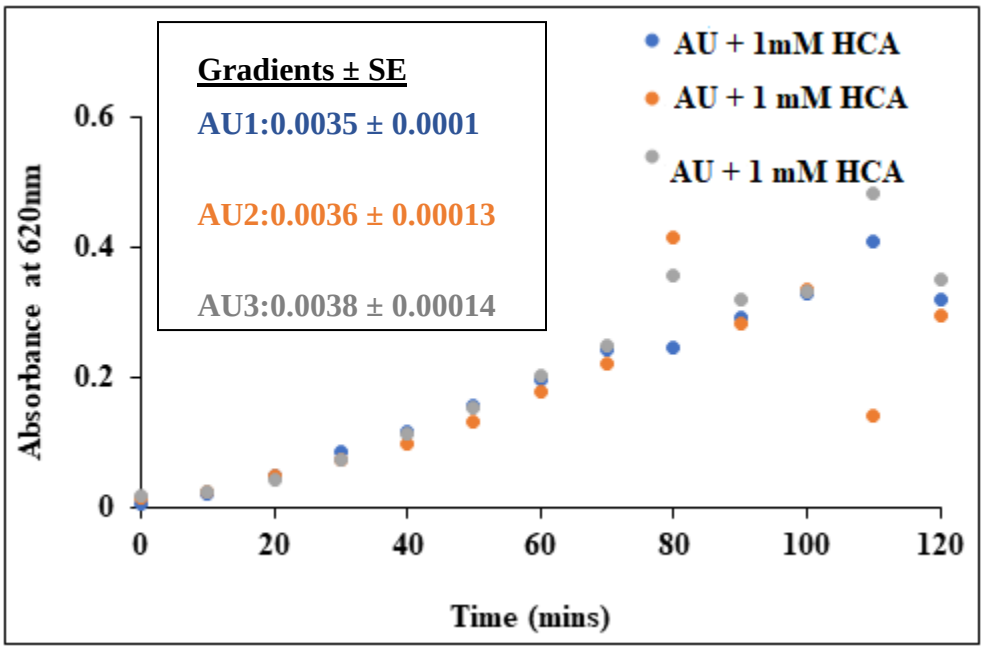

Figure 5.8. Absorbance versus time for CaOx crystallisation kinetics in AU containing 1.0 mM HCA.

5.4.3. Comment

Figure 5.9 summaries the crystallisation rates as a function of the concentration of HCA.

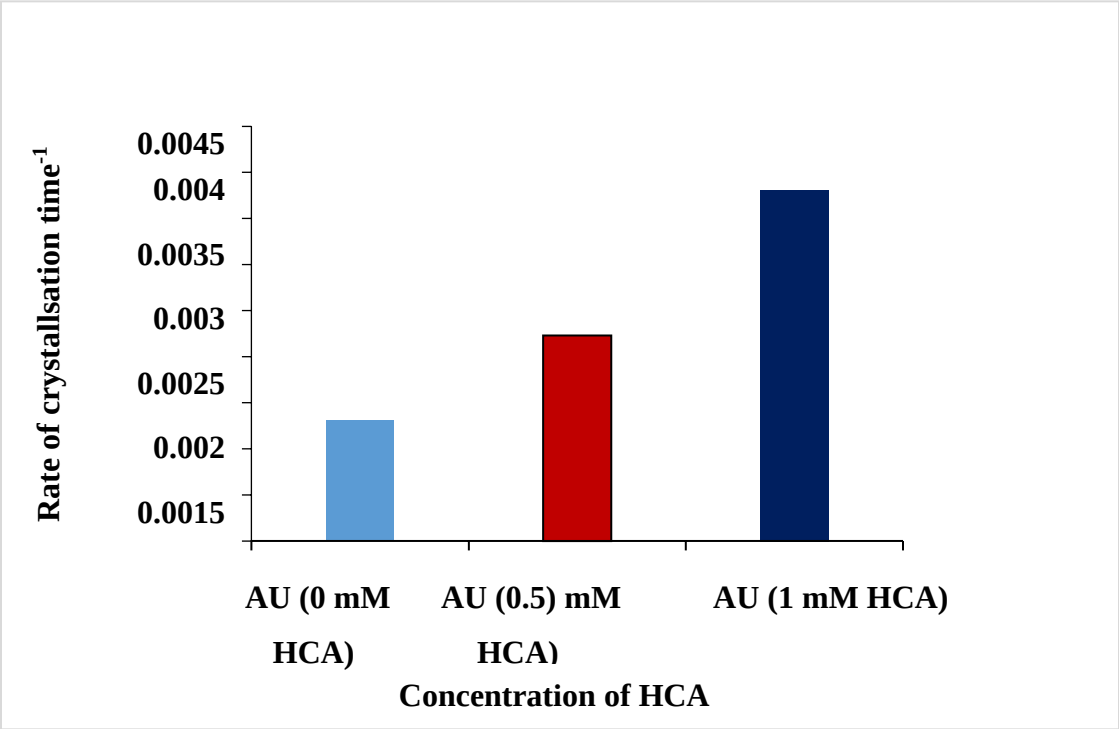

Figure 5.9. CaOx crystallisation rates as a function of HCA concentration in AU.

It can be seen that the crystallisation rate increases with increasing HCA concentration. In addition, induction times appear to decrease dramatically after the addition of HCA irrespective of the latter's concentration. Both of these effects are regarded as being favorable in terms of reducing the risk of CaOx stone formation. Firstly, a decrease in the induction time means that crystals start forming much more quickly in the presence of HCA in AU.[6, 12] Secondly, an increase in the

crystallisation rate means the small crystal formed in AU continue to form more rapidly. This reduces the supersaturation rapidly, and this is good because, in *vivo*, crystals would pass through the urinary tract prior to aggregation. [13, 14] As in a previous chapter, it was shown that HCA is a strong chelator of Ca^{+2} to form $[Ca(HCA)]^{-}$. This $[Ca(HCA)]^{-}$ complex reduced the CaOx supersaturation, thereby supporting the notion of HCA playing a kinetic role in inhibiting CaOx crystallisation.

5.5. Discussion

In the study described in this chapter, the thermodynamic and kinetic effects of HCA on the CaOx metastable limit and the overall rate of CaOx crystallisation respectively were investigated.

For HCA to be an effective therapy for kidney stones, it must be secreted in the urine. A previous study by Jahi and *et al*.[15],[8] revealed that HCA was detectable in blood and urine, making it a very good candidate as a stone therapeutic.[6] Various trials of HCA in humans have reported HCA to be well tolerated, with no important dangerous side-effects.[7]

As regarding crystallisation propensity, the CaOx MSL is defined as the capability of the solution to resist spontaneous nucleation. [9] In the present study, the effect of two different concentrations of HCA on MSL values was investigated. The addition of 1 mM HCA in AU leads to an increase in the CaOx MSL, indicating that it retards crystal nucleation at this concentration. This is

encouraging as it suggests that HCA might achieve the same result in *vivo* when administered to humans.

For the investigation of crystallisation kinetics, the addition of 0.5 mM and 1 mM HCA to AU increased the rate of CaOx crystallisation. As stated previously, this is a favorable outcome because it suggests that small crystals would be formed rapidly (to reduce the supersaturation) [13], allowing them to pass relatively quickly and harmlessly through the urinary tract in the event of HCA being ingested. [13, 16] This supports the notion that investigations involving AU help provide insight into protocols and conditions applied *in vivo*. [9]

The previous review by Kim *et al*.[6] reported that the calcium-binding capacity of HCA and citrate at pH 5 to 7 and at concentrations up to 3 mM were not significantly different. However, the results of the present study showed the calcium-binding capacity of HCA is significantly greater than citrate (Chapter 2). A possible explanation for the lack of agreement between the two studies could be that in their measurement of HCA as a calcium complexing agent, Kim *et al*. used a calcium ion-specific electrode to measure residual concentrations of Ca^{2+}, whereas, in the present study, actual stability constants were determined by potentiometric titration using a pH glass electrode. Kim *et al*. also reported that there was no difference between the CaOx MSL of urine in the presence of HCA and Cit whereas the present study demonstrated that HCA significantly affects this thermodynamic factor and that it does so to a greater extent than Cit. A possible explanation for this difference is that Kim *et al*. estimated crystallisation visually whereas, in the present study, crystallisation was measured photometrically. Thus, regarding both differences

between the studies (Ca-binding capacity and CaOx MSL), more sensitive techniques were used in the present study.

In conclusion, the results obtained from the studies described here are important for two reasons. Firstly, stability constants for Ca-HCA complexation are reported for the first time.

Secondly, the findings of favorable effects by HCA on retarding CaOx crystallisation indicate its potential for use as a curative agent in the therapy of kidney stones in humans.

References

1. Hess B, Ryall R, Kavanagh JP, Khan SR, Kok D, Rodgers AL, Tiselius HG, Methods for measuring crystallisation in urolithiasis research: why, how and when. *Eur. Urol*, 2001, **40**, 220-30.

2. Gupta M, Bhayana S, and Sikka SK, Role of urinary inhibitors and promoters in calcium oxalate crystallization. *IJRPC,* 2011, **1**(4), 793-798.

3. Vijaya T, Sathish Kumar M, Ramarao NV, Narendra Babu A, Ramarao N, Urolithiasis and Its Causes- Short Review. *JPHYTO*, 2013, **2** (3), 1-6.

4. Ryall RL, Glyeosaminoglyeans proteins and stone formation: adult themes and child's play. *Pediatr. Nephrol*, 1996, **10**, 656- 666.

5. Walton RC, Kavanagh JP, Rao PN, Heywood BR, The association of different urinary proteins with calcium oxalate hydromorphs. Evidence for non-specific interactions. *Biochim. Biophys. Acta*, 2005, **1723**(1-3), 175-83.

6. Kim D, Rimer JD, and Asplin JR, Hydroxycitrate: a potential new therapy for calcium urolithiasis. *Urolithiasis,* 2019, **47**(4), 311-320.

7. Soni MG, Burdock GA, Preuss HG, Stohs SJ, Ohia SE, Bagchi DS, Safety assessment (−)-hydroxycitrate, Super CitriMax, a novel calcium/potassium salt. *Food. Chem. Toxicol* , 2004, 42(9), 1513-1529.

8. Chung J, Inhibition of calcium oxalate monohydrate crystallization using organic growth modifiers. *MSc Thesis*, 2013, University of Houston.

9. Kavanagh JP, In vitro calcium oxalate crystallisation methods. *Urol. Res*, 2006,**34**(2), 139–145.

10. Ryall RL, Hibberd CM, Marshall VR, A method for studying inhibitory activity in whole urine. *Urol. Res*, 1985, **13**, 285-289.

11. Fakier S, The effect of inositol-hexakisphosphate (phytate) on urinary risk factors for calcium oxalate urolithiasis in South African population groups with different kidney stone risk profiles: theoretical modelling, in vitro crystallisation experiments and in vivo human studies. *Thesis. PhD*, 2015, University of Cape Town.

12. Costa-Bauza A, Rodriguez A, Grases F, Efficacy of mixtures of magnesium, citrate, and phytate as calcium oxalate crystallisation inhibitors in urine. *J. Urol*, 2015, **194**(3), 812-819.

13. Cerini C, Geider S, Dussol B, Hennequin C, Daudon M, Veesler S et al., Nucleation of calcium oxalate crystals by albumin: involvement in the prevention of stone formation. *Kidney. Int*, 1999, **55**(5), 1776-86.

14. Hallson PC, Rose GA, Seasonal variations in urinary crystals. *British Journal of Urology*, 1977, **49**(4), 277-84

15. Loe YCC, Bergeron N, Schwarz JM, Rodriguez N, Gas chromatography/mass spectrometry method to quantify blood hydroxycitrate concentration,. *Anal. Biochem,* 2001, **292**(1), 148-54.

16. Kavanagh JP, Methods for the study calcium oxalate crystallisation and their application to urolithiasis research. *Scan. Microsc* ,1992 ,**6**(3), 685-704.

Chapter Six

6.1. Conclusion

The inhibition of urinary kidney stone formation can occur via a thermodynamic and/or kinetic route. The present study aimed to establish whether hydroxycitric acid citrate affects and/or inhibits calcium oxalate crystallisation and, if so, how it achieves this and how it compares with inhibition by citrate. Since the equilibrium constants of HCA with H^+ and Ca^{2+} are unknown, the first step in the investigation was to measure these using glass electrode potentiometry. The thermodynamic binding constants for complexes for Ca(II)-HCA showed three species with log equilibrium constants (ML = 3.93, MLH_2 = 3.32, and MLH = 4.51) all higher than those for citrate.[1] Equilibrium constants for these three species are being reported here for the first time and hence will be invaluable for future speciation and modelling projects involving calcium and HCA.

Since HCA forms more stable complexes than citrate, it was of fundamental chemical interest to determine the structure of the different species. This was attempted using ^{1}H-NMR, as described in Chapter 3. The results showed all protons shifted in response to changes in pH. Thus these data could not be used to estimate the pK_a values of HCA or to assign protonation sites to individual microstates.

Solution structures of metal (Ca^{2+}, Mg^{2+}, and Zn^{2+})-HCA complexes were also investigated using ^{1}H-NMR, the idea being that those protons closest to the coordination site would be most affected

(Chapter 3). On the addition of the metal ion, however, all the peaks shifted and/or broadened. Shifting of the proton signals is due to the inductive effect of the metal ion. Since none of the metal ions is paramagnetic, it was concluded that the broadening must be exchange broadening. That is, several different structural isomers of a species must exist simultaneously in solution. Since the chemical shifts of the various isomers will be different, rapid or intermediate (on the NMR time-scale) exchange between them will lead to signal broadening. Thus, the NMR results were inconclusive or showed that even for the metal complexes, several microstates co-exist in solution. Indeed, it is concluded that the existence of these microstates is a contributory factor for explaining the superior binding capacity of HCA to calcium.

After the HCA-Ca equilibrium constants were determined, there was still a need to know if its complexes are strong enough to affect the speciation of Ca(II) in urine. This was modelled by including the measured equilibrium constants in the JESS thermodynamic database [2] and simulating their effect on urine. The results showed that a moderate concentration of 1 mM HCA significantly affects the *in vitro* speciation of calcium. At this concentration, in artificial urine, 33% of the calcium is in the form of $[Ca(HCA)]^-$. A result of this complexation of Ca^{2+} is that the free calcium concentration decreased. This, in turn, affected the calcium oxalate and phosphate speciation.

Additionally, the SI values of different calcium salts as a function of HCA concentration were investigated. This showed that increasing the concentration of HCA decreased the SI of COM, hydroxyapatite, and brushite. Since various trials of HCA in humans have reported HCA to be well tolerated, with no important adverse events [2,3] these findings are important because they suggest that HCA could be considered for the treatment of calcium-containing kidney stones, provided that its effect on crystal inhibition could be demonstrated in *in vitro* experiments. This was achieved in studies described in Chapter 5.

The results of the *in vitro* experiments showed that the addition of 1 mM HCA to artificial urine leads to an increase in the CaOx MSL, indicating that it retards crystallisation. This is a thermodynamic effect governed by the saturation of CaOx.

In the kinetic experiments, the addition of 0.5 mM and 1 mM HCA to AU increased the rate of CaOx crystallization. This is a favourable outcome because it suggests that small crystals would be formed rapidly (thereby reducing the supersaturation), allowing them to pass relatively quickly and harmlessly through the urinary tract in an *in vivo* situation. This observation is supported by the decrease in the induction time with increasing concentrations of HCA. Since induction time measure how long it takes for crystallisation to be detected after exceeding the MSL, a reduction in this time indicates a more rapid formation of crystals to reduce supersaturation.

Limitations of the present study include

1. The use of mercantile salts instead of HCA extracted from the plant (*Garcinia*) might have affected the result.

2. The experimental crystallisation work in the present study needs to be concluded with *in vivo* studies in humans.

3.The experimentally used 1 mM HCA and showed the effect of HCA in *vitro* ,but this 1 mM HCA may be enough or not to in *vivo* ,so what is the convenient volume of doses per day this could be used from HCA to prevention measures from kidney stones diseases .

Despite these limitations, it is concluded that the studies described in this thesis have shown that HCA plays thermodynamic and kinetic roles in decreasing important crystallisation danger factors for CaOx kidney stone formation. This is the first time that these effects have been demonstrated theoretically and experimentally for HCA. Thus, future studies involving the administration of HCA in human trials is encouraged.

References

1. Field TB, Coburn J, Mccourt JL, and Mcbryde WAE, Composition and stability of some Metal citrate and diglycolate complexes in aqueous solution. *Analytica.Chimica. Acta*, 1975, **74**, 101-106.

2. Muray K, May PM, Jess, a joint expert speciation system-II, The thermodynamic Database. *Talanta*, 1991, **38**, 1419-26.

3. Soni MG, Burdock GA, Preuss HG, Stohs SJ, Ohia SE, Bagchi D, Safety assessment of (−)-hydroxycitric acid and super citrimax, a novel calcium/potassium salt. *Food. Chem.Toxicol,* 2004, **42**, 151.